Aalto University
School of Engineering

Master's Program in Mechanical Engineering

CFD MODELLING OF MATTE DROPLET COALESCENCE IN FLASH SMELTING SETTLER

-SHREYAS KARADAHALLI NAGESH

School of Engineering

Thesis submitted in partial fulfillment of the requirements for the degree of Master of Science (Technology).

Espoo, April 2019

Supervisor: Prof.Ari Jokilaakso

Thesis Advisor: M.Sc.Nadir Khan

Author Shreyas Karadahalli Nagesh

Title of thesis CFD Modelling of Matte droplet coalescence in Flash smelting settler

Degree program M.Sc in Mechanical Engineering

Major/minor Minor **Code** Kirjoita tekstiä napsauttamalla tätä.

Thesis supervisor Prof. Ari Jokilaakso

Thesis advisor M.Sc.Nadir Khan

Date 3.04.2019 **Number of pages** 83 **Language** English

Computer simulations are popular due to difficulty in setup of conventional experimental methods at high temperature processes. Computational Fluid dynamics is an important tool to study settling mechanism in Outotec's flash smelting settler. Commercial Ansys Fluent model was used to study settling previously by researchers, but no study was done to model coalescence. The thesis aims in studying the suitability of the Ansys fluent built in code to model coalescence for flash smelting settler. The success of the model helps to understand copper loss mechanisms and find ways to increase copper recovery.

Firstly, collision theory and coalescence mechanism is reviewed thoroughly. Secondly, Ansys fluent built in models for modeling coalescence are listed and compared to select best mathematical model. The primary criteria for selection was ability to model collisions, coalescence, particle tracking and better visualization capacities. The selected discrete phase model is parametrized to model coalescence during settling of matte droplets through slag phase. It is noted that DPM could be used to simulate settling and coalescence of matte droplets. DPM can be used to get the idea of the process/coalescence phenomenon in a short period. The simulation showed droplets change trajectory after collisions/coalescence. Simulation also revealed coalescence dramatically affects settling time. Settling time is not only affected by increase in droplet diameter but also due to change in droplet trajectory after coalescences. However, Parametrized DPM model uses parcels injection technique that makes it difficult to track droplets individually for accurate comparison. In future user defined function should be written to identify and track droplets individually for accurate analysis of individual droplets.

Keywords Flash smelting, copper loss, Coalescence, Discrete Phase Modelling(DPM), Ansys Fluent, Weber Number, O'Rourke's Algorithm

Acknowledgement

I like to thank my supervisor Prof. Ari Jokilaakso for giving me an opportunity to do my master thesis in the interesting topic of computational fluid dynamics. During my master thesis study, I learned lot of practical stuff related to execution of algorithms in multiphase flows. I like to thank my instructor Nadir Khan for helping me out to solve the problem when I was stuck. I also like to express my gratitude to Aalto University IT service desk for the continuous support in installing Ansys, updating it and fixing the problems when asked.

Finally, I like to thank my parents, friends for their support offered during my master thesis program at Aalto University, Finland.

Espoo April 3, 2019

[SHREYAS KARADAHALLI NAGESH]

Contents

1 Introduction

In order to minimize copper loss and increase copper recovery, settling mechanism should be thoroughly understood. Previously researchers studied settling of matte droplets through slag in industrial flash smelting settler [Xia, J. L. et al (2007)], [Zhou, P et.al (2006)], [Taskinen, Pekka. et.al (2005)]. Most researchers inferred that settling rate is inversely proportional to droplet diameter. Xia et.al (2017) concluded that copper losses could be minimized by increasing matte droplet diameter. Coalescence of matte droplets increases the droplet diameter. Hence it is necessary to investigate effect of coalescence in matte settling processes in the settler of the copper flash smelting furnace.

Studying coalescence in Flash smelting settler is not possible by experimental methods. Setup of PIV cameras, analyzing coalescences and relating to settling mechanism is impossible in industrial scale. Hence computer simulations provide an alternative to these issues. Using computer simulations coalescences could be visualized in different sections of the settler safely. Different parameters controlling settling time could be studied by computer simulations in an economical way.

In the recent years, computational capacities of the computers have increased. The number of built-in mathematical models to model different phenomena are also more in number. Complicated phenomena like coalescence and breakup could be modeled by computational fluid dynamics technique. CFD is used to understand coalescence mechanism in lot of industrial processes like solvent extraction settler, kühni column, liquid-liquid extraction and agitated column. Computational coalescence helps to analyze the phenomenon safely from different angles.

The target of the work is to parametrize a built-in mathematical model to simulate coalescence of matte droplets through slag in flash smelting settler. Coalescence modeling is considered as one of the difficult point in polydispersed flows [Liao, Y., & Lucas, D. (2010)]. Simulating coalescences is very complicated because it involves not only interaction between droplet and continuous phase but also interaction between two colliding droplets. Relative velocity between two droplets causes collisions. The outcome of collision might be bouncing, coalescence, separation and shattering. After collision if the contact time is longer than drainage time coalescence happens otherwise the outcome is bouncing. Commercial CFD packages measure contact and drainage time by built in parameters. Built in parameters are smartly arranged in built in models to simulate collisions/coalescences. Some of the commercial simulation packages for modeling fluid flow problems are Ansys Fluent, Ansys CFX, starccm+, comsol multiphysics, CONVERGE CFD, NUMECA OMNIS, autodesk CFD, etc. In this master thesis Ansys fluent is used for modeling coalescence.

Some of the built-in mathematical models provided in Ansys Fluent for coalescence modeling include VOF method, discrete phase model, MUSIG model, etc. Most of the built models use collision frequency as a parameter in determining collision outcome. In this thesis, DPM and MUSIG model are studied in detail and two case studies are done with respect to VOF method. Previously researchers used volume of fluid for simulating binary droplet coalescence [Mohammadi, M et.al (2011, May)], [Yuan et al (2018)]. MUSIG model uses collision frequency and coalescence efficiency for modeling coalescences. DPM uses built in O'Rourke method for modeling coalescences. O'Rourke method uses offset distance and Weber number as the parameters to determine the outcome of collision. If the offset distance is lower than critically measured offset distance the outcome is coalescence otherwise the outcome is bouncing.

Critical comparison is drawn between different mathematical models and the built-in model is critically selected. DPM is selected based on its ability to model collisions, coalescence, particle

tracking and better visualization capacities. The aim of the thesis is to investigate the feasibility of the selected built-in model in modeling coalescence. As mentioned before DPM uses offset distance between the two droplets and critical offset distance in determining the collision outcome. Matte droplets of size 100-900 μm enter into the flash smelting settler of size 18m long and 6m wide. Inside the settler tiny matte droplets have to be simulated for collisions and coalescence outcome. The coordinates are defined in meters for settler modeling. However, matte droplets are in the order of 10^{-6} m. If three-dimensional simulation is carried out then it is difficult to parametrize the DPM model for collisions and coalescences due to big settler and very tiny matte droplets. Imagining collisions in 10^{-6} m coordinates and making offset distance lower than critical offset distance is quite challenging. In the DPM code, injections should be suitably made such that droplets undergo collisions and the outcome should be coalescences. To simplify computational domain of the settler is reduced in dimensions. The viability is checked by coalescences in particle tracking history, post visualizations and realistic settling time. DPM built in model displays clearly, if the collision outcome is coalescences. Coalescence pattern visualized in post processing visualizations are compared to the coalescence pattern observed by previous researchers. Literature review on settling of matte droplets through slag showed with increase in droplet diameter settling is faster. Hence, simulation is considered realistic if settling time decreases with coalescences. Suitability of the built in code is further studied by its ability to calculate the settling time of individual droplets in realistic conditions. This is extended to account copper losses. Chemical reactions and user-defined models are ignored in this work.

The main tasks carried out in this master thesis project could be written as follows:

1. To introduce flash smelting and the reason for carrying out this work. Settler part of the furnace is studied in detail.
2. Carry out a literature review on settling of matte droplets through slag in the settler of a flash smelting furnace. CFD research papers related to settling are studied and influencing parameters are documented.
3. Collision theory and coalescence is described. Mechanisms and mathematical models for coalescence are studied in detail.
4. Previous CFD simulation studies related to coalescence is documented. One case study is done with respect to each algorithm.
5. Search experimental data regarding properties of matte, slag, and mass flow rate.
6. By critically comparing different mathematical models best mathematical model is selected.
7. CFD modeling is done with the selected mathematical model.
8. Simulation results are compared with the collision theory, coalescence mechanism, settling and case studies.
9. Feasibility of the selected built in model is documented by considering settling time and copper losses.

The master thesis is written in five sections. In section 1 introduction is given by describing research targets and goals. In section 2 detailed background information is written. First flash smelting and compuational fluid dynamics are described. Also some previous studies related to settler modeling are documented. Then the collision theory and coalescence modeling is studied thoroughly. Next the computational methods are elaborated with some previous studies. The computational methods are compared and the best method is taken for modeling setup. In section 3, computational setup settings are written in detail. This is followed by results and discussion. Summary and conclusions are documented in the final section.

2 Background information

2.1 Flash smelting

Outokumpu (today known as Outotec FS) developed flash smelting in 1949 for smelting copper ore. Flash smelting does today 50% of primary copper smelting. In this process oxygen enriched air, sulphide concentrate ore and silica flux are introduced into the furnace at high temperature. The sulphide concentrate ore undergo an exothermic reaction in presence of oxygen gas and forms matte. The reactions between the copper concentrate, flux and oxygen takes place in less than one second at the reaction shaft; hence, the name is flash smelting. The reactions are presented in (1), (2) and (3) [Davenport, W. G., & Partelpoeg, E. H. (2015)]:

$$2CuFeS_2 + 13/4O_2 \xrightarrow{\Delta H=-450MJ/Kgmol} (Cu_2S + 1/2\ FeS) + 3/2\ FeO + 5/2\ SO_2 \quad (1)$$

$$FeS_2 + 5/2\ O_2 \xrightarrow{\Delta H=-700MJ/Kgmol} FeO + 2\ SO_2 \quad (2)$$

$$2FeO + SiO_2 \xrightarrow{\Delta H=-20MJ/Kgmol} 2\ FeO.\ SiO_2 \quad (3)$$

The flash smelting is a continuous process. The products of flash smelting are molten matte, slag and off gas. Molten matte is a mixture of copper, iron and sulphur. The percentage of copper in matte varies between 45-75%. Molten slag is iron oxide and gangue. The off gas is hot and dusty sulphur dioxide gas (SO_2) and Nitrogen (N_2) [Davenport, W. G et al., 2015].

Figure 1 shows the schematic representation of flash smelting furnace. The flash smelting furnace have concentrate burner, reaction shaft, settler, and uptake [Davenport et.al (2002)]. The primary function of concentrate burner is to combine sulphide concentrate particles and oxygen feed for even suspension. The raw materials from burners move into the reaction shaft. In the reaction shaft, oxygen reacts with concentrate particles and oxidation of sulphide concentrate happens at high temperature [Davenport et.al (2015)]. The formation of matte and slag takes place in the region beneath the reaction shaft. In addition, matte grade is determined at the region underneath the reaction shaft. The molten particles undergo chemical reactions inside the settler [WHITE, M. (2015)]. Copper-Iron-Sulphur matte phase settles due to gravity through the slag phase. Molten matte and slag are removed at regular intervals through the matte and slag tap holes respectively. Both matte and slag tapholes are water-cooled. An uptake removes the off-gas out from the furnace.

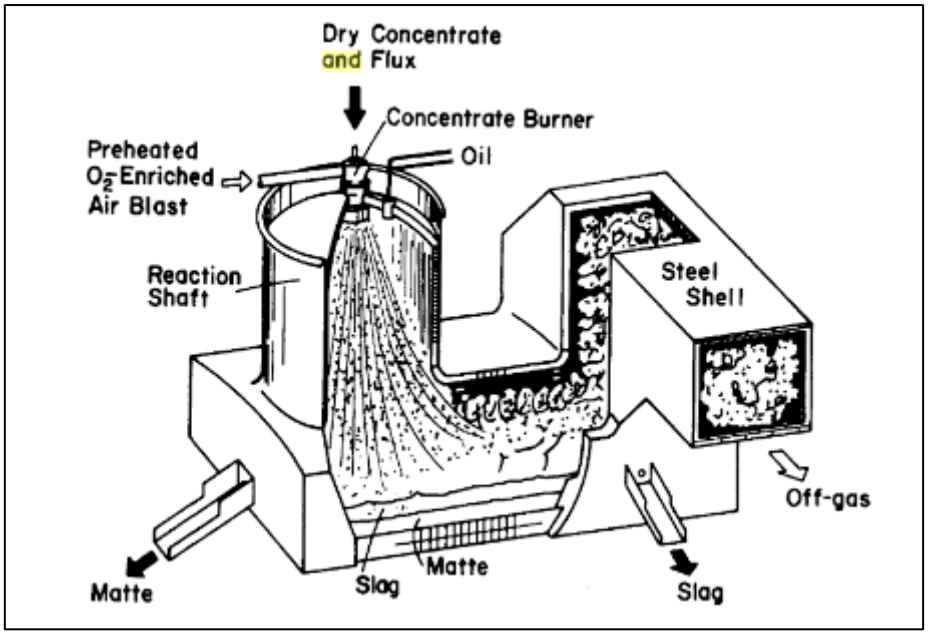

Figure 1: Flash smelting [Davenport et al, 2002)].

The Outotec's flash smelting furnaces vary in size and shape significantly [Davenport et.al (2015)]. The details of Boliden Harjavalta (Finland) furnace are shown in table 1 and figure two [Davenport et.al (2015)]. The Outotec flash furnace interior is made of high quality Magnesium oxide (MgO) and Cr_2O_3-Mgo refractory bricks. The bricks are backed by steel shell and water-cooled copper cooling elements in the areas of sever wear [Davenport et al, 2015]. Steel casing of 1cm thick covers most parts of the furnace. Large portions of the settler and reaction shaft are water cooled to account overheating.

Table 1: Table showing the details of Outokumpu's Flash smelting Furnace [Davenport et.al (2015)]

Company	Boliden Harjavalta Finland
Date of Furnace commissioning	1949
size, hearth in m	5*18.5*2
diameter of reaction shaft in meter	4.5
height of the reaction shaft above settler roof in meter	6.5
number of concentrate burners	1
Active matte tapholes	1
Active Slag tapholes	1
Slag layer thickness	0.25
Matte layer thickness	0.3

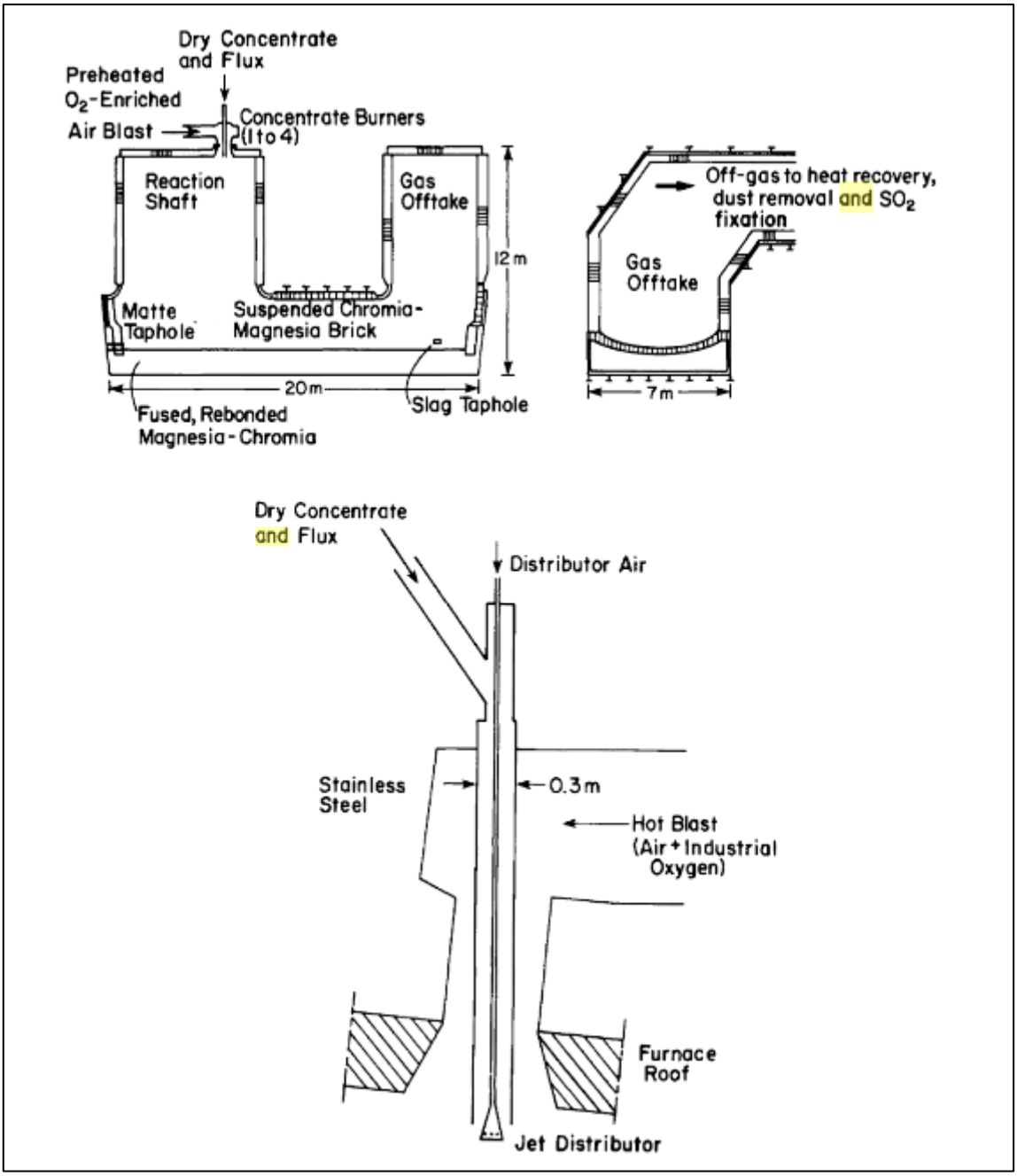

Figure 2: Side views and end views of Outotec's flash furnace [Davenport et.al (2015)]

Besides flash smelting, other smelting techniques to extract copper are reverberatory smelting and electric furnace smelting. The fuel for reverberatory smelting is a fossil fuel. Reverberatory smelting produces molten matte and molten iron-silicate slag. Reverberatory smelting was very popular during 20th Century. However, the use of reverberatory smelting declined after the development of flash smelting [Davenport et al (2002)]. The main reason for the downfall of reverberatory smelting is offgass sulphur dioxide, which is less than 2% volume fraction. The amount of energy used during reverberatory smelting is high compared to other smelting techniques. Electric smelting contains an electrically heated hearth furnace that requires feed of Cu-Fe-S and gives the products of matte containing 50-60% copper, molten slag, and the off gas. Even though flash smelting produces off-gas of sulphur dioxide, it performs better.

Copper loss in smelting

In any copper smelting process, the production of slag and copper is in the ratio of 2:1. Copper losses in smelting slags comprises 30% chemically soluble copper and 70% mechanically entrained matte droplets. This is one of the biggest economical concern for copper industries. Copper losses entrapped in waste slag strongly influence the cost of copper extraction process [Ma, X. et.al (2016)]. For instance, by minimizing 0.1 weight percentage of Copper loss in the slag over the year the company can save over several million dollars. Hence, the companies give high priority to recover copper from smelting slag.

It is widely accepted by researchers that copper losses in slag can be of mechanical or chemical in nature [Suh, I. K et.al (1988)]. During primary copper production copper dissolve as sulphide or oxide. During secondary copper production copper dissolve as oxide. This is termed as chemical copper loss. Chemical copper loss is determined by system thermodynamics and is intrinsic. Mechanical copper loss refers to mechanically entrained metal. Entrapped or floating unsettled droplets refers to mechanical copper loss [Minto, R. et.al (1972)].

Copper loss in Flash smelting settler

Different physical phenomena happening in the settler part are settling and separation of matte/slag phases, heat transfer between slag/matte phases and settler walls [Khan, N. A., & Jokilaakso, A. (2018)]. During settling of matte droplets through slag, not all matte droplets settle through the slag. There exist some copper droplets suspended in the molten slag. This unsettled matte droplets accounts for copper loss. Studying settling is important to minimize this copper loss and find ways to enhance copper recovery.

Researchers applied three methodologies to study copper loss in slag [De Wilde et.al (2016)]. First methodology is water-based systems. Water based systems represents different phases in the process. Second methodology uses models like computational fluid dynamics, phase field models, other numerical models. Third method uses industrial and/or lab scale procedures. Previous studies have shown that fluid dynamics greatly influences settling mechanism of matte droplets [Ma, X. et.al (2016)]. Computational fluid dynamics is used in this thesis to study settling of matte droplets through slag.

2.2 Computational Fluid dynamics

"We are literally at a significant point in history. A third branch of the scientific method, computer simulation, is emerging as a day-to-day tool. It is taking its place next to experimental development and mathematical theory as a way to new discoveries in science and engineering". John Rollwagen, CEO of Cray Research in his 1989 speech [Moukalled, F. et al (2016), said these words.

It is worth to quote such/similar statements in 2019 by witnessing the progress of simulation tools in present day industries. It is now evident that the application of simulation tools is vital to the development of industries. Numerical modeling/simulation tools has taken the role of technology enablers. The Computational Fluid Dynamics (CFD) is one of those tools. CFD was initially developed for aeronautics and aerospace industries. Compared to other well-established computer aided engineering techniques like Finite Element Analysis (FEA) CFD took more time to get the mainstream usage in other industries. The reason for the slow evolution is the complexity of the equations that are solved in CFD technique. However, with the advancement of computer technology and increase

in computational capacities CFD is used in wide range of industries like chemical, automotive, electronics, power, building industries, Fire safety, nuclear industries, etc.

CFD uses numerical analysis and data structures for analyzing fluid flows. CFD analyzes fluid flow and heat transfer phenomena by the use of computer codes, thus replacing governing equations by numbers. Later these numbers are advanced with respect to space and time giving final solution of the problem. The computer code is written by defining the mathematical models suitable for the particular fluid flow problem. CFD involves three conservation laws of physics namely mass, momentum and energy conservation laws. The mass, energy and momentum conservation equations together are partial differential equations called as Navier-Stokes equations. Besides Navier-Stokes equations, CFD takes care of empirical equations and Multiphase models as well. Empirical equation accounts the effect of turbulence while multiphase models takes care of different phases during CFD modeling. For flows, which are incompressible in nature, density remains constant and is not linked to pressure. However, for compressible flows density varies and thus linked to pressure.

With the increase in usage of CFD simulation in various industrial sectors lot of commercial software are available in the market. Some of the commercial software packages to solve fluid flow problems are Ansys Fluent, Ansys CFX, starccm+, comsol CFD, CONVERGE CFD, NUMECA OMNIS, autodesk CFD, atlair, etc. Today's CFD analyst has the luxury of getting high number of built in models for one flow problem. The large number of built in models developed by commercial software vendors shows the importance of CFD in industries and academia. Commercial software companies have spent lot of time and investment to provide a user-friendly graphical interface in the models. The open source package used for CFD analysis is openfoam. Ansys fluent is used in this master thesis.

Ansys Fluent solves the fluid flow problem by two steps namely preprocessor, solver. The typical steps done during pre-processor stage are defining computational domain, generating mesh, defining the fluids and boundary conditions. The steps done during solver stage are checking and repairing the mesh, approximation of mathematical models, which accounts for flow and heat transfer variables. Finally governing equations are discretized, solution of algebraic equations. The post processing analyzes the results. Post processing also involve reporting and calculating variables at specific points/ planes. The typical CFD steps to solve fluid flow problem could be written as shown in figure 3.

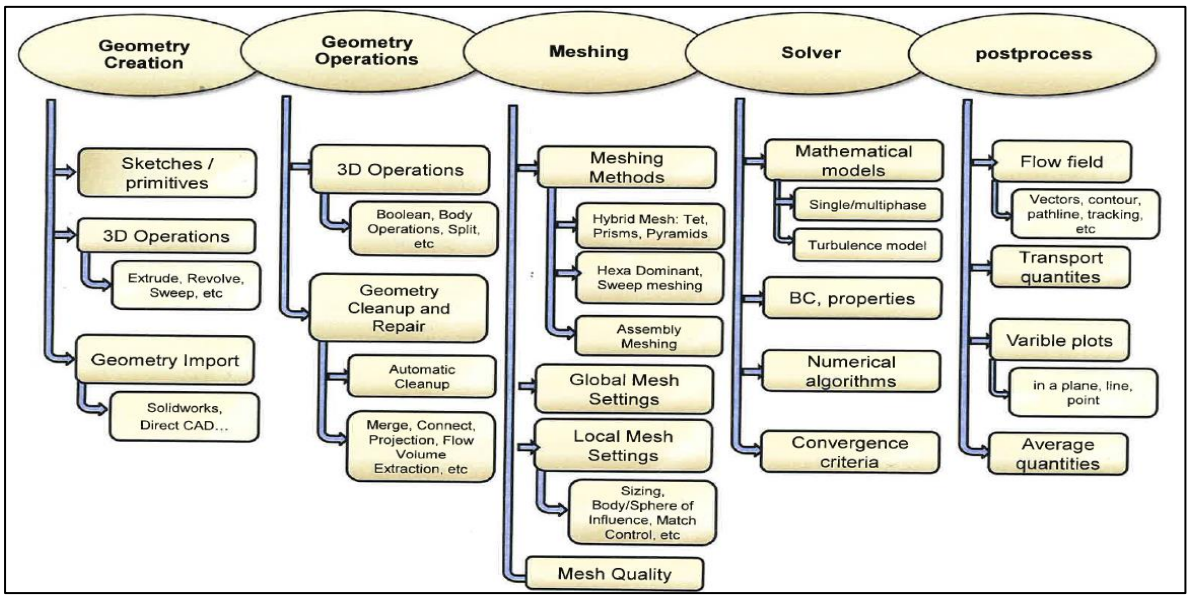

Figure 3: Basic flowsheet to solve a fluid flow problem via a CFD code

CFD history in Outotec

It is very complicated to take direct measurements in industrial process because of aggressive and hostile conditions. CFD modeling/numerical simulations could compensate this problem with the help of mathematical models. Outotec started using numerical simulations in 1980's by the collaboration between Columbia University and university of Utah. After starting several research projects, chalcopyrite combustion was modeled by one-dimensional code. Two-dimensional flows were simulated in late 1980's. During 1980's phoenics, the first commercial fluid flow program was launched. In 1990's powerful computers made possible to simulate three dimensional flows. Outotec started considering CFD as an important research area from 1990's. The company realized new platform could be reached by numerical simulations. The decision was made to collaborate and work with university of Helsinki in fluid flow modeling research. During the time commercial software packages were decided to use. Large CFD research group was established in Helsinki university of technology. The group published several researches during the time. Both experimental group and modeling group worked in the area of sulfide combustion kinetics. From 1995 sub models are developed and validated. Some of the models developed are model for chalcopyrite particle combustion, model for chalcocite particle combustion, model for mixed particle combustion, model for magnetohydrodynamic flows, model for NOx-formation, model for heat recovery boiler and off-gas cooling, etc [Ahokainen, T. et al(2006)]. CFD modeling of Outokumpu flash smelting process began in 1992. The study aimed at improving the energy efficiency of flash smelting. From then on flash smelting is a target of CFD simulation due to its hostile conditions. Some of the earlier works regarding this include Ahokainen et al 1997, Koh et al 1998, and Šutalo et al (1998a b). With the increase in computational power, new models were developed over time by researchers. This thesis focusses on settler part of the flash smelting furnace.

2.2.1 Literature review on settler modeling

The Outotec's flash smelting settler is 18m long and 6m wide. The inlet of settler has a diameter of 4.5m [Xia, J. L. et al (2007)]. Slag and matte layer thickness vary as they are tapped at regular intervals. Matte layer is in the range of 0.3 m while slag layer is in the range of 0.15-0.8m. The schematic of Outokumpu flash smelting is as shown in figure 4. Studying flash smelting settling is important because of phenomena like slag/matte interactions, slag/matte reactions, and copper losses during slag tapping [Khan, N. A., & Jokilaakso, A. (2018)]. It is impossible to visualize the settling phenomena, particle tracks and flow field inside settler by direct methods. In order to minimize the copper loss in flash smelting settler and increase the direct recovery of copper CFD simulation is used. The flash smelting settler model is quite complicated because it contains two phase gas/ paticle flows, turbulent flow, radiation, and chemical reactions at high temperature.

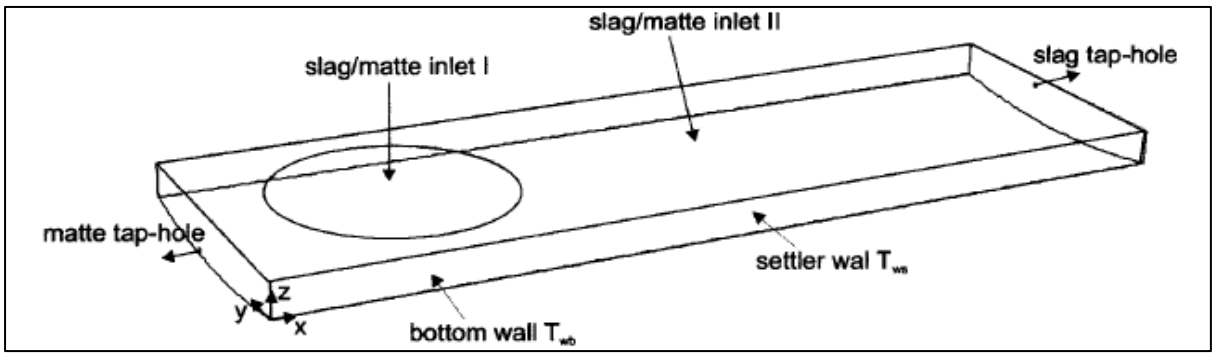

Figure 4: Schematic representation of Outotec's settler [Xia, J. L. et al (2007)]

Some of the previous publications to study settling mechanism are Xia, J. L. et al ((2007), [Zhou, P et.al (2006)] and Taskinen, Pekka. et.al (2005). Most researchers utilized a modified version of the Stokes law as a governing equation to explain the mechanism of settling process [Zhou, P et.al (2006)]. Xia, J. L. et al ((2007) conducted a detailed simulation to study settling behavior for matte droplets of different diameters. The researchers proved that time taken for settling is inversely proportional to droplet diameter [Zhou, P et.al (2006)] [Taskinen, Pekka. et.al (2005)] [Davenport, W. G et.al(2002)] [Jiang, T et.al(2016)]. The variation of settling time with respect to matte droplet diameter is as shown in figure 5.

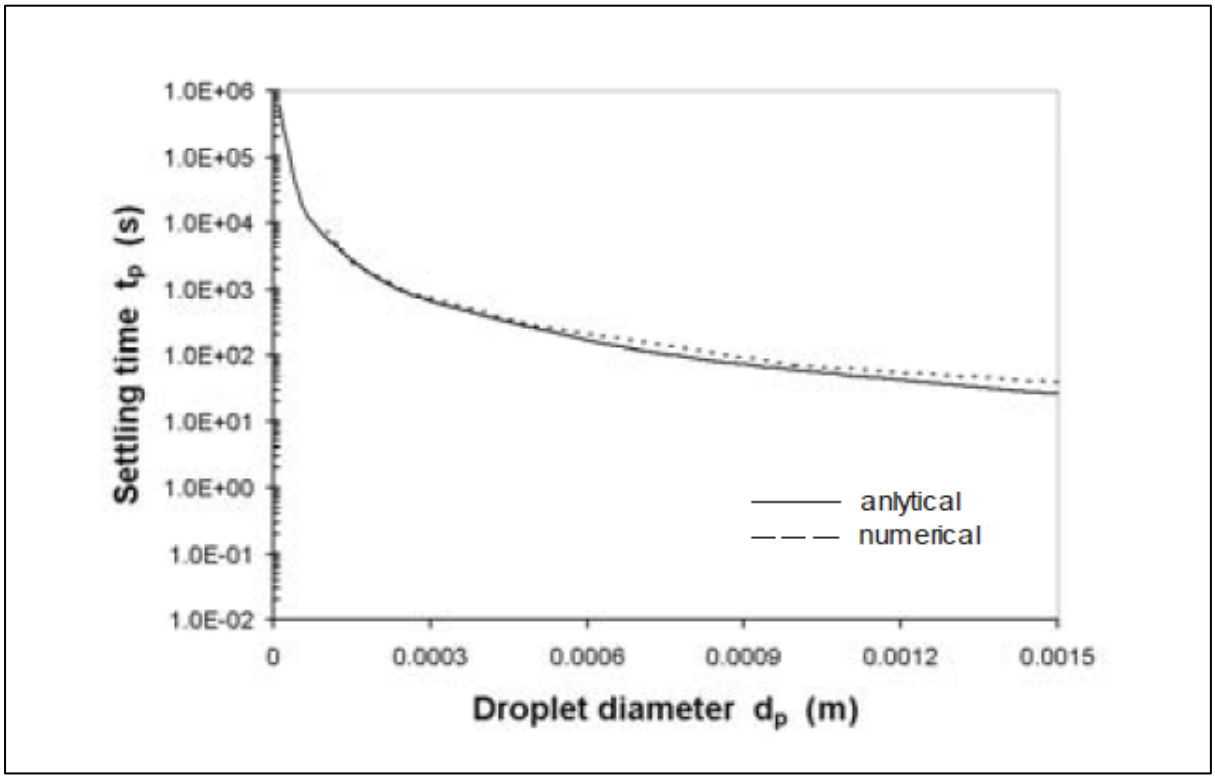

Figure 5: Graph of settling velocity versus matte droplet diameter, results obtained from Taskinen, Pekka. et.al (2005)

The settling of a matte droplet in slag is primarily influenced by terminal velocity. The formulae of terminal velocity during creeping flow is called Hadamard – Rybczynki equation [Jiang, T et al,. 2016] which is given by equation 4.

$$U_T = \frac{2gr^2\Delta\rho}{3\mu}\left(\frac{1+k}{2+3k}\right) \quad (4)$$

In equation 4, U_T is the terminal velocity, g is the acceleration due gravity, r is the radius of the matte droplet, $\Delta\rho$ is the density difference, μ is the viscosity of the slag, k is the viscosity ratio of droplet to slag. Settling velocity varies exponentially with respect to Matte droplet diameter as shown in figure 6. Similarly, stokes law will solve settling velocity when slag tapping is not done [Zhou, P et al (2006)]:

$$V_s = \frac{g(\rho_m-\rho_s)d_p^2}{18\mu} \quad (5)$$

In equation 5, V_s is the settling velocity, g is the acceleration due to gravity, ρ_m is the density of the matte, ρ_s is the density of the slag, μ is the viscosity, H_s is the slag height or slag thickness and d_p is the particle diameter.

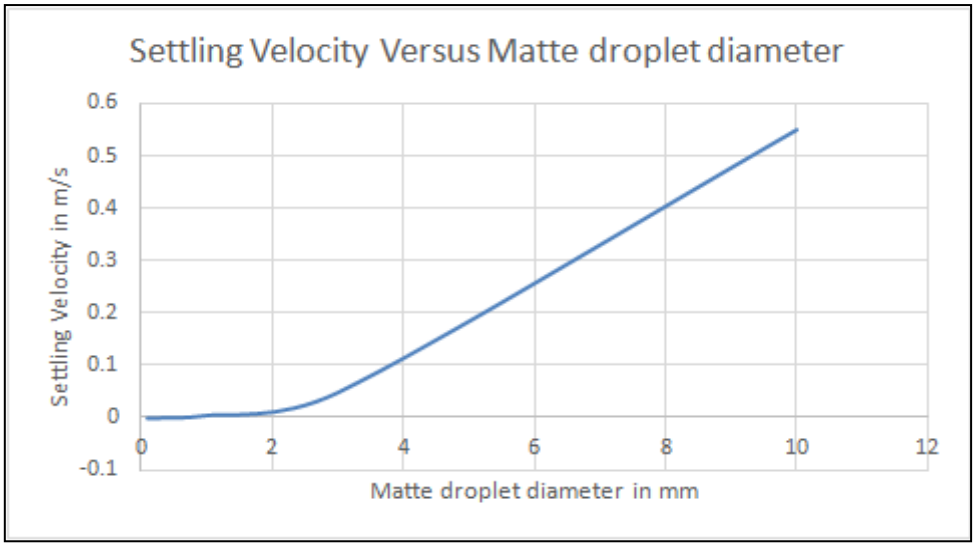

Figure 6: Graph of settling velocity versus matte droplet diameter, data obtained from Davenport, W. G., et al (2002)

Taskinen, Pekka. et.al (2005) and Xia, J. L(2007) concluded that settling does not happen below a minimum droplet size. P Zhou, J Yu, H Chen and C Mei derived the maximum droplet size diameter formulae of the matte droplets during flash smelting [Zhou, P et al (2006)]. The derivation showed that maximum droplet diameter was found by equation 6.

$$d_{max} = \sqrt{\left(\frac{18}{g}\,\frac{\mu_s}{(\rho_m-\rho_s)\rho_s}\,\frac{q}{l\,w}\,\frac{r}{r+1}\right)} \qquad (6)$$

Xia et.al (2007) studied copper losses with respect to matte droplet diameter. The researchers concluded that copper losses could be minimized by increasing the droplet diameter. In other words, copper losses are inversely proportional to droplet diameter.

The above results of Taskinen, Pekka. et.al (2005), Zhou, P et.al (2006), and Xia, J. L. et al ((2007) indicate that with increase in matte droplet diameter settling is faster. Therefore, settling efficiency increases with increase in droplet size. Larger droplet diameter results in less number of suspended particles and hence will minimize matte loss in slag[Xia et.al (2007)]. However, these studies considered average droplet diameter in their simulation that is not the true representation of the actual process. To understand realistic settling mechanism coalescence should be simulated and investigated. Simulation is carried out by considering coalescence and it is compared with inference of Taskinen, Pekka. et.al (2005), Zhou, P et.al (2006), Xia et.al (2016) and Xia, J. L. et al ((2007).

To simulate coalescence in Ansys fluent firstly collision theory and coalescence mechanism is understood in section 2.3. In section 2.4 Ansys fluent built in mathematical models are studied. Comparison is made between them and the best built in model is selected for simulation. The present study focusses on clarifying copper losses with respect to coalescence and the ability of the built in model to simulate it.

2.3 Collision and coalescence

When two droplets collide, they interact for a certain time known as contact time. If the contact time is long, enough for the film to drain called drainage time and reach critical thickness coalescence occur. Otherwise, the droplets rebound. In other words, Bouncing will happen when the droplet surface

contact does not happen because of the presence of thin intervening gas film [Dhainaut, M. (2002)]. Shattering happens when the relative velocity between two droplets is high [Svanberg, M. et al (1998)]. Separation happens because of two droplets connect temporarily and go away from each other. Separation process can be classified into two types: reflexive separation and stretching separation [Ashgriz, N., & Poo, J. Y. (1990)]. Thus collision of two droplets will lead to four different possible outcomes [Dhainaut, M. (2002)] namely, coalescence, bouncing, separation and shattering. Bouncing, coalescence and separation are shown in figure 7. Shattering outcome is shown in figure 8. Similar patterns were observed by different researchers. Figure 9 shows the time sequence of coalescence and bouncing for a research done by Hu, Y. T. et.al (2000). Pattern of reflexive separation captured by Orme, M. (1997)] is shown in figure 10.

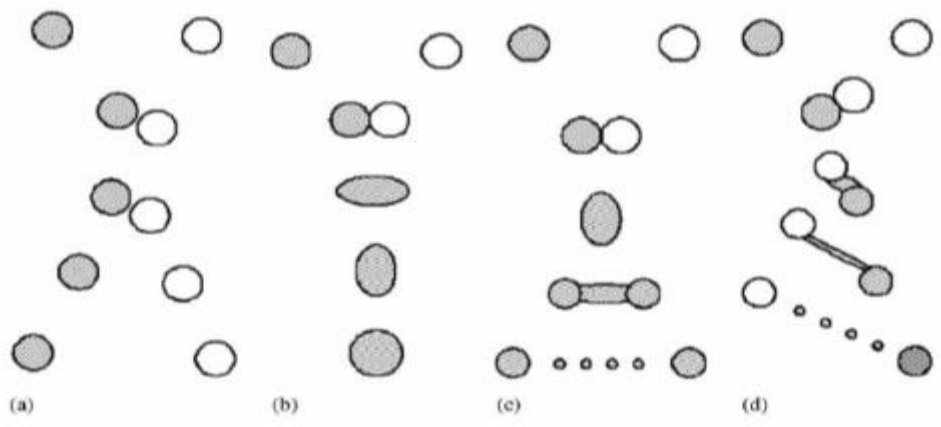

Figure 7: Illustration of a. bouncing, b. coalescence, c. reflexive separation and d. stretching separation [Gao, S. et al. (2010)]

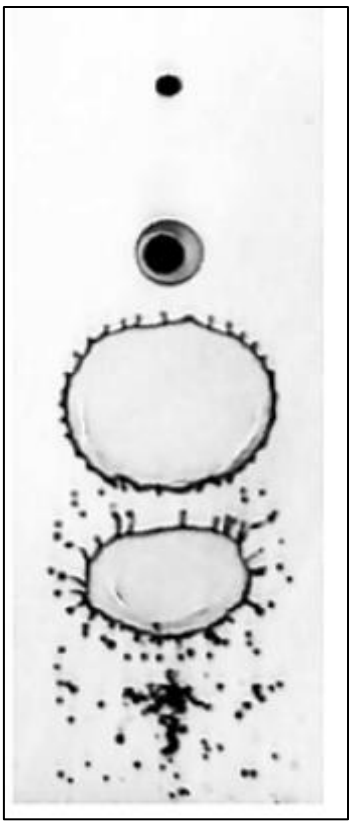

Figure 8: Illustration of shattering [Roth et al.(1999)]

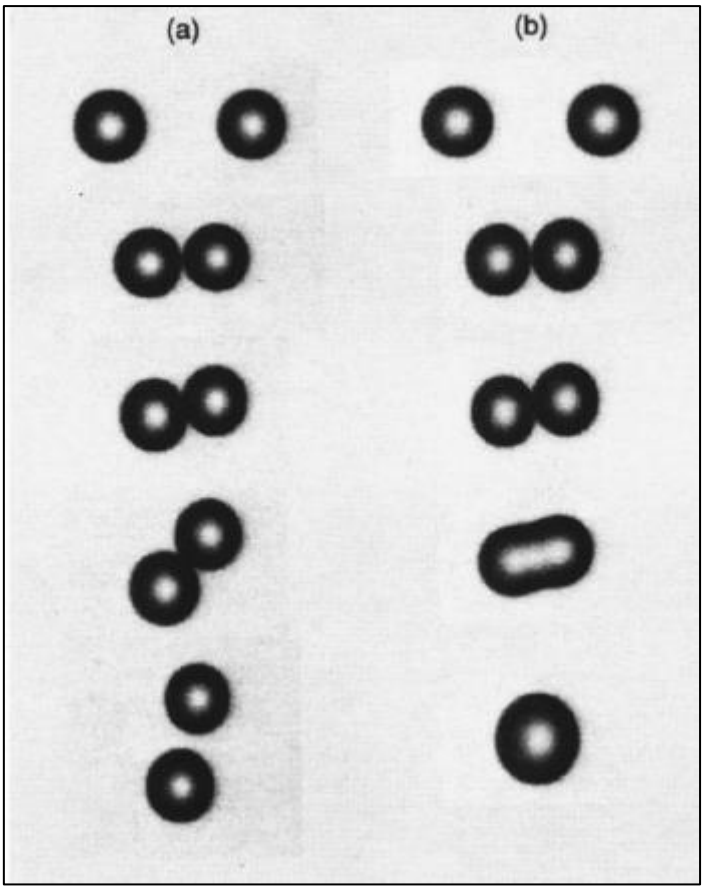

Figure 9: Time sequence of two-droplet coalescence. In case a coalescence does not happen and lead to bouncing but in case b coalescence happens [Hu, Y. T. et.al (2000)]

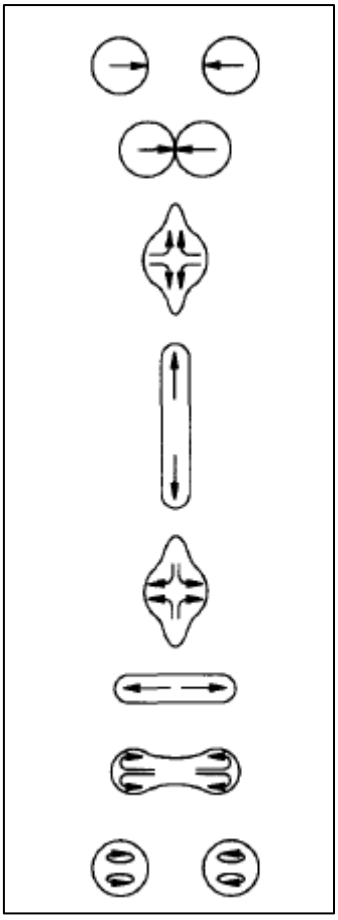

Figure 10: Figure representing head on collisions leading to reflexive separation [Orme, M. (1997)]

The four parameters that determine the outcome of collisions are Weber number, diameter ratio, impact diameter and Reynold's number [Ashgriz, N., & Poo, J. Y. (1990)].

In figure 11,

d_1 and d_s = diameters of large and small droplets respectively

X= Distance between the center of droplet 1 and the relative velocity vector on the drop 2 center

U_1 and U_s = Terminal velocities of droplet 1 and droplet 2 respectively

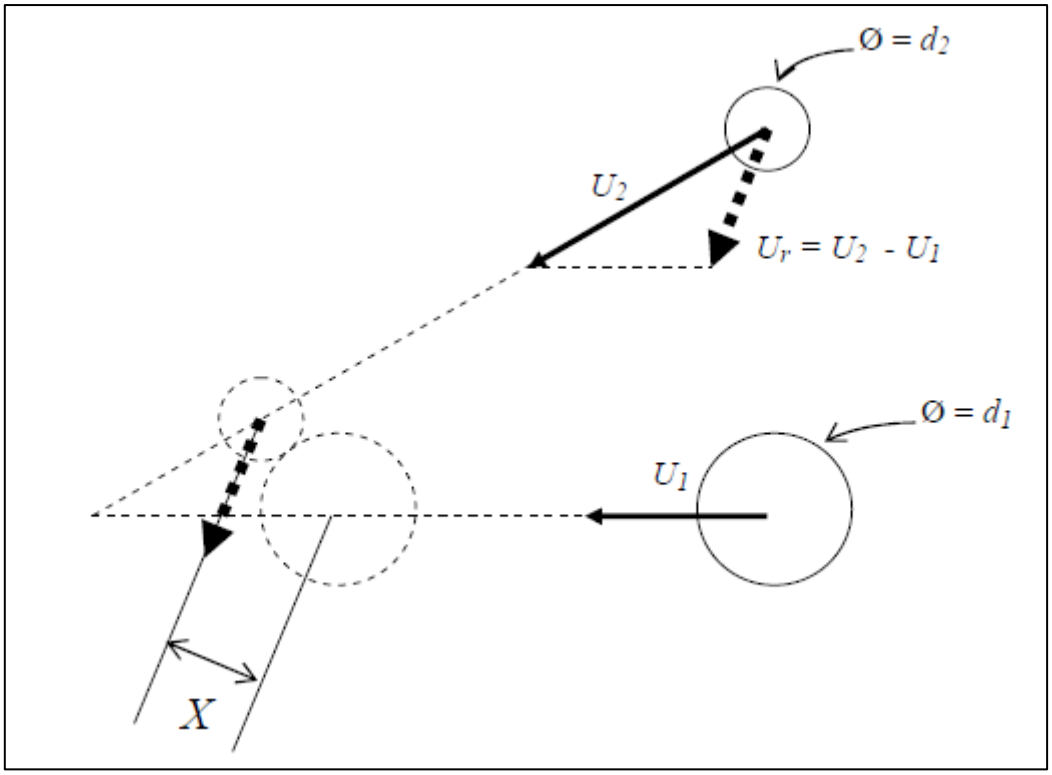

Figure 11: Figure representing the collision of droplets [Dhainaut, M. (2002).]

Weber number is the ratio of inertial force to surface tension force.

Hence,

$$\mathrm{We} = \frac{\rho d_s U^2}{\sigma} \tag{7}$$

where,

ρ = Density

U= relative velocity between two droplets

Diameter ratio is the ratio between small droplet diameters to large droplet diameter.

$$\Delta = \frac{d_s}{d_1} \tag{8}$$

d_1 and d_s are diameters of large and small droplets respectively.

Impact diameter is the ratio between two times the distance between the center of droplet 1 and the relative velocity vector on drop 2 center to the sum of large diameter to small diameter. It could be written as

$$x = \frac{2*X}{d_1+d_s} \tag{9}$$

Reynold's number is a dimensionless number in fluid mechanics that is used to predict fluid flow in different situations. Flow is said to be laminar at low Reynold's number while flow is said to be turbulent at high Reynold's number.

$$\mathrm{Re} = \frac{\rho d_1 \mathrm{U}_{rel}}{\mu} \tag{10}$$

Previous studies have shown that collision outcome is not dependent on one parameter but it depends on several parameters as a whole [Orme, M. (1997)] [Ashgriz, N., & Poo, J. Y. (1990)]. Figure 12 shows the outcome of collision as dependent on two parameters namely Weber number and diameter ratio. It could be observed from figure 12 that outcome of collision is coalescence for high droplet ratio and low Weber number.

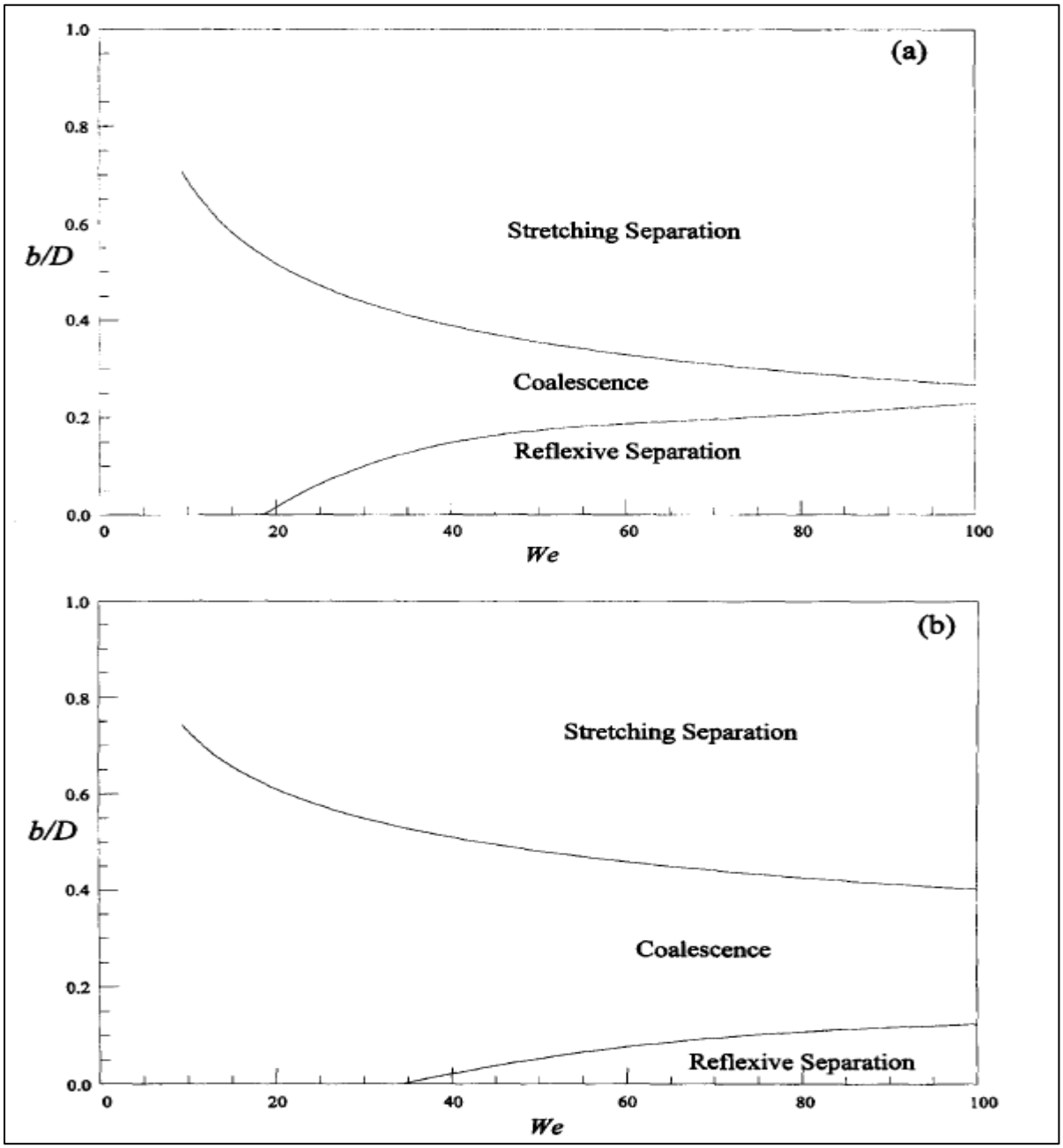

Figure 12: Outcome of collisions (a) when droplet size ratio is 1.0 (b) when droplet size ratio is 2.0[Orme, M. (1997)].

Figure 13 shows range of Weber number values and droplet ratio whether the coalescence will reach stable or unstable depending on the Weber number and the diameter ratio:

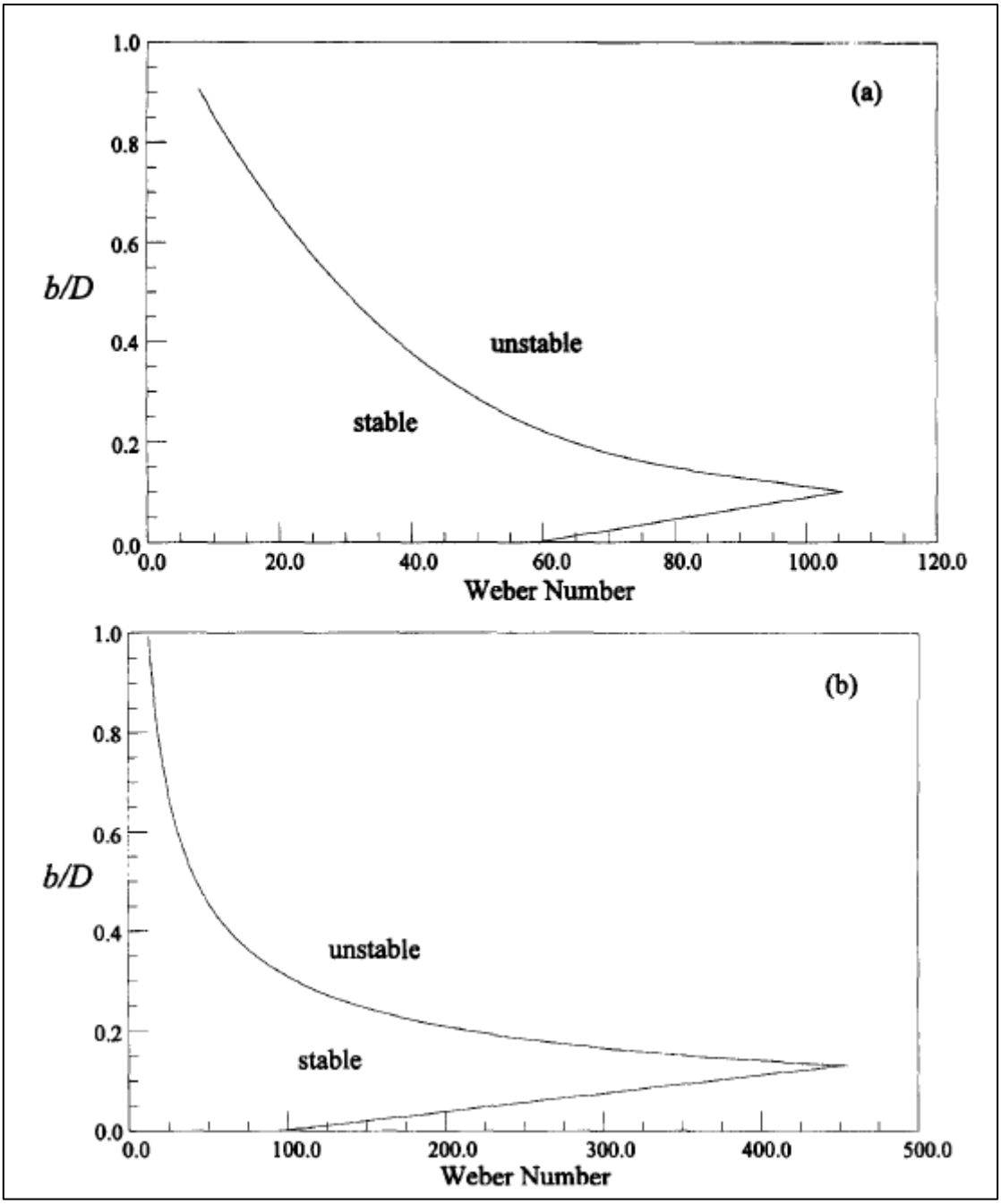

Figure 13: Collisions leading to stable or unstable coalescence when (a) droplet diameters are 120 µm and (b) droplet diameters are 600 µm [Orme, M. (1997)].

Besides the above four parameters coalescence outcome is also dependent on whether the collision happens head-on or off center. It is proved by researchers that head-on collisions lead to coalescence while oblique collisions lead to bouncing outcome. Park in his research on streams of water droplets proved that head-on collisions between pair of droplets will lead to stable coalescence. On the other hand off-center collisions between pair of droplets will lead to transient coalescence [Park, R. W. (1970).

Coalescence being one of the outcomes of collision, lot of researches is done over time to model and analyze coalescence mechanism of droplets. During coalescence, two droplets join to form one single droplet as shown in figure 14. Perhaps understanding the mechanism and mathematical models of coalescence is of superior interest for researchers because coalescence is seen in lot of multiphase flow applications like solvent extraction settler, kühni column, liquid-liquid extraction, agitated column. Droplet coalescence and breakup modeling is considered as the difficult point in polydispersed flow simulation [Lucas, D et al., 2007]. Even today, no satisfactory model that takes care of all coalescence mechanisms and mathematical models applicable to different conditions are available in the literature [Jakobsen et al.,2005]. The modeling is usually done on the basis of collision/ break-up frequencies, breakage daughter droplet size distribution and probabilities of breakage and coalescence [Liao, Y., & Lucas, D. (2010)]. In other words, large number of mathematical models have been formulated and documented in terms of collision frequency and coalescence efficiency for coalescence problem.

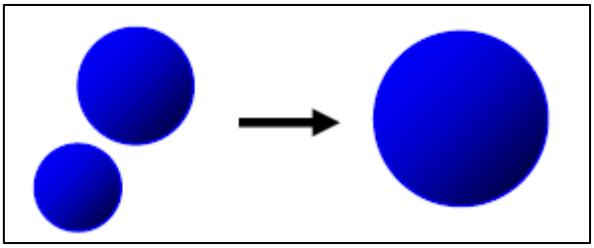

Figure14: Representation of coalescence (Espejo,2008)

Relative motion between two droplets causes collision [Liao, Y., & Lucas, D. (2010)]. When two droplets collide they interact for a certain time known as contact time. If the contact time is long enough for the film to drain called drainage time and reach critical thickness, coalescence occur [ANSYS 18.2 documentation]. The typical steps during coalescence is as shown in figure 15. Hence, it is clear that contact and drainage times also have high importance besides coalescence mechanism in studying coalescence. Ross (1971) assumed coalescence and contact time as random variables and computed coalescence efficiency by applying probability density function of a normal distribution. If λ is considered as the coalescence efficiency then it is given by the formulae:

$$\lambda(\mathrm{d}_1,\mathrm{d}_2) = \frac{1}{2}\exp\left(-\frac{\mathrm{t_{drainage}}}{\mathrm{t_{contact}}}\right) exp\left(\frac{1}{2}\frac{\sigma^2_{drainage}}{\sigma^2_{contact}}\right) * erfc\left(\frac{\sqrt{2}\,\sigma^2_{t_{drainage}} - t_{drainage}t_{contact}}{2t_{contact}\sigma_{t_{drainage}}}\right) \quad (11)$$

Coulaloglou, C.A (1975) simplified the above equation and modified as

$$\lambda(\mathrm{d}_1,\mathrm{d}_2) = \exp\left(-\frac{\mathrm{t_{drainage}}}{\mathrm{t_{contact}}}\right) \quad (12)$$

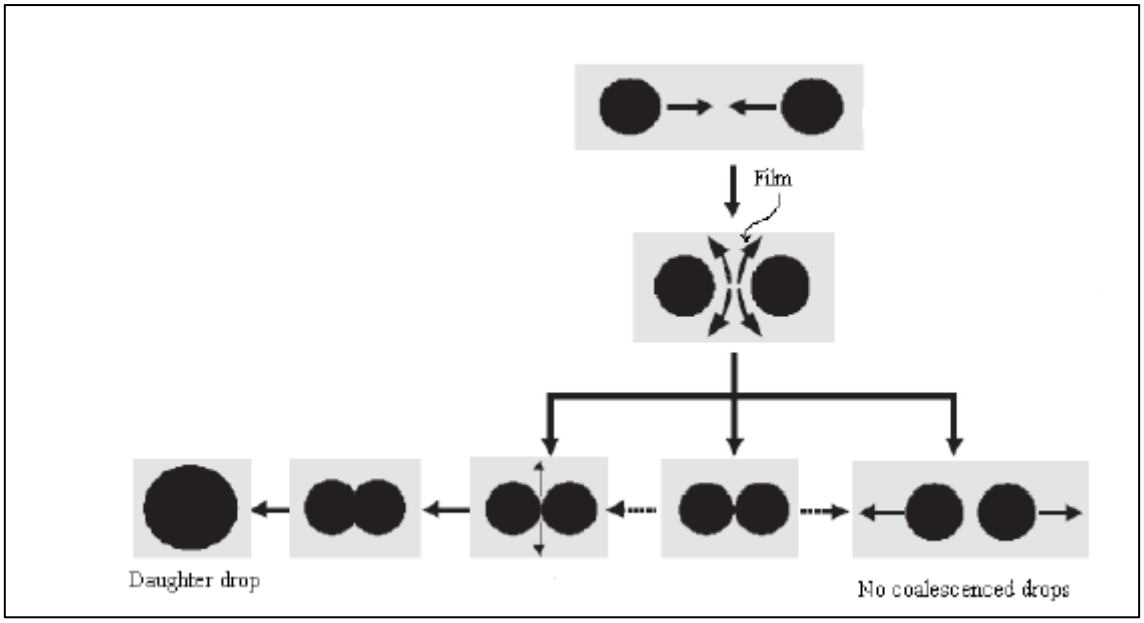

Figure 15: Steps in Coalescence (Schuchmann and Danner, 2004)

Relative motion between two droplets causes coalescence. In turbulent conditions, the mechanisms responsible for relative motion could be classified into five different types as below:

1. Relative motion due to turbulent fluctuations around the continuous phase as shown in figure 16.a.
2. Bubble/Droplet capture in turbulent eddy as shown in figure 16.b.
3. Relative motion because of mean velocity gradients in the flow as shown in figure 16.c.
4. Buoyant forces/Body forces as shown in figure 16.d.
5. Zigzag/helical trajectories also called as wake interactions. The mechanism is shown in figure 16.e.

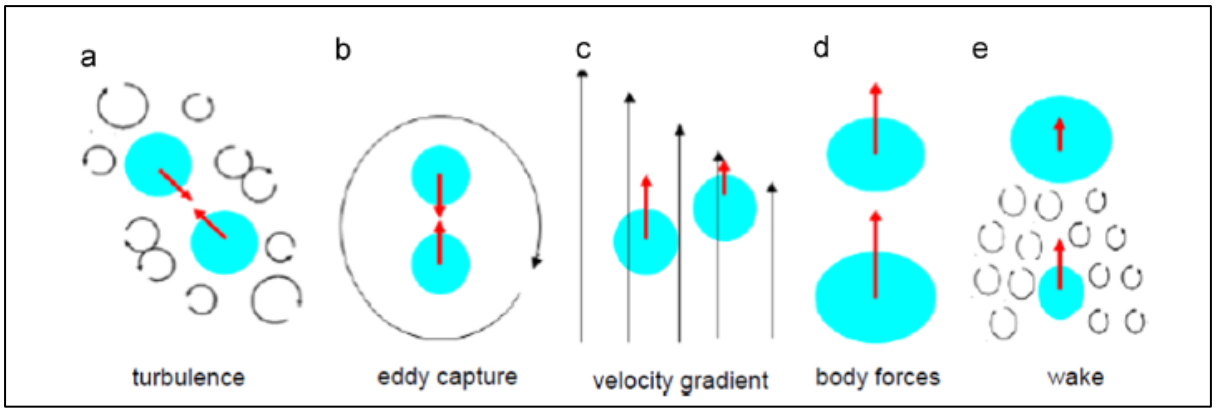

Figure 16: Various mechanisms leading to collision in turbulent flow [Liao, Y et al.2015].

Even though bubble and droplets are very much different from the perspective of chemical engineer but from the perspective of CFD there is not much difference. The mechanism by which bubble coalescence happens is very much similar to the coalescence mechanism of droplets. Also physical effects of droplet coalescence and the physical effects of bubble coalescence are comparable in nature [Liao, Y., & Lucas, D. (2010)]. In other words, the mathematical models describing the bubble coalescence is used for modeling the droplet coalescence as well. Hence the term droplet is used instead of bubble when explaining the mechanisms or mathematical models responsible for

coalescence. This should not be misunderstood with the experimental setup made to understand the coalescence phenomenon during chemical processes. Also this should not be misunderstood with the experimental results of bubble and droplets coalescence. From various literatures and theories, it could be concluded that parameters mainly influencing the coalescence process in polydispersed flow are as follows:

- Droplet diameter,
- External force,
- Physical Properties,
- Impurities,
- Collision frequency parameters and
- Coalescence Efficiency.

Droplet diameter: Droplet size has to be sufficiently large for coalescence to occur [Magiera, R., & Blass, E. (1997)]. After the threshold diameter, the coalescence rate increases at the interface when droplet diameter decreases. In other words, droplet diameter and coalescence rate are inversely proportional to each other. At the interface, the stability of coalescence decreases when droplet size is less. Coalescence happens in some kind of droplet size range [Liu, S., & Li, D. (1999)]. There is a minimum droplet diameter and maximum droplet diameter at which the coalescence is more likely to happen. The researchers observed different collision frequency and coalescence efficiency when different mechanism is used to model coalescence [Liao, Y., & Lucas, D. (2010)]. The variation for different mechanisms is according to figure 17 and figure 18.

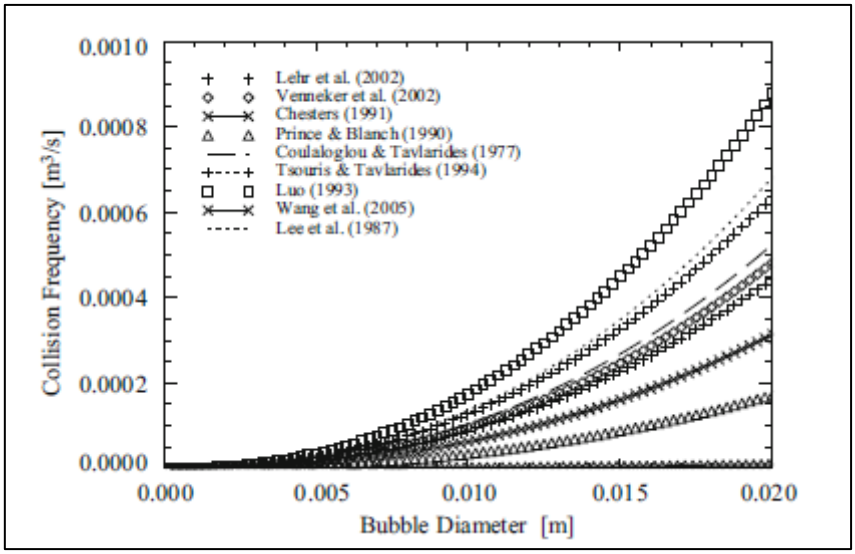

Figure 17: Figure showing the variation of collision frequency with respect to droplet diameter for various mathematical models [Liao, Y., & Lucas, D. (2010)].

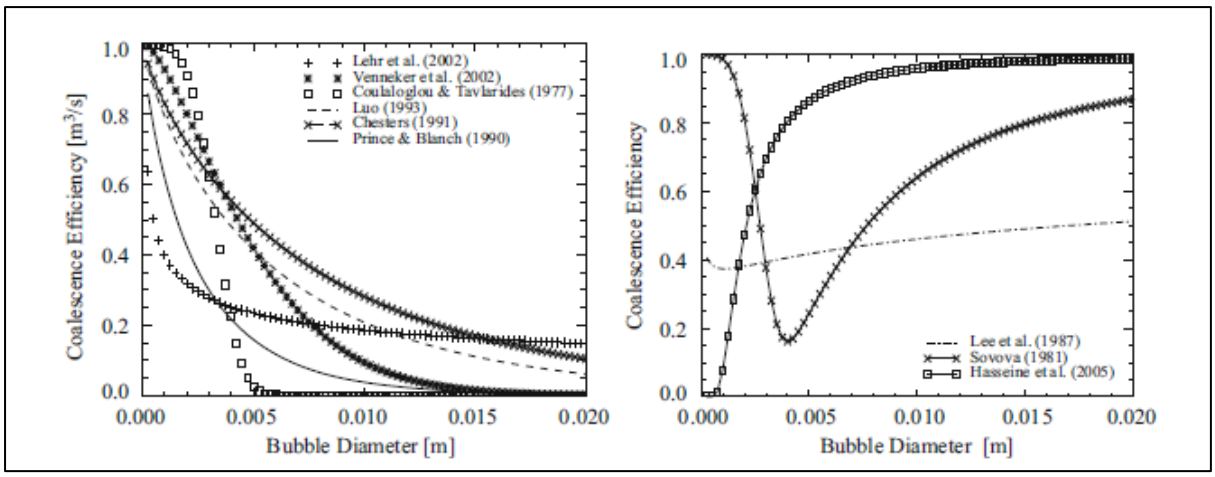

Figure 18: Figure showing the variation of coalescence Efficiency with respect to droplet diameter for various mathematical models [Liao, Y., & Lucas, D. (2010)].

External Force: The coalescence rate is higher when external force is high and droplets are little far from each other because collision events are often. But if the distance between two droplets is very small, droplets might deform and flatten. Hence, the contact surface area and film drainage time increases [Leng, D. E., & Calabrese, R. V. (2004)]. If droplets are oscillating during collision then coalescence rate decreases.

Physical Properties: Physical properties include viscosity and temperature. Temperature increases the coalescence rate [Charles, G. E., & Mason, S. G. (1960)]. Temperature also has a control on mobility of the interface. The coalescence rate is inversely proportional to viscosity of the continuous phase. In other words, coalescence rate increases when continuous phase viscosity decreases [Charles, G. E., & Mason, S. G. (1960)].

Impurities: Coalescence rate decreases when there are impurities in the injector [Charles, G. E., & Mason, S. G. (1960)]. It should be also noted that coalescence rate varies as per the wetting properties of solid impurities. Coalescence rate increases upon wetting.

2.4 Computational methods for coalescence modeling

Two authors named Liao, Y., & Lucas, D. (2010) has done an excellent literature review of mechanisms governing the coalescence process in different chemical process and categorized the coalescence models. Some of the mathematical models are written for a particular chemical process by correlating with the experimental data called empirical models while other mathematical models are written by calculating coalescence frequency as a product of coalescence efficiency and collision frequency called physical models [Liao, Y., & Lucas, D. (2010)]. In other words, mathematical models describe coalescence frequency as the product of coalescence Efficiency and collision Frequency. Figure 19 shows the excellent category done by the researchers explaining the coalescence mechanism.

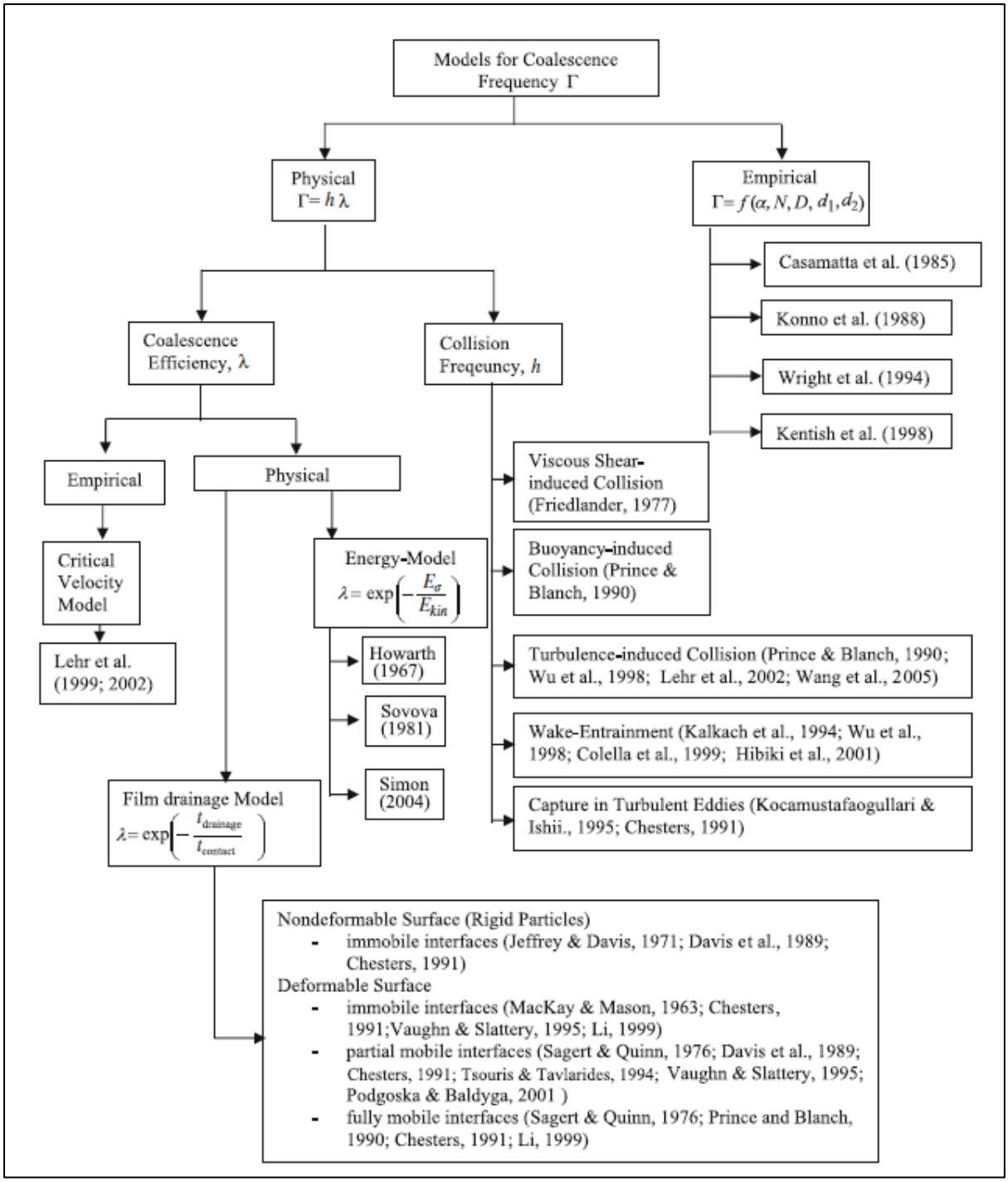

Figure 19: Different mechanisms for coalescence modeling categorized by Liao, Y., & Lucas, D. (2010)

Collision frequency formulae for some of the mathematical models could be written in the table 2. On the other hand, coalescence Efficiency could be written in the table 3.

Table 2: Collision frequency for different mathematical models

Mathematical Model	**Collision frequency** $h(d_1, d_2)$	**Constants**
Carrica et al.(1999)	$C_4' \left(\frac{\epsilon}{\gamma}\right)^{1/2} \left(\gamma_1^{\frac{1}{3}} + \gamma_2^{\frac{1}{3}}\right)^3$ (13)	

	It should be noted in the above equation that, $d_1 < l_e$ (14) also, $d_2 < l_e$	
Wang et al.(2005a,b)	$C_6' \gamma pi (d_1 + d_2)^2 \left(d_1^{2/3} + d_2^{2/3}\right)^{1/2} \varepsilon^{1/3}$..... .....(15)	$C_6' = 1.11$ $\gamma \; and \; pi$ are two modifications applied

Table 3: Coalescence Efficiency for different mathematical models

Mathematical Model	Coalescence Efficiency	Constants
Carrica et al.(1999)	$exp\left(-\frac{10^3\left(\frac{r_{eq}^3\rho_c}{16\sigma}\right)^{\frac{1}{2}} ln\left(\frac{h_i}{h_f}\right)\left(\lvert u_{real}\rvert (r_1+r_2)^{\frac{2}{3}} + 2(r_1+r_2)\epsilon^{\frac{1}{3}}\right)}{2(r_1+r_2)^{\frac{5}{3}}}\right)$ (16) $h_f = 10^{-7}$ $h_i = 10^{-4}$	
Wang et al.(2005a,b)	$P_{C,t} = exp\left(-\frac{\left(0.75(1+\epsilon_{12}^2)(1+\epsilon_{12}^3)\right)^{1/2}}{\rho_g / (\rho_t + C_{VM})(1+\epsilon_{12})^3} We_{12}^{1/2}\right)$ (17)	$\epsilon_{12} = \frac{d_1}{d_2}$

Finally, coalescence frequency is calculated as the product of collision frequency and coalescence Efficiency. Ansys Fluent 18.2 provides an option to build a coalescence rate kernel $Q(m_i; m_j)$.

The Q could be of two types:

- CEL expression or
- User Routine consisting of mass or diameter denoted by groups i and j by any fluid variables.

Ansys Fluent provides the built in mathematical models for modeling coalescence. The mathematical models provided by Fluent are volume of fluid method, Level set method, MUSIG model and discrete phase model (uses O'rourke method). In this master thesis, MUSIG model and discrete phase model are studied in detail. However, a brief overview is given and two previous studies are done with respect to VOF method.

2.4.1 Volume of Fluid Model

Volume of fluid model is used for modeling two or more immiscible fluids by solving a set of momentum equations [ANSYS 18.2 Documentation]. VOF tracks the volume fraction of each fluids through domain. The interface(s) tracking is done by solving continuity equation for volume fraction of one or more phases.

Previous studies

Mohammadi, M et al, (2011, May) solved continuity and momentum equations and simulated binary water droplets coalescence in a continuous phase of oil. Water oil interphase was tracked by solving continuity equation for volume fraction of one or more phases. The VOF method solves the added transport equation by defining a parameter called volume fraction α(X,t). Volume fraction α(X,t) notes the fraction of a computational cell filled with water. If α(X,t)=1 then the computational cell is completely filled with water. If α(X,t)=0 then water is absent in the computational cell. If the value is between zero and one then it is water oil interphase. The motion of interface is followed by solving transport equation.

The researchers compared the pattern of water droplets coalescence with the experimental data of Qian, J., & Law, C. K. (1997) and identified reasonable similarities. They carried out a parametric study and analyzed the effect of collision velocity, oil viscosity, interfacial tension and off-center collision on coalescence. Figure 20 shows the pattern of coalescence of water droplets in oil at different instant of time. The research results from their CFD analysis are as shown in table 4.

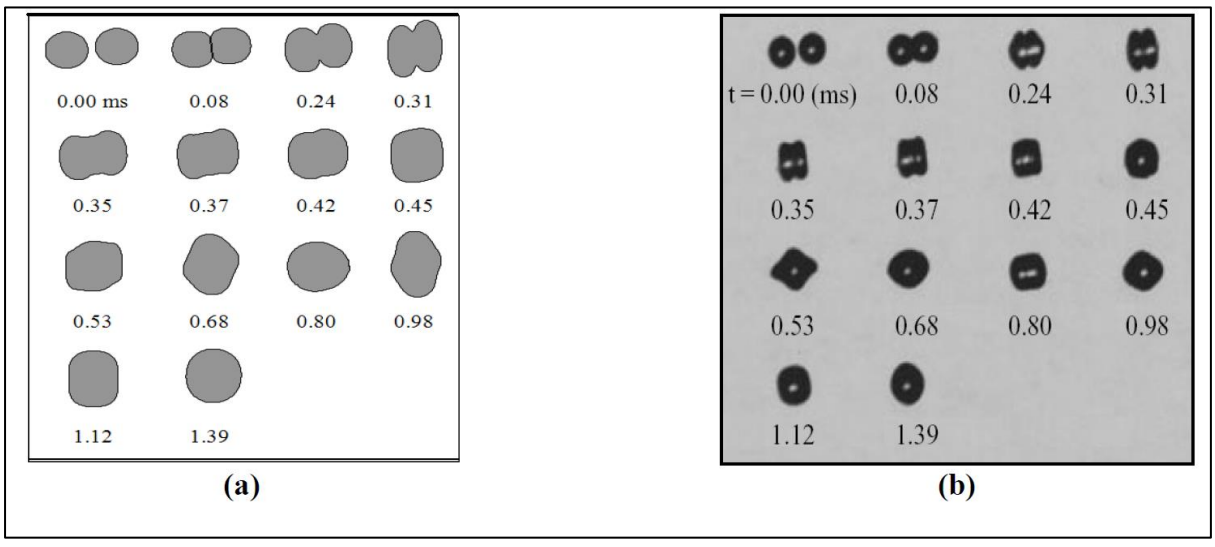

Figure 20: (a) Coalescence of water droplets in oil at different time scales, Mohammadi, M et.al (2011, May) compared with Qian, J., & Law, C. K. (1997) experimental results

Table 4: Effect of collision velocity, oil viscosity, interfacial tension and off-center collision on coalescence

Parameter	Results/Conclusions
Collision velocity	With increase in collision velocity Kinetic energy of droplets increases. With increase in Kinetic Energy rate of coalescence increases.
Water-oil interfacial tension	With increase in water-oil interfacial tension, surface force becomes higher. Due to this, the rate of coalescence increases.
Oil viscosity	High oil viscosity increases film-thinning force. With increase in oil viscosity rate of coalescence decreases.
Off-center parameter	With increase in off-center parameter rate of coalescence decreases.

Similar to Mohammadi, M Yuan et al, 2018 performed CFD analysis and tracked the droplet-droplet coalescence and breakup of water in oil. They compared their results with the experimental data of Qian, J., & Law, C. K. (1997) and identified reasonable similarities. The interphase was tracked by VOF method. Addition of collision time and shape recovery time is used for calculating coalescence time. The researchers noted that collision time decreases with the rise in relative velocity. Shape recovery time does not undergo any modification with higher relative velocity. Coalescence time reduces to minimal with the rise in relative velocity. When the droplet diameter is more, the coalescence time is also high. Droplet diameter and shape recovery time have a very complicated relation. For a droplet of smaller diameter, the shape recovery time in the coalescence time is increasing. The researchers noted that both relative velocity and absolute velocity are factors, which determine the coalescence process. According to researchers, the probability of coalescence is higher under two cases; firstly, when two droplets move towards each other with equal velocity, secondly when one droplet move towards a stagnant droplet. In addition, two droplets moving in the same direction is less likely to coalesce. Figures 21-25 are some of the results of their simulation:

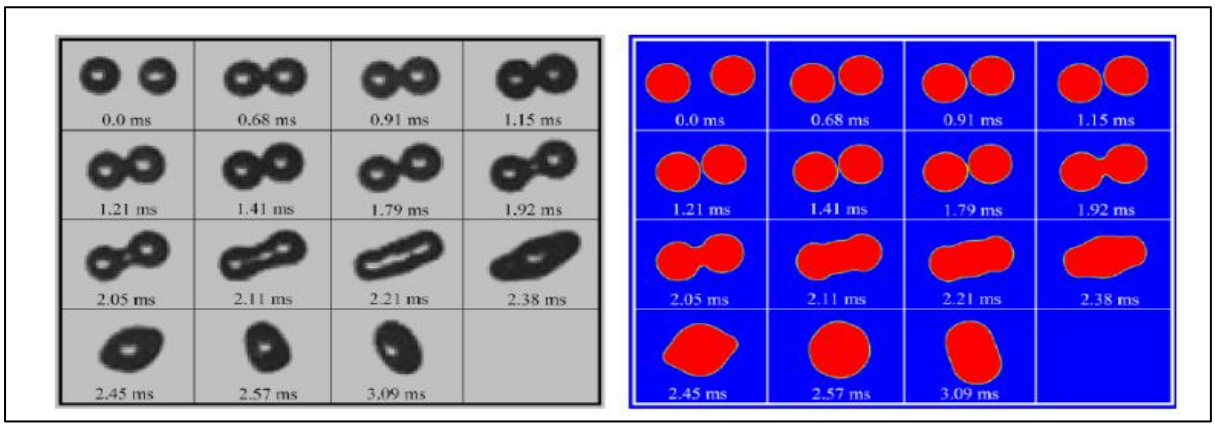

Qian and Law data from Experiments CFD simulation result

Figure 21: Comparison of CFD results obtained by researchers with Qian and Law data from experimental results, Yuan et al (2018)

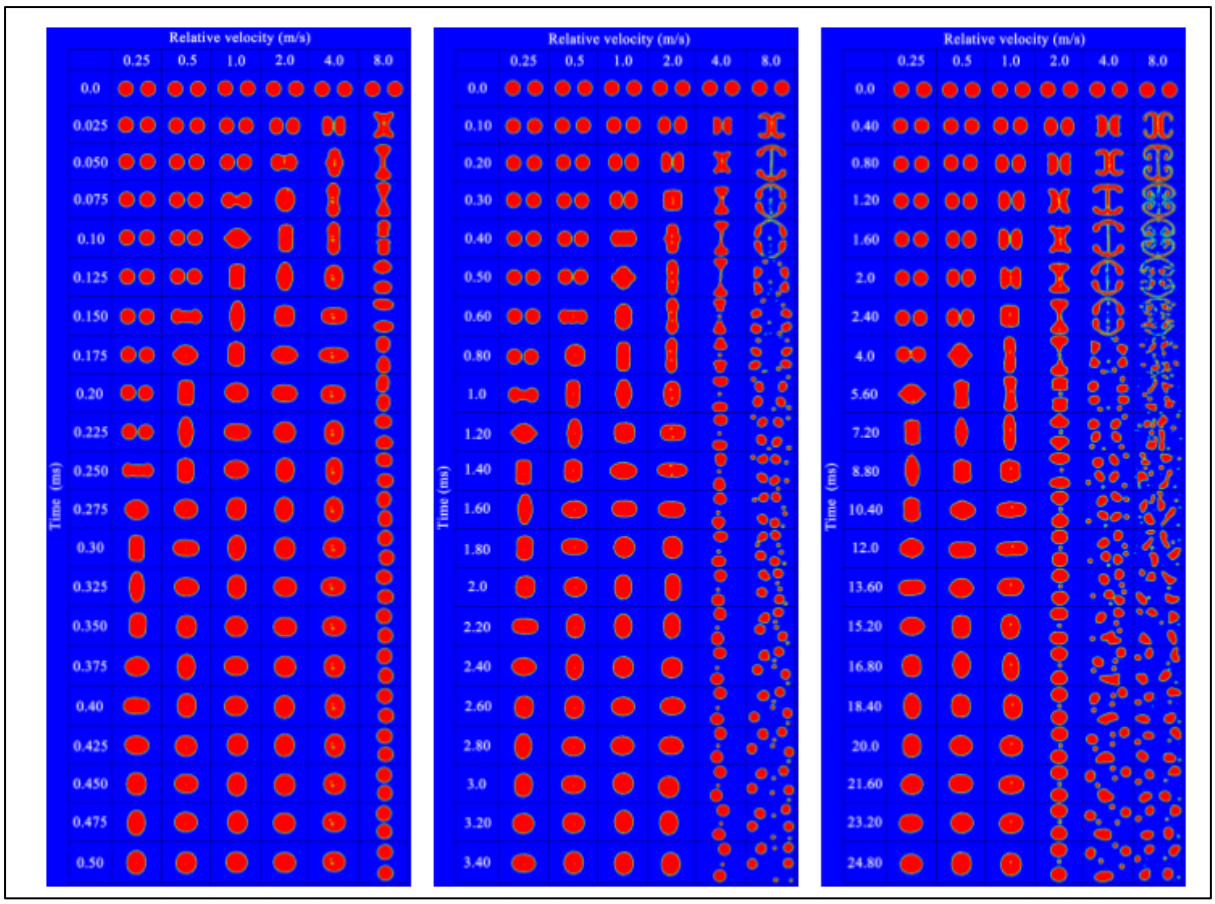

Figure 22: Coalescence happening at different time intervals for droplet sizes of diameter 50,200 and 800 µm, Yuan et al (2018)

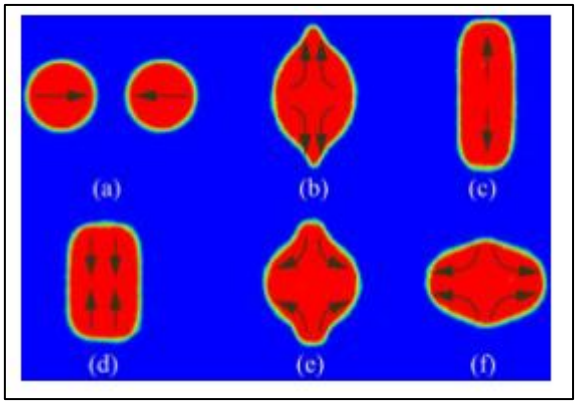

Figure 23: Droplet deformation after coalescence, Yuan et al (2018)

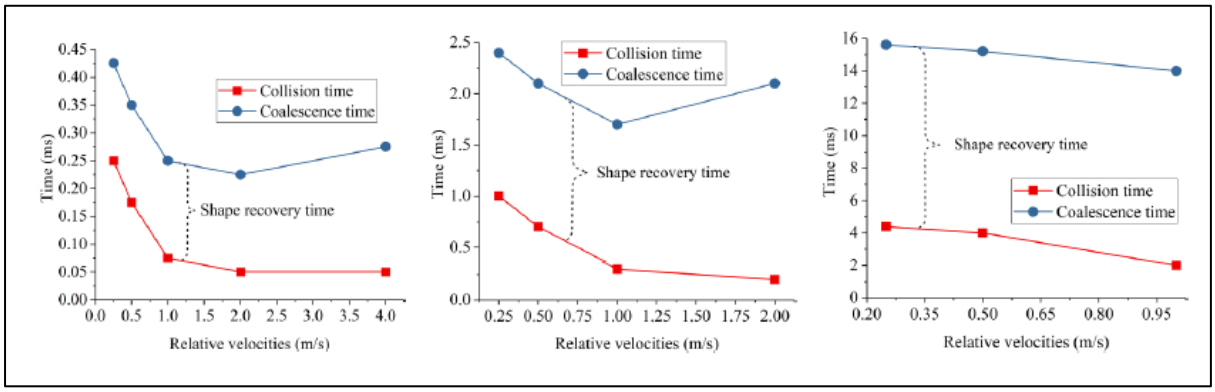

Figure 24: The change of relative velocities with respect to time for collision time and coalescence time, Yuan et al (2018)

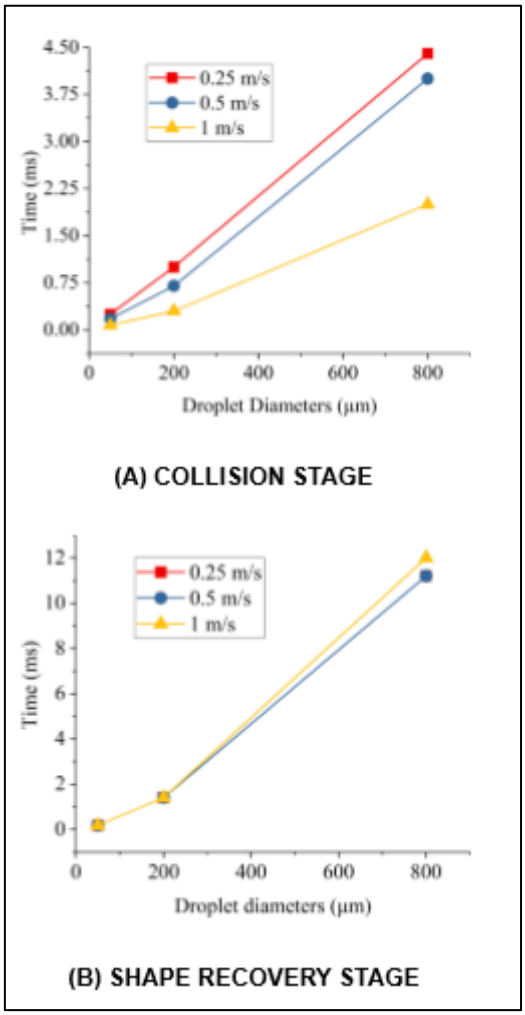

Figure 25: The variation of droplet diameters with respect to time at different velocities, Yuan et al (2018)

2.4.2 MUSIG model

The Musig stands for multiple size group models which is developed by Lo, S. in 1996. It is developed for modeling polydispersed multiphase flow. It should be noted that in polydispersed multiphase flows dispersed phase has big variation in size. Also, variant size particles interact with each other through the breakup and coalescence mechanisms in polydispersed multiphase flows. Musig model considers population balance model for modeling breakup and coalescence. Population balance model is mainly considered for three-dimensional CFD calculations and it calculates size distribution of polydispersed flows [Ramkrishna, D. (2000)]. Ansys Fluent 18.2 provides the built in model for coalescence and breakup modeling for Musig model.

One of the most famous and promising equation to model and describe the coalescence and breakage process in various chemical industries like solvent extraction settler, kühni column, agitated column is population balance equation [Kentish, S. E et al., 1998] [Konno, M., et al 1988] [Lucas, D et al., 2007]. The population balance model takes care of birth rate and death rate of droplets/bubbles due to coalescence and breakup [Ramkrishna, D. (2000)]. The population balance model could be written and explained as below [ANSYS 18.2 Documentaion]:

$S = B_b - D_B + B_C - D_C$ (18)

In the above equation,

B_b= Birth rate due to break-up

$B_b = \int_m^\infty g(\varepsilon; m) n(\varepsilon; t)$ (19)

B_C= Birth rate due to coalescence

$B_C = 1/2 \int_0^m Q(m-\varepsilon; \varepsilon) n(m-\varepsilon, t) n(m, t) d\varepsilon$ (20)

D_B= Death rate due to break-up

$D_B = n(m, t) \int_0^m g(m; \varepsilon) d\varepsilon$ (21)

D_C= Death rate due to coalescence

$D_C = n(m, t) \int_0^\infty Q(m; \varepsilon) n(\varepsilon; t) dt$ (22)

In the above equations,

$g(m; \varepsilon)$ defines the specific breakup rate,

$Q(m; \varepsilon)$ defines the specific coalescence rate.

Population balance model considers the Prince and Balsch model for coalescence modeling and Luo and Svendsen model for break-up modeling. Prince, M. J., & Blanch, H. W. (1990) formulated a theory that coalescence of two droplets occurs in the following three steps:

1. Firstly collision of droplets happen leading to trapping of little amount of liquid film in between them.
2. Secondly, drainage of liquid film takes place until liquid film separating the droplets reach a critical thickness.
3. Finally rupturing of the film is noticed leading to joining of droplets.

The steps are represented as in figure 26.

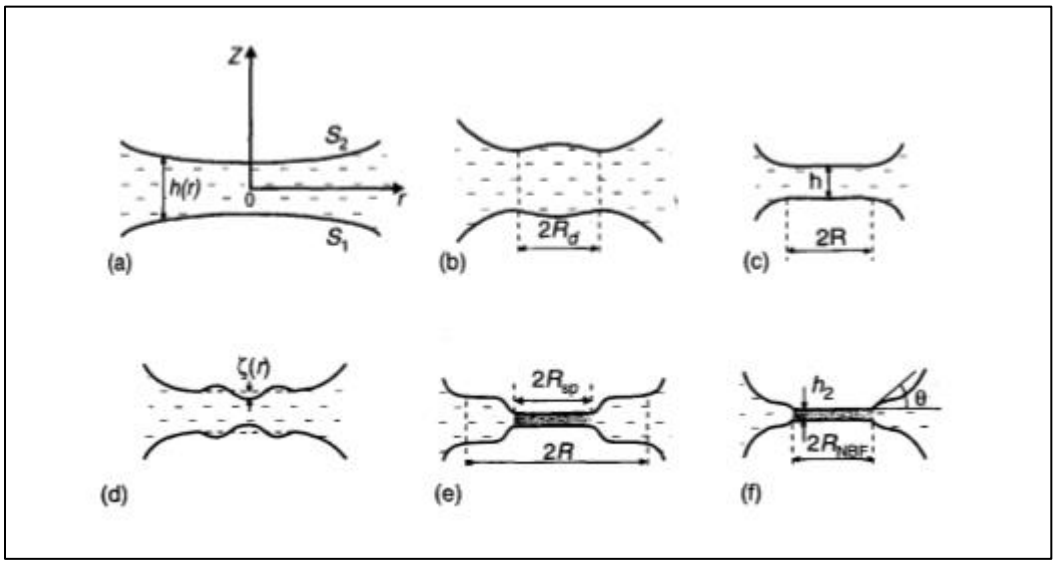

Figure 26: The steps involved in thin liquid film formation and evolution between two droplets [Kralchevsky et al(1997)]

Prince and Blanch model is applied for turbulent fluctuation collisions. It tries to model coalescence frequency as the product of collision efficiency and collision frequency.

If Q is considered as the collision rate of two bubbles, θ_{ij} as the collision frequency and η_{ij} as the collision efficiency then,

$$Q= \theta_{ij}\eta_{ij} \quad (23)$$

The prince and Blansch model give collision frequency as the sum of coalescence frequencies due to turbulence, Buoyancy and Source terms.

If θ_{ij} is considered as the collision frequency, then collision frequency could be given as the sum of collision frequency due to turbulence (θ_{ij}^{T}), Buoyancy (θ_{ij}^{B})and source terms (θ_{ij}^{S}).

Hence the final formulae for collision frequency could be written as below.

$$(\theta_{ij}) = \theta_{ij}^{T} + \theta_{ij}^{B} + \theta_{ij}^{S} \quad (24)$$

The collision frequency due to turbulence could be written as below:

$$\theta_{ij}^{T} = F_{CT} S_{ij} (u_{ti}^2 + u_{tj}^2)^{1/2} \quad (25)$$

In the above equation, S_{ij} represents the area of cross section of the colliding particles,

$$S_{ij} = \frac{pi}{4}(d_i + d_j)^2 \quad (26)$$

Similarly, turbulent velocity is given by the equation,

$$u_{ti} = \sqrt{2}\, \epsilon^{1/3}\, d^{1/3} \quad (27)$$

Collision frequency due to Buoyancy is given by the equation,

$$\theta_{\mathrm{ij}}^{\mathrm{B}} = F_{CB} S_{ij} |U_{rj} - U_{ri}| \quad (28)$$

In the above equation F_{CB} is a calibration factor,

and

$$U_{ri} = \sqrt{\frac{2.14\sigma}{\rho_c d_i} + 0.505 g d_i} \quad (29)$$

If η_{ij} is considered as the collision efficiency, Prince and Blanch model uses time required for coalescence t_{ij} and actual contact time τ_{ij} to model collision efficiency.

The collision efficiency could be formulated by Prince and Blanch model as below:

$$\eta_{ij} = e^{t_{ij}/\tau_{ij}} \quad (30)$$

$$t_{ij} = (\rho_c r_{ij}^3 / 16\sigma)^{1/2} \ln(h_0 / h_f) \quad (31)$$

In the above equation it should be noted that h_0 refers to initial thickness, h_f refers to critical film thickness during rupture and r_{ij} is the equivalent radius which could be calculated by the below formulae

$$r_{ij} = \left(\frac{1}{2}\left(\frac{1}{r_i} + \frac{1}{r_j}\right)\right)^{-1} \quad (32)$$

The actual contact time during collision could be calculated by the below formulae:

$$\tau = \frac{r_{ij}^{2/3}}{\varepsilon_c^{1/3}} \quad (33)$$

2.4.3 Discrete phase model and O'Rourke's method

Discrete phase modeling abbreviated as DPM calculates the trajectory of discrete phase droplets by Lagrangian formulation. It contains the inertia of discrete phase, hydrodynamic drag, force of gravity, steady and unsteady state flows. On the other hand, it uses Eulerian frame gas phase for calculating the exchange of heat, mass and momentum. It also predicts the turbulence effect on the dispersed particles because of turbulent eddies in continuous phase. The limitation of Discrete phase modeling is that volume fraction of the dispersed phase should be less than 10%. It models turbulent dispersion by stochastic tracking and particle cloud model. Ansys Fluent 18.2 provides the built in model for coalescence modeling for discrete phase model.

The outcome of collision is according to O'Rourke's algorithm. P. J. O'Rourke in his PhD thesis postulated an algorithm called O'Rourke algorithm, which decreases the computational cost during spray droplet collision [P. J. O'Rourke (1981)]. The algorithm assumes that collision of two parcels happens only if they are located in the same continuous phase cell. The theories mentioned in the previous sections do not completely hold well with the O'Rourke algorithm. The reason is Roorke's algorithm takes account of only Weber number as the parameter determining the outcome of collision. It should be also noted that only coalescence and bouncing are considered as the outcome of collision forgetting reflexive separation and stretching. The algorithm being widely applicable for

low Weber number collisions that is below 100 [P. J. O'Rourke (1981)]. For N droplets in the control Volume, every droplet has N-1 probable collision outcome [ANSYS 18.2 Documentation]. Hence, it could be considered that

Number of collision pairs= $\frac{1}{2}$ N^2 (34)

The factor $\frac{1}{2}$ is used because if droplet 1 collides with another droplet 2 then droplet 2 colliding with droplet 1 is considered similar. This symmetry makes the number of collisions to half [ANSYS 18.2 Documentation]. It should be noted here that in every time steps collision algorithm calculates $\frac{1}{2}$ N^2 probable collision events.

The algorithm uses conservation of mass, conservation of momentum and energy to model post-characteristics of droplets after collisions. O'Rourke classified the droplets based on their size. If there are two droplets of different diameters then droplet 1 has a diameter lower than the diameter of droplet 2. Droplet with bigger diameter is called collector droplet. Probability of collision is calculated with respect to frame of reference of collector droplet. Hence O'Rourke's algorithm considers velocity of collector droplet to be zero. In the algorithm, the relative distance between smaller and larger droplet diameter is important.

The probability of bigger droplet colliding with the smaller droplet is given by the formulae:

$$P_1 = \frac{Pi(r_1+r_2)^2 V_{rel}\Delta t}{V} \quad (35)$$

r_1 and r_2 are radius of bigger and smaller droplets respectively.

The mean expected number of collisions is:

$$\bar{n} = \frac{n_2 pi(r_1+r_2)^2 v_{rel}\Delta t}{V} \quad (36)$$

If n is the number of collisions between bigger droplets and the other droplets, the probability distribution is as per the Poisson distribution which is given by the formulae:

$$P(n) = e^{-n\frac{n^n}{n!}} \quad (37)$$

After collision, the droplets might experience coalescence, bouncing, shattering and reflexive separation as mentioned in the previous chapter 4.1. However, the O'Roorke algorithm models only coalescence and bouncing as the outcome of collision. According to O'Roorke algorithm collision leads to coalescence if it is head-on collision or if it is oblique collision it leads to bouncing. The coalescence probability is related to offset of collector droplet center and small droplet trajectory. The critical offset is given by:

$$b_{crit} = (r_1 + r_2)\sqrt{min\left(1.0, \frac{2.4f}{We}\right)} \quad (38)$$

It should be noted here that f is a function of $\frac{r_1}{r_2}$

Where in r_1 and r_2 are radius of droplet 1 and droplet 2 respectively.

$$f\left(\frac{r_1}{r_2}\right) = \left(\frac{r_1}{r_2}\right)^3 - \left(\frac{r_1}{r_2}\right)^2 + 2.7\left(\frac{r_1}{r_2}\right) \quad (39)$$

If Y is considered as a random number between 0 to 1, the actual collision parameter is given by the formulae,

$b = (r_1 + r_2)\sqrt{Y}$ (40)

If $b < b_{crit}$, the outcome is coalescence or else the outcome is bouncing.

DPM integrates particle force balance equation for calculating the particle trajectory by using Lagrangian frame of reference. The particle force balance equation could be written as below:

$\frac{du_i^p}{dt}$ = drag force + Gravity force+ extra forces (41)

It could be noted here that,

Drag force=$F_D(u_i - u_i^p)$ (42)

Gravity force= $\frac{g_i(\rho_p - \rho)}{\rho_g}$ (43)

Extra forces = F_i (44)

Extra forces may be due to varied reasons like pressure gradient, thermophoretic, rotating reference frame, brownian motion and saffman lift which will be discussed in the succeeding sections.

It should be noted in the above equations that

$F_D = \frac{18\mu C_D Re_{rel}}{\rho_p d_p^2 24}$ (45)

Here,

Re_{rel} is the relative Reynold's number which could be written by the below formulae:

$Re_{rel} = \frac{\rho_p d_p |u_i^p - u_i|}{\mu}$ (46)

C_D is the drag coefficient. There are number of laws for calculating C_D like spherical drag law, non-spherical drag law, Stokes-Cunningham law, high-mach-number drag law, dynamic drag model theory, dense discrete phase model drag laws, bubbly flow drag laws, rotational drag law [ANSYS fluent 18.2 Documentation].The drag coefficient formulae for different drag law is written in table 5.

Table 5: Table showing the drag coefficient formulae for different drag laws.

Laws	Drag coefficient C_D	Constants
Spherical Drag Law [S. A. Morsi and A. J. Alexander]	$a_1 + \frac{a_2}{Re} + \frac{a_3}{Re^2}$ (47)	
Non-Spherical Drag law [A. Haider and O. Levenspiel]	$\frac{24}{Re_{rel}}(1 + b_1 Re_{sph}^{b_2}) + \frac{b_3 Re_{rel}}{b_4 + Re_{rel}}$ (48)	$b_1 = \exp(2.3288 - 6.4581\varphi + 2.4486\varphi^2)$ (49) $b_2 = 0.964 + 0.5565\varphi$ (50) $b_3 = \exp(4.905 - 13.8944\varphi + 18.4222\varphi^2 - 10.2599\varphi^3)$ (51) $b_4 = \exp(1.4681 + 12.2584\varphi - 20.7322\varphi^2 + 15.8855\varphi^3)$ (52)

		φ is the shape factor If you consider s as the surface area of the sphere, S is the actual surface area of the sphere $\varphi = \frac{s}{S}$ (53)
Rotational Drag Law [S. C. R. Dennis et al,.]	$\frac{6.45}{\sqrt{Re_\omega}} + \frac{32.1}{Re_\omega}$ (54)	$Re_\omega = \frac{\rho_f \lvert\Omega\rvert d_p^2}{4\mu_f}$ (55)
Stokes-Cunningham Drag Law[H. Ounis et al,.]	This law calculates F_D directly instead of C_D. The formulae for F_D could be given as $F_D = \frac{18\mu}{d_p^2 \rho_p C_c}$ (56)	$C_c = 1 + \frac{2\lambda}{d_p}(1.257 + 0.4e^{-(\frac{1.1 d_p}{2\lambda})}$ (57) It should be noted in the above equation that, $\lambda =$ Molecular mean free path.
High-Mach Number Drag Law[Clift, Grace, and Weber]	$a_1 + \frac{a_2}{Re} + \frac{a_3}{Re^2}$ (58) Mach number should be greater than 0.4 and Reynolds number should be greater than 20	
Dynamic Drag model theory [A. B. Liu et al,.]	$C_{d,sphere}$(1+2.632y) (59)	$C_{d,sphere} = 0.424$ if $Re > 1000$ (60) $C_{d,sphere} = \frac{24}{Re}\left(1 + \frac{Re^{\frac{2}{3}}}{6}\right)$ (61) if Re≤1000 (62) y is a droplet distortion determined by the double integral equation

It should be noted in the Particle force balance equation that there is a term called extra forces. The extra forces are added under special circumstances. The extra forces may be due to reference frame rotation, virtual mass force, brownian force, temperature gradient, lift caused by shear, rotational lift [Ansy Fluent 18.2 documentation]. Extra force formulae is written in table 6.

Table 6: Table showing the extra force formulae

Extra force reason	Theory	Formulae
		F_i
virtual mass force	Virtual mass force accelerate the fluid surrounding the particle.	if $\rho_p > \rho$ $\frac{1\rho}{2\rho_p}\frac{d}{dt}(u_i - u_i^p)$ else, $F_i = \left(\frac{\rho}{\rho_p}\right) u_p \frac{\partial u}{\partial x}$ (63)

temperature gradient	Force experienced by temperature gradient is called thermophoresis. Small particles of gas having temperature gradient possess an opposite force to the temperature gradient.	$\mathrm{F}_i = -D_{T,p}\frac{1}{m_p T}\frac{\partial T}{\partial x}$ (64) $D_{T,p}$ is the thermophoretic coefficient
Lift caused by shear	The additional term may include the lift caused by shear force	$\frac{2\mathrm{K}\gamma^{1/2}\rho d_{ij}}{\rho_p d_p (d_{ik}d_{kl})^{1/4}}((u_\mathrm{i} - \mathrm{u}_\mathrm{i}^\mathrm{p})$ (65)

The Particle force balance equation is integrated to calculate the velocity of the particle along a trajectory at each point. The velocity equation of the particle is given by:

$$\frac{dX}{dt} = u_i^p \quad (66)$$

After solving particle force balance equation and the above equation in each coordinate direction, the equation takes the form,

$$\frac{du_i^p}{dt} = \frac{1}{\tau_p}(u_\mathrm{i} - \mathrm{u}_\mathrm{i}^\mathrm{p}) \quad (67)$$

In the above equation,

τ_p refers to particle relaxation time.

Ansys fluent adapts trapezoidal scheme and integrates the above equation and the equation becomes:

$$\frac{u_p^{n+1} - u_p^n}{\Delta t} = \frac{1}{\tau}\left(u^* - u_p^{n+1}\right) + \cdots \quad (68)$$

In the above equation n gives the iteration number

$$u^* = \frac{1}{2}(u^n + u^{n+1}) \quad (69)$$

$$u^{n+1} = u^n + \Delta t u_p^n . \nabla u^n \quad (70)$$

The equations $\frac{dX}{dt} = u_i^p$ and $\frac{du_i^p}{dt} = \frac{1}{\tau_p}(u_\mathrm{i} - \mathrm{u}_\mathrm{i}^\mathrm{p})$ are solved to obtain particle's velocity and position at any instant of time.

Besides particle tracking DPM also calculates heat and mass exchange, physical property averaging, wall-jet model, wall film model, etc.

Previous study

In the past DPM was used to study settling of matte droplets through slag by Xia, J. L. et.al (2004). The researchers' numerically modeled three-dimensional magneto-hydrodynamic flow and simulated nickel droplet trajectories in an electric furnace smelting. The publication was limited to study settling

of Nickel droplets and coalescence was not studied. However, the authors suggested that droplet coagulation to form bigger droplets would influence the settling.

They simulated slag flow and nickel droplet settling behavior by varying the droplet size and initial droplet location systematically. They introduced droplet-settling ratio for better understanding the droplet settling behavior. The characteristic curve of droplet diameter versus settling ratio is plotted. They observed complex three-dimensional slag flow. Some of the findings from their simulation are as follows

- The droplet coagulation to form bigger droplets should play an important role in the behavior of droplet settling.
- The droplet turbulent dispersion affects the droplet trajectory significantly and it is taken into account during simulation.
- Steps taken to improve the coagulation process will enhance the settling of droplets as well.
- Majority of the droplets settle in the central region of the furnace.
- The droplet settling ratio is directly proportional to the droplet diameter. In other words as droplet diameter increases settling ratio also increases as shown in figure 29.
- A droplet whose diameter is less than 50 μm makes movement with the slag or suspend in the slag.
- The residence time of small droplets could be long.

Below are the figures from their simulation results showing the droplet trajectories during various trials

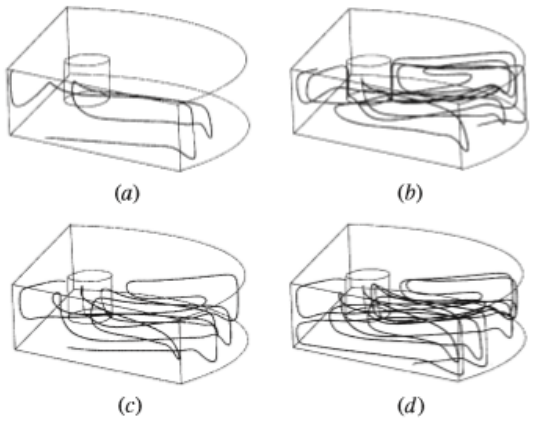

Fig. 6—Examples of the droplet trajectories starting at four different initial positions. $d_p = 500$ μm, turbulent particle dispersion excluded. Initial droplet positions: $z = 1.16$ m, $\theta = 0$ deg with (*a*) $r = 0.106$ m, (*b*) $r = 0.488$ m, (*c*) $r = 0.974$ m, and (*d*) $r = 1.03$ m.

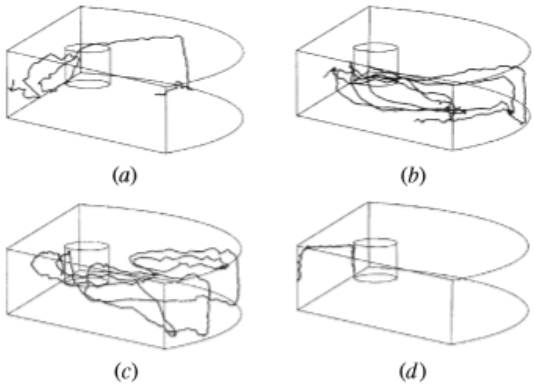

Fig. 8—Examples of the droplet trajectories starting at four different initial positions. $d_p = 500$ μm, turbulent particle dispersion included. Initial droplet positions: $z = 0.687$ m, $\theta = 0$ deg with (*a*) $r = 0.106$ m, (*b*) $r = 0.488$ m, (*c*) $r = 0.974$ m, and (*d*) $r = 1.03$ m.

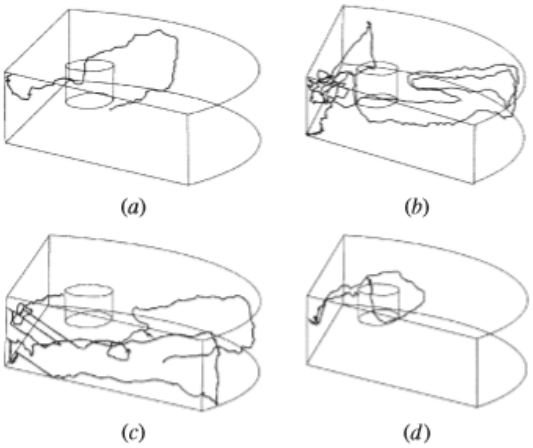

Fig. 7—Examples of the droplet trajectories starting at four different initial positions. $d_p = 500$ μm, turbulent particle dispersion included. Initial droplet positions: $z = 1.16$ m, $\theta = 0$ deg with (*a*) $r = 0.106$ m, (*b*) $r = 0.488$ m, (*c*) $r = 0.974$ m, and (*d*) $r = 1.03$ m.

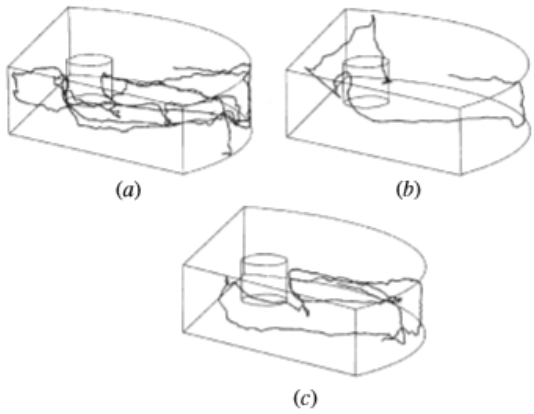

Fig. 9—Examples of the droplet trajectories starting at three different initial positions. $d_p = 500$ μm, turbulent particle dispersion included. The initial droplet positions: $z = 1.16$ m, $r = 2.85$ m with (*a*) $\theta = 16.6$ deg, (*b*) $\theta = 25.55$ deg, and (*c*) $\theta = 36.9$ deg.

Figure 27: Figures showing the droplet trajectories at different positions [Xia, J. L. et.al (2004)]

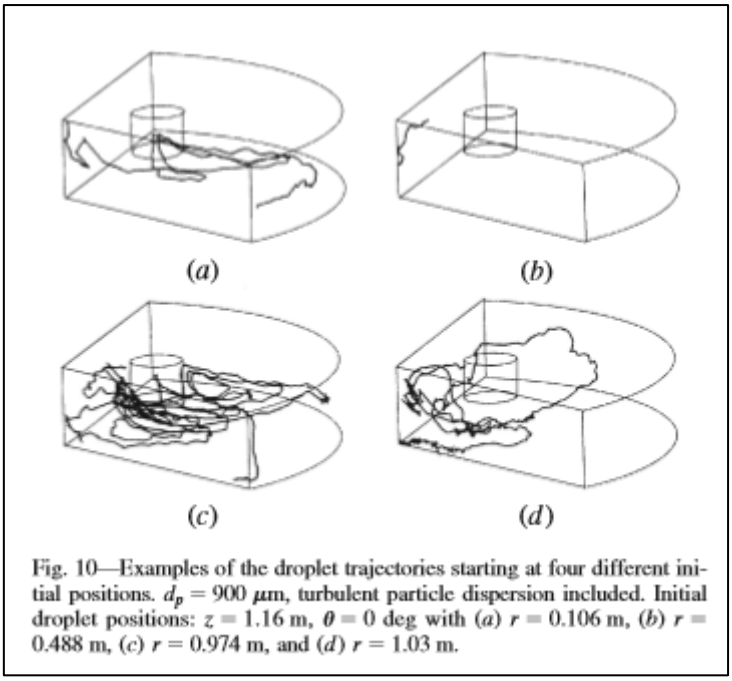

Fig. 10—Examples of the droplet trajectories starting at four different initial positions. $d_p = 900$ μm, turbulent particle dispersion included. Initial droplet positions: $z = 1.16$ m, $\theta = 0$ deg with (*a*) $r = 0.106$ m, (*b*) $r = 0.488$ m, (*c*) $r = 0.974$ m, and (*d*) $r = 1.03$ m.

Figure 28: Figure showing the droplet trajectories at different positions [Xia, J. L. et.al (2004)]

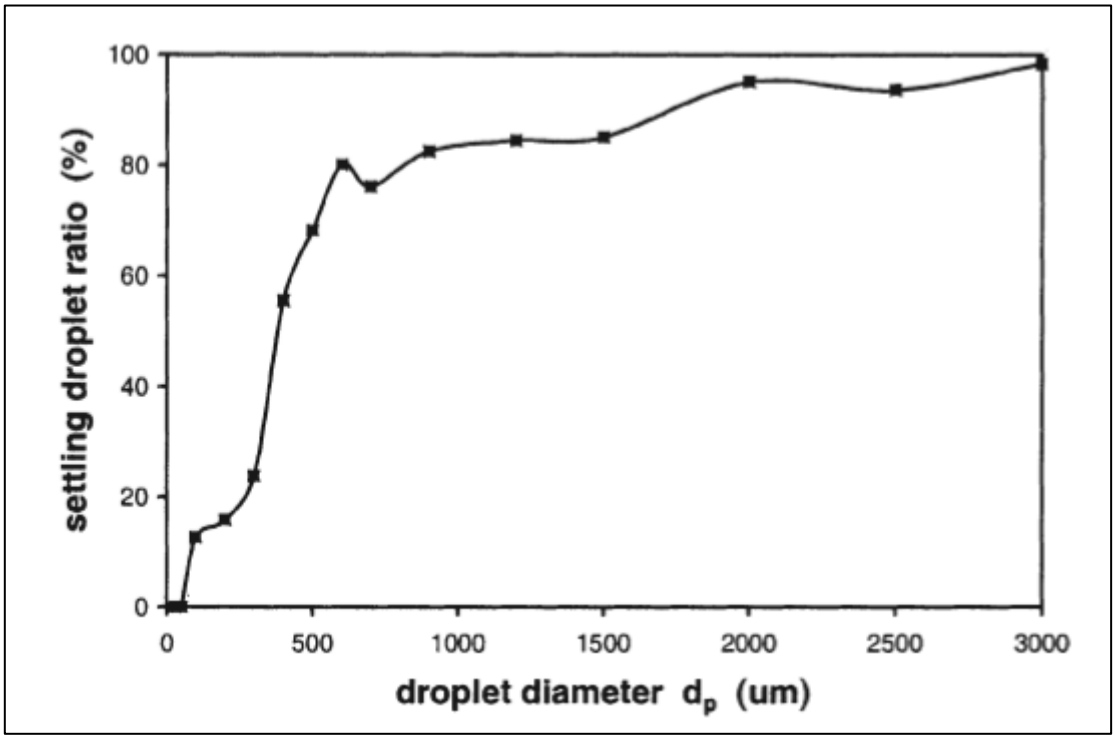

Figure 29: variation of droplet settling ratio with droplet diameter [Xia, J. L. et.al (2004)]

2.5 Comparison of computational methods

MUSIG model and DPM are studied in detail in this master thesis. User defined models are not included. A brief comparison between Musig Model and DPM is given in table 7.

Table 7: Comparison between Musig Model and discrete phase model

Attributes	Musig Model	Discrete Phase model
Size distribution	MUSIG model breaks the droplet coalescence phenomenon into various size classes based on the process. It considers minimum and maximum size distribution. Simulation case is setup based on the process.	Different diameter size distribution could be provided in DPM as well. However, Musig model gives higher possibilities to include size distributions. It has an upper hand here due to higher definition possibilities and user-friendly options based on the process requirements.
Familiarity	MUSIG is a proven method for coalescence modeling. Lot of researchers implemented MUSIG method for modeling the phenomenon. Hence adaptation of Musig to Flash smelting is quite easy.	DPM is popular to model settling, identify droplet trajectory. However, sparse literature is available to model coalescence with DPM technique. Hence combining O'rourke algorithm with DPM is quite challenging. The pain of parametrizing exist.
Post processing visualization	Musig model does allow particle-tracking visualization. However, particle trajectory cannot individually be tracked here.	DPM integrates particle force balance equation to track the droplet trajectory. Hence, trajectory of individual droplets could be visualized in post processing animation. The tracking of individual droplet trajectory helps to study copper losses with better visualization.
Transport Equations	New transport equations should be implemented in MUSIG model.	Adding transport equations is quite easy here.
Computation time	Musig model takes more computation time due to different size classes.	DPM takes less computation time due to parcel injection technique.

It is evident from table 7; both MUSIG model and DPM are good choices in their own respects. DPM is checked for feasibility in this thesis. Since sparse literature is available to model coalescence by DPM technique, the parametrization might yield some unknown benefits/disadvantages. If parametrized DPM gives good results, it will be taken for the next stage of the project. If it does not fulfill the requirements, modifications/alternative model will be proposed.

3 Computational setup

In the computational part, matte droplets coalescence inside the settler is studied by using CFD simulation. The commercial software used is Ansys Fluent 18.2. DPM model was combined with O'Rourke algorithm for modeling coalescence. The target was to parametrize the model and check its viability. In this parameterization, chemical reactions and user-defined models are excluded.

3.1 Calculation domain and discretization

The computational domain was created in the design modeler. Modeling full-scale settler is computationally intensive and analysis is quite difficult with big settler and tiny matte droplets. Moreover, maximum coalescence occur underneath the reaction shaft; therefore, it is better to focus around the reaction shaft instead of the complete flash smelting settler. Hence, the length of the settler was shortened from 18 m to 8 m to reduce computation demand. The dimensions of the settler are presented in the Table 8. Geometry modeled is as shown in figure 30 and 31.

Table 8: Table showing the dimensions of the settler

Settler Geometry									
Length	Width	Height from wall end	Height from center end	Slag tap hole (m)		Matte tap hole (m)		slag/matte inlet (m)	
(m)	(m)	(m)	(m)	Radius	coordinates(m)	Radius	coordinates	Radius	coordinates
8	6	0.70	0.87	0.045	0.5,0.5, 8	0.045	0.5,-0.1, 0	2.25	0,0,3.75

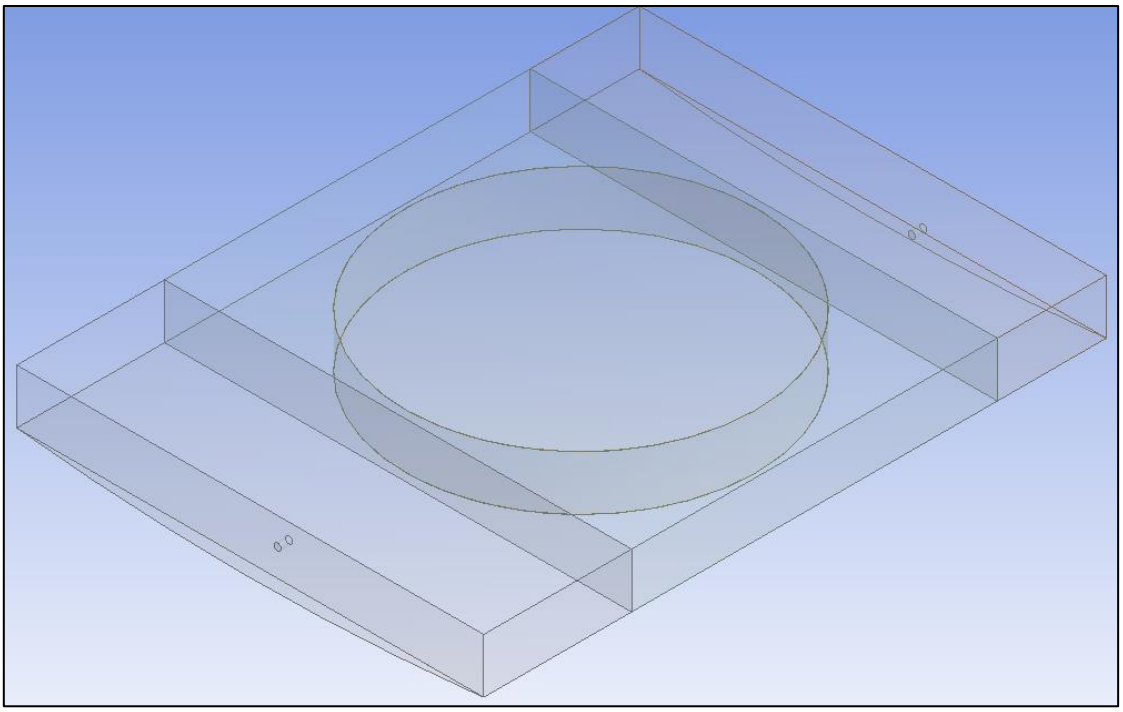

Figure 30: Geometry created using Ansys Design modeler

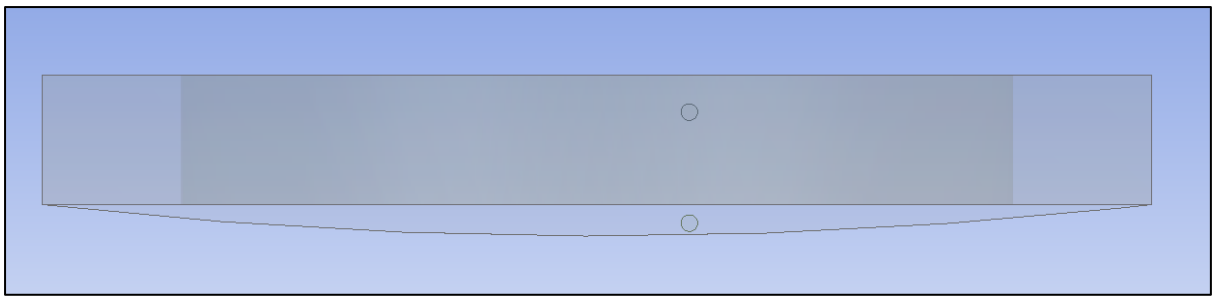

Figure 31: Curved bottom settler

The number of cells was adjusted to get the initial results. Several discretized tetrahedral cell volumes were tested to achieve coalescence. Mesh dependency was checked using the higher discretized volume cells which showed that there was not any significant difference in the results therefore, 107228 was used as the final mesh size. The discretized domain is as shown in figure 32.

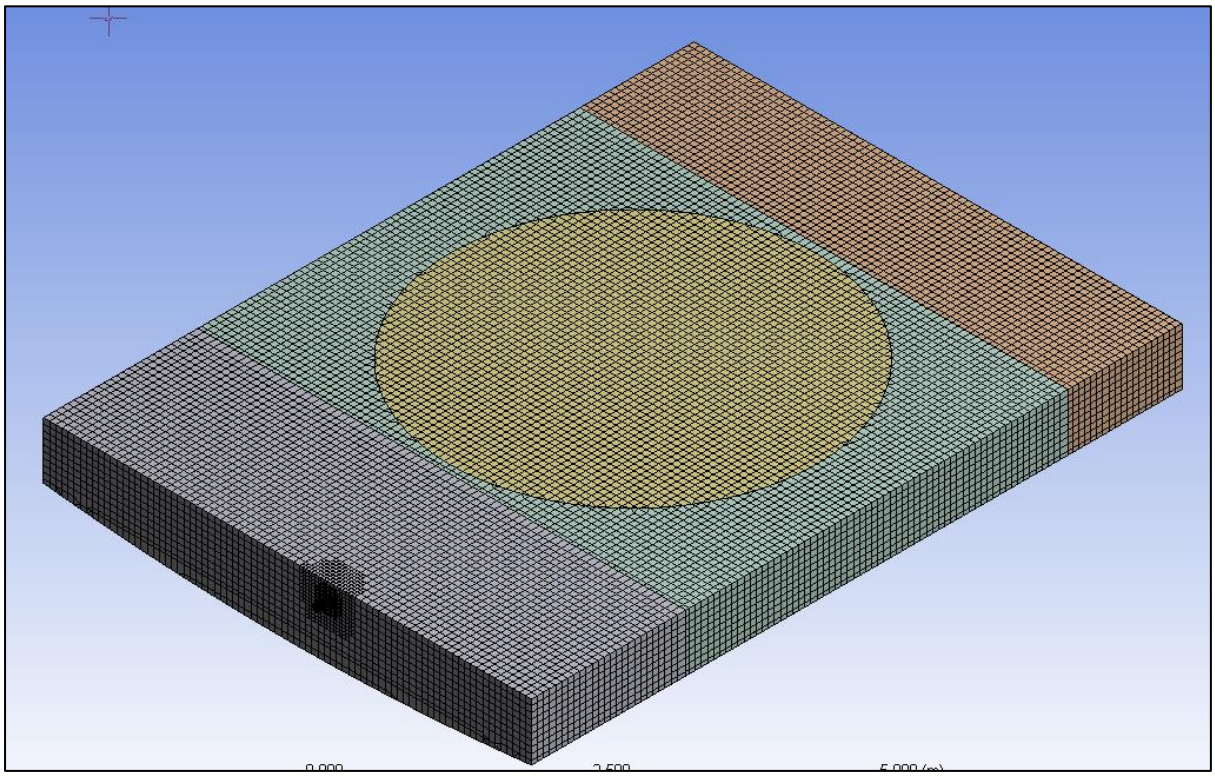

Figure 32: Meshed settler Geometry

3.2 Governing equations and models

Transient simulation is carried out for two-phase flow. Ansys Fluent built in model implemented is discrete phase model. DPM integrates particle force balance equation given by equation 41. This integration yields droplet trajectory. Rewriting equation 41:

$\frac{du_i^p}{dt}$= drag force + Gravity force+ extra forces (41)

For calculating drag force, gravity force and extra force, the algorithm uses the equations from 42-66 documented in section 2.4.3.

After calculating the droplet trajectory, DPM uses O'Rourke's algorithm for determining the outcome of collision as in equations 34-40. The algorithm calculates Weber number, critical offset distance, offset distance parameter given by equations 7, 38 and 40. Rewriting the equations,

$$\mathrm{We} = \frac{\rho d_s U^2}{\sigma} \tag{7}$$

$$b_{crit} = (r_1 + r_2)\sqrt{min\left(1.0, \frac{2.4\mathrm{f}}{\mathrm{We}}\right)} \tag{38}$$

$$\mathrm{b} = (r_1 + r_2)\sqrt{Y} \tag{40}$$

As mentioned in the section 2.4.3 coalescence happens when the distance between two colliding droplets is lower than the critical offset distance. Hence, parametrization is done to achieve b<b_{crit}.

Eulerain-Lagrangian algorithm is implemented for the overall simulation. The reason for going with Eulerian-Lagrangian algorithm is that it is suitable for tracking secondary phase or individual particles. Continuous phase is considered as primary phase while secondary phase is fluid particle or solid [Ansys fluent 18.2]. In this setup continuous phase is slag while secondary phase is matte droplets undergoing settling with coalescence. Thus, Eulerain method is used for modeling continuous slag phase while Lagrangian method is used for modeling the copper matte droplet motion in the continuous slag phase.

The solution used is a pressure-based solver with absolute velocity formulation. The continuity equation of the velocity field is solved by pressure correction equation. Ansys Fluent provides options for both steady state and transient conditions. In this solution, transient solution is adapted. Gravity is included to include the gravitational force during settling of matte droplets through slag. Implicit formulation is adapted because it is iterative and feasible for running transient simulation. The energy equation is also included.

The interactions between two droplets happens with the turbulent eddies of the continuous phase in turbulent dispersed flows. Since coalescence happens in turbulent conditions its necessary to select turbulent model over laminar model. Turbulent models provided by Ansys Fluent include k-epsilon, k-omega, and Reynold's stress models. The comparison between them is as shown in figure 33.

Selection of appropriate turbulence model is very important in coalescence modeling [B. Andersson et.al (2011)]. For this solution k-epsilon, realizable model is selected. The reasons for going with this model are

- Low level of approximation.
- High level of resolution.
- Under adverse pressure gradients performs better for boundary layers.
- Good for simulating flows which involve high mean shear rate.
- For simulating swirling, rotation, recirculation and robost streamline curvature this model is best.

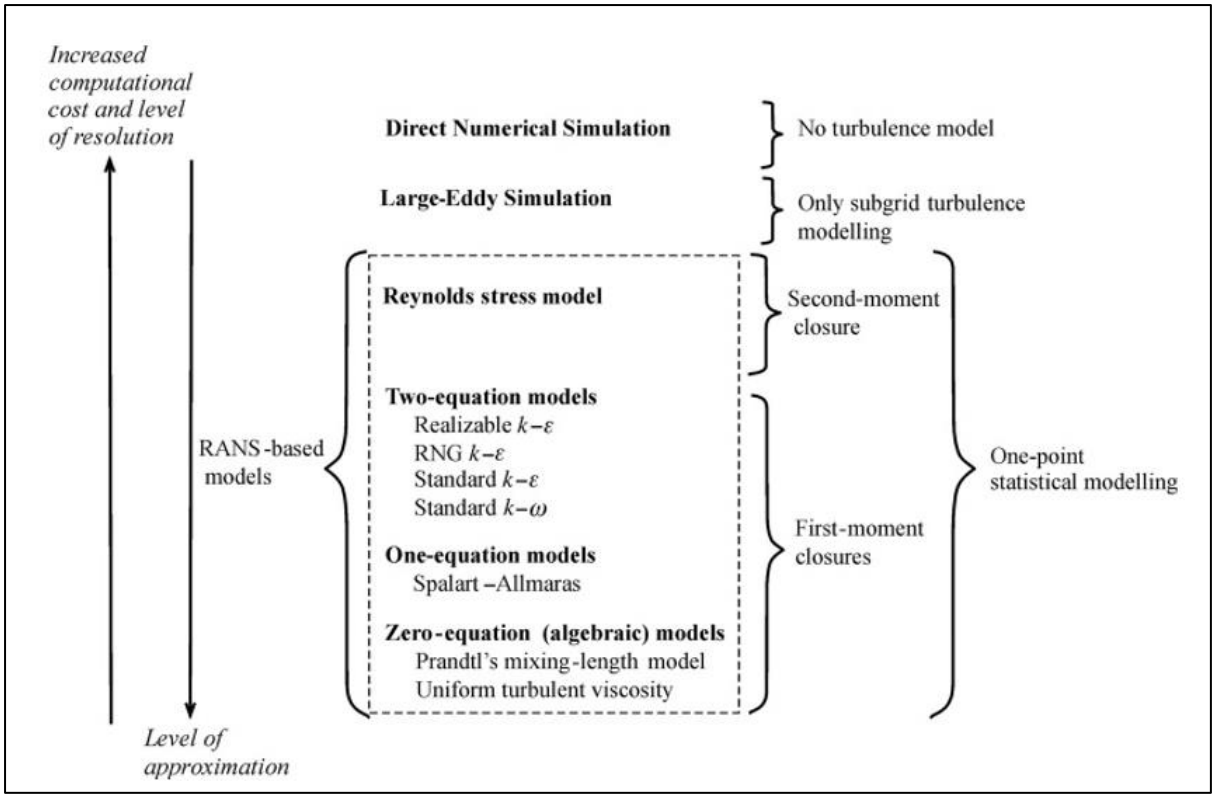

Figure 33: schematics of turbulence modeling[B. Andersson et.al(2011)]

The interaction is made possible between the discrete phase and the continuous phase. The DPM sources are updated for every flow iteration. This simulation is restricted only for coalescence modeling. Hence, only coalescence is included and breakup is not included. Also user defined function is not written in the simulation. The accuracy is controlled with a tolerance of 1e-05 and maximum refinements of 20. Hybrid parallel processing is employed in the algorithm. Automated tracking scheme is implemented with trapezoidal high order scheme and lower order scheme being implicit.

3.3 Material Properties and Injections

Slag is used as the continuous phase whereas matte is used as dispersed phase in the form of droplet parcels. The properties of matte and slag are taken from [Xia, J et al (2007)] for this master thesis project. Physical properties of both slag and matte are presented in Table 9.

Table 9: Properties of matte and slag [Xia, J et al (2007)]

Properties	Matte	Slag
Density (kg/m^3)	5100	3150
Viscosity (kg/m.s)	0.04	0.45
Specific heat (J/kg.K)	850	1100
Thermal conductivity (W/m.K)	15	6

Ansys fluent DPM module provide three injection types named single, group, cone, surface and file type of injections as shown in figure 34. The single point injections and surface injectors did not achieve coalescences. The results of single point injectors and surface injectors are described in section 4.6 and 4.7 respectively. Hence, cone injector is used in the setup. When the number of collisions are higher, the probability of coalescence will be higher as per equation 36. Rewriting equation 37:

$$P(n) = e^{-n\frac{n^n}{n!}} \quad (37)$$

Where n is the number of collisions between bigger droplets and the other droplets, the probability distribution is as per the Poisson distribution. Hence, to account more number of coalescences matte droplets were injected with a cone distribution pattern. Entry of matte droplets from cone creates high turbulence at the inlet and large number of collisions/coalescences.

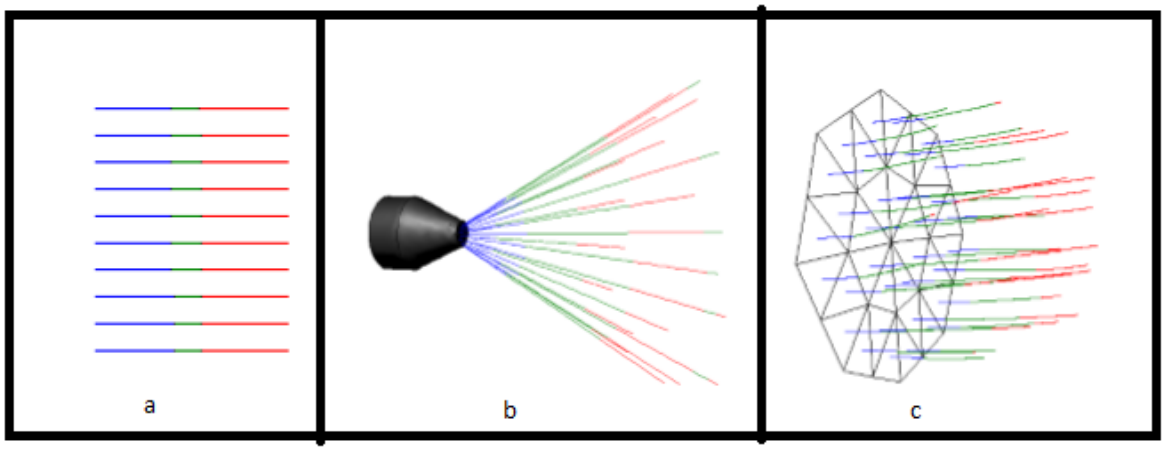

Figure 34: injection types illustration a. group injection b. cone injection c. surface injection

The computational domain was completely filled by slag phase. Cone injectors with an angle of 60° are placed at three coordinates (0, 0.698, 4), (0, 0.698, 3.5) and (0,0.698,3). The matte droplets of 300 µm were injected as particle parcels to strike the slag phase. Discrete random walk model is implemented for modeling turbulent dispersion. Rest of the injection settings are as shown in table 10.

Table 10: Matte injection settings

Temperature of matte droplets (K)	**1603**
number of streams in one injector	50
Total flow rate (kg/s)	4.45
velocity of injection (m/s)	1

3.4 Boundary conditions and solution algorithm

Matte droplet parcels enter into the settler part of the furnace from the top wall at 1420 K. The boundary conditions of top wall, sidewall and slag outlet is set to reflect the parcels hitting them. Slag tapping pressure outlet is used and matte droplets can escape from it. The boundary conditions of bottom wall are set to escape the parcels hitting them. The temperature of bottom wall was set 1100 K.

Phase coupled simple scheme is used for achieving pressure velocity coupling. Gradient selected is least squares cell based, momentum used is second order upwind, volume fraction used is modified HRIC, turbulent kinetic energy is second order upwind, turbulent dissipation rate is second order upwind and energy is second order upwind. Transient formulation is first order implicit and warped-face gradient correction is applied. The other settings and values are as shown in the table 11, 12, 13, 14 and 15.

Table 11: Solution Methods Settings

Pressure-Velocity Coupling	
Scheme	Phase Coupled Simple
Solve N-Phase Volume Fraction Equations	Off
Spatial Discretization	
Gradient	Least Squares Cell based
Momentum	Second Order upwind
Volume Fraction	Modified HRIC
Turbulent Kinetic Energy	Second Order Upwind
Turbulent Dissipation Rate	Second Order Upwind
Energy	Second Order Upwind
Transient Formulation	First Order Implicit
Non-Iterative Time Advancement	Off
Warped-Face Gradient Correction	On
High order Term Relaxation	Off

Table 12: Solution Controls Settings

Pressure	**0.3**
Density	1
Body Forces	1
Momentum	0.3
Volume Fraction	0.3
Turbulent Kinetic Energy	0.6
Turbulent Dissipation Rate	0.6
Turbulent Viscosity	1
Energy	1
Discrete Phase Sources	0.9

Table 13: Residual Monitors Settings

Options	**Print to console**	**on**
	Plot	on
	Window	1
	Iterations to plot	1000
Iterations to store	1000	
Equations Residuals (monitor and convergence is turned on for all the cases)	Continuity	0.001
	u-phase 1	0.001
	v-phase 1	0.001
	w-phase 1	0.001
	energy-p1	0.001
	k	0.001
	epsilon	0.001
Convergence criterion	Absolute	
Convergence condition	choose condition	All conditions are met
	Every time step	1
Residual values	Normalize	off
	Scale	on
	Compute Local Scale	off

Table 14: Solution Initialization Settings

Initialization Methods	**Standard Initialization**
Reference frame	Relative to cell zone
Initial values	
Gauge Pressure(pascal)	0
Turbulent Kinetic Energy(m^2/ s^2)	1.56e-06
Turbulent Dissipation Rate(m^2/ s^3)	9.583148e-10
Phase-1 X Velocity(m/s)	0
Phase-1 Y Velocity(m/s)	-0.000741
Phase-1 Z Velocity(m/s)	0
Phase-1 Temperature(K)	1318.894
Phase-2 X Velocity(m/s)	0
Phase-2 Y Velocity(m/s)	0
Phase-2 Z Velocity(m/s)	0
Phase-2 Temperature(K)	1318.894

Table 15: Calculation Settings

Time Stepping Method	**Fixed**
Time Step Size(s)	0.05
Number of Time Steps	50000
Extrapolate Variables	off
Data Sampling for Time statistics	off
solid time step	off
Max Iterations/ Time Step	120
Reporting Interval	1
Profile Update Interval	1

4 Results and discussions

The objective of the work is to study the effect of coalescence on settling mechanism and the feasibility of DPM model to simulate the phenomenon effectively. This is further extended to study copper losses.

At first, the parameterized DPM model is checked by viewing coalescences in particle tracking history and post processing animation. Then velocity vectors, droplet trajectory/copper losses, settling time, number of coalescences and other influencing parameters are studied in detail.

4.1 Particle tracking

Particle tracking history in DPM model displays number of particles tracked, number of particles escaped, aborted, evaporated, incomplete, parallel, coalescence at every time step. The corresponding flow time is also observed. The particle tracking showed coalescences and hence the built in model is parametrized well to model the phenomenon. Particle tracking history also showed that the solution converged with the set convergence criteria.

4.2 Post processing

The collision of two matte droplets leads to four possible outcomes namely coalescence, bouncing, separation and shattering. Parametrized DPM model cannot simulate separation and shattering outcomes. Hence, the post processing showed only coalescence and bouncing as the collision outcome. Some of the coalescences happening in different parts of the settler are shown in figures 35-37. Since coalescence is observed in particle tracking history and post processing, it could be concluded that the distance between two droplets achieved is lower than the critical offset distance in the parametrized dpm code. In other words, contact time is achieved longer than drainage time.

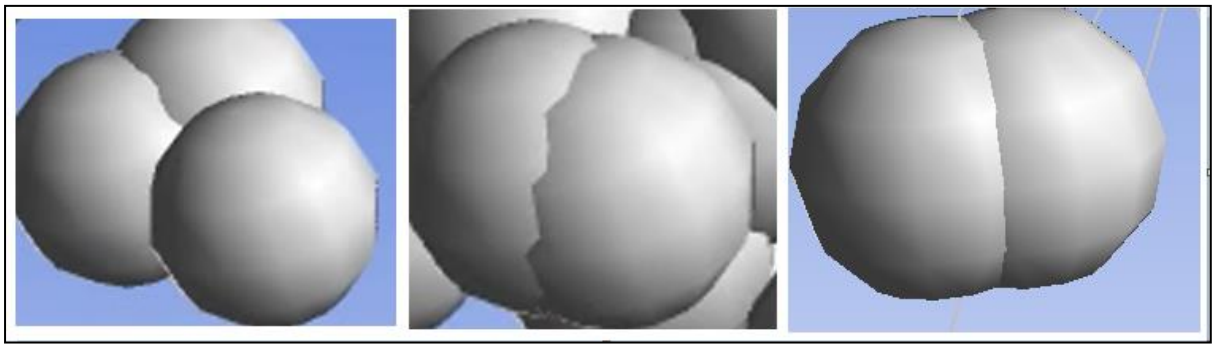

Figure 35: The coalescence in post processing

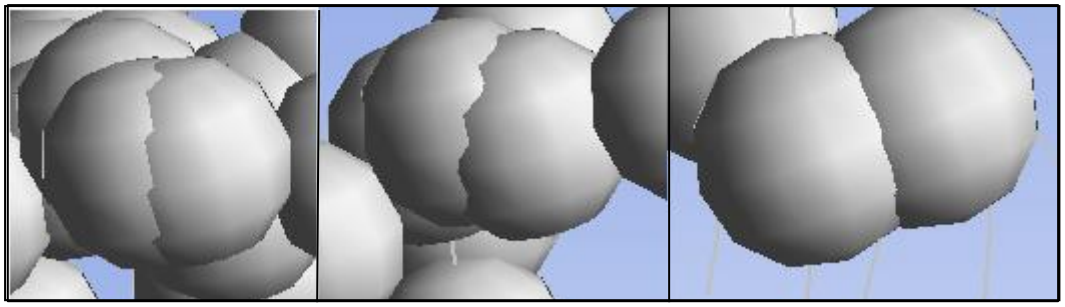

Figure 36: Coalescence at different positions of the settler

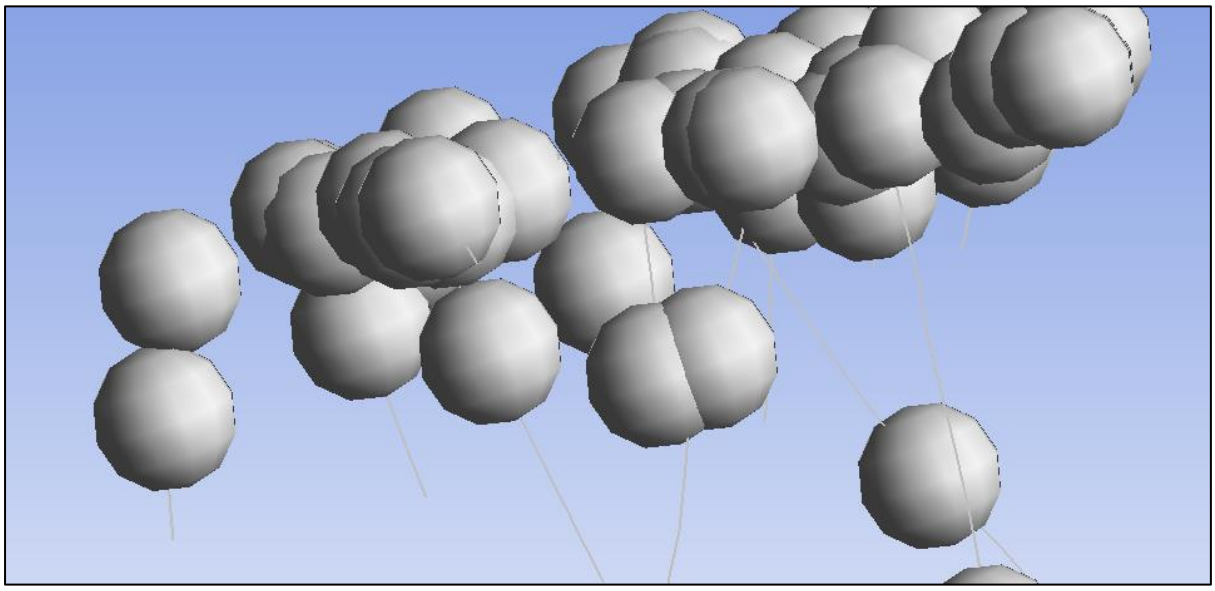

Figure 37: Coalescences

4.3 High turbulence

Velocity vectors are plotted at the inlet of the settler, different iso surfaces with inlet and middle surface as shown in figure 38, 39 and 40.

Figure 38 and 39 showed high turbulence at the inlet of the settler. The high turbulence is caused by entry of 150 matte droplets from cone injection. Droplets injected as parcels strikes the slag phase leading to collisions/coalescences. Figure 40 showed significant turbulent dispersion at different points. Turbulent dispersion is modeled by discrete random walk model. This is similar to the turbulent dispersion viewed by previous researchers Xia, J. L. et.al (2007).

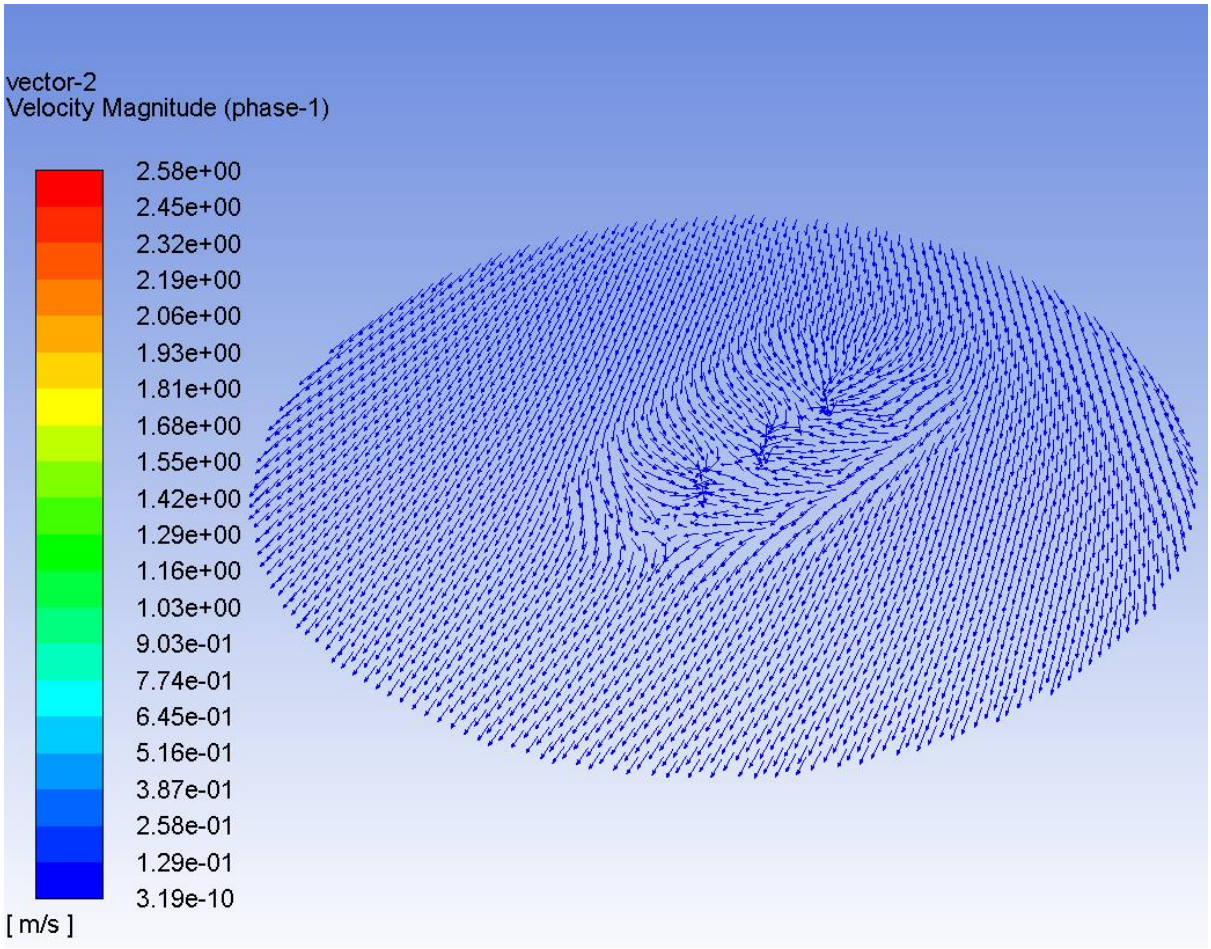

Figure 38: Velocity vectors at the inlet of the settler

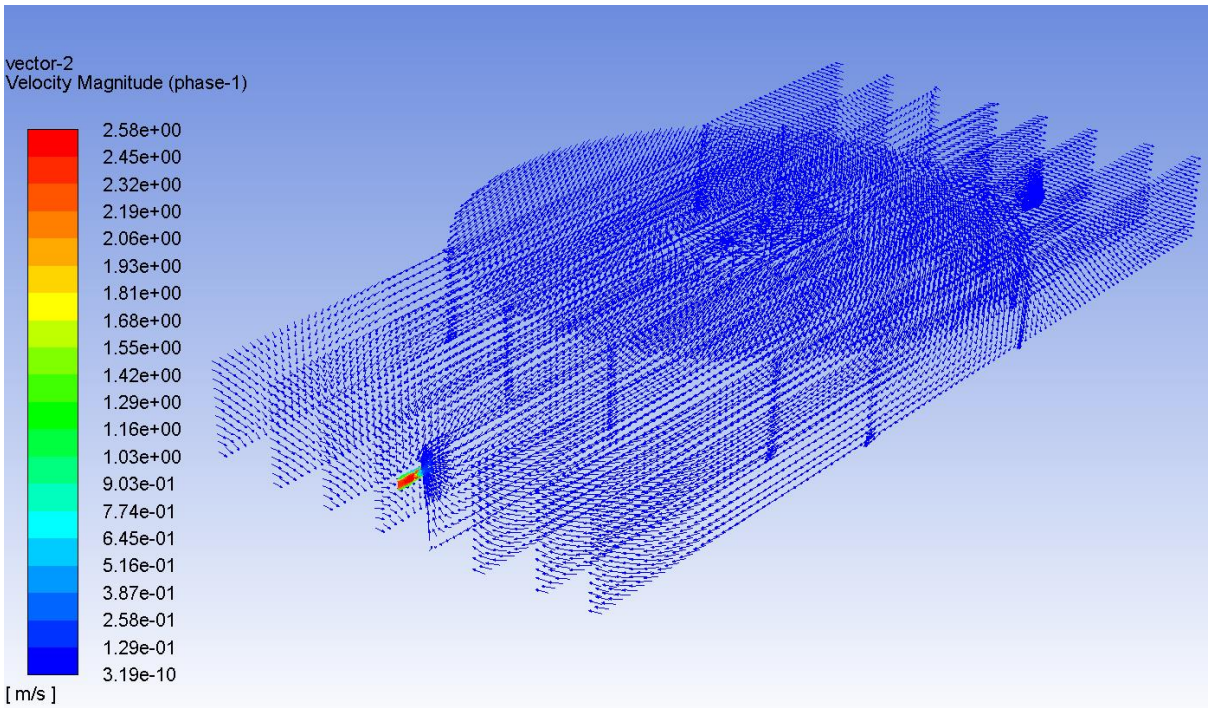

Figure 39: Velocity vectors at the inlet of the settler and different iso surfaces

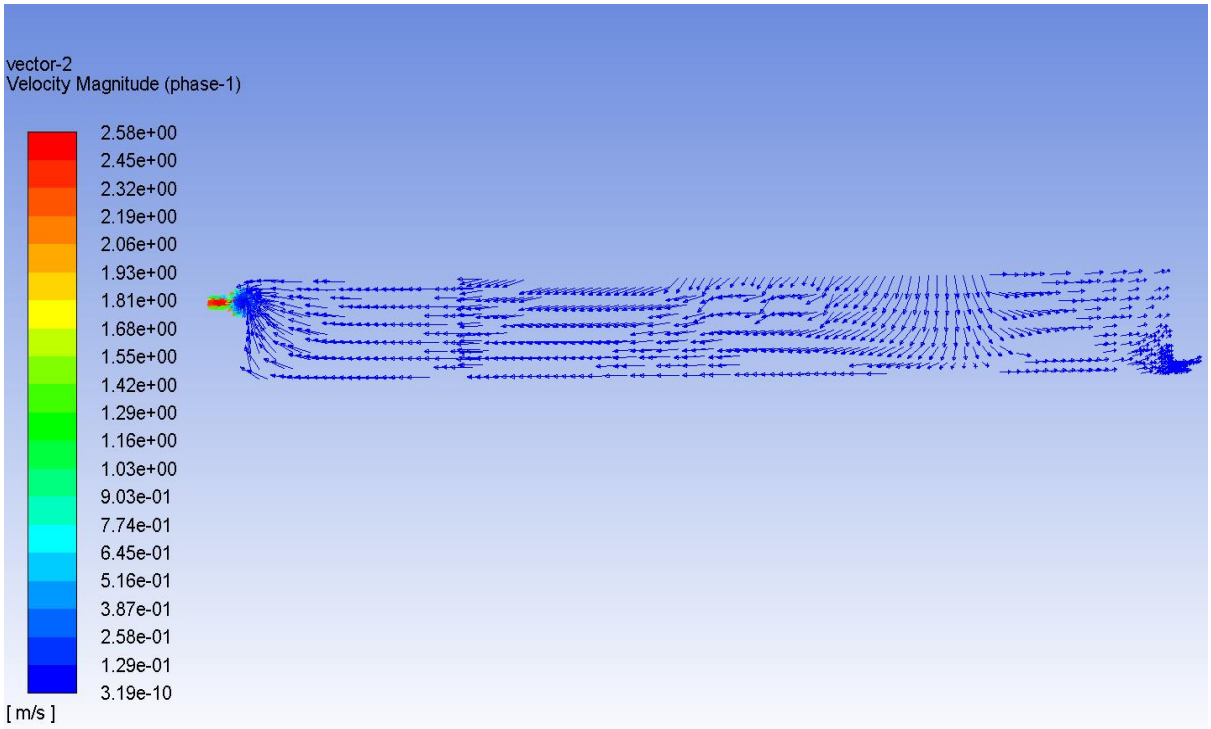

Figure 40: Velocity vectors at middle of the settler

4.4 Droplet trajectory and copper loss

Collision/coalescence of matte droplets might happen during settling through slag phase. The core activity of this thesis work is to understand the settling mechanism with respect to coalescence and DPM viability to model the phenomenon. To understand settling mechanism, droplet trajectory is analyzed with respect to collisions/coalescences. DPM determines droplet trajectory by integrating particle force balance equation.

Computation 1

In computation 1, two cases are simulated for settling of 300 µm matte droplets through slag phase. Variation in droplet trajectories is compared for two different cases. The cases vary by injection definition.

Case 1

In case 1, three matte droplets of 300 µm diameter are injected at three coordinate points named as point 1, point 2 and point 3. The injection definitions are as shown in table 16. During settling process, three matte droplets did not interact with each other at all. Droplets injected from point 2 and point 3 moved out from the tap hole while droplets injected from point 1 settled at the bottom wall. The post-processing results are as shown in figure 41 and 42.

Table 16: Injection definitions in computation 1

Matte diameter	Injection type	coordinate points
300 µm	single	point1= (0,0.698,3.0)
300 µm	single	point2= (0,0.698,3.5)
300 µm	single	point 3= (0,0.698,4.0)

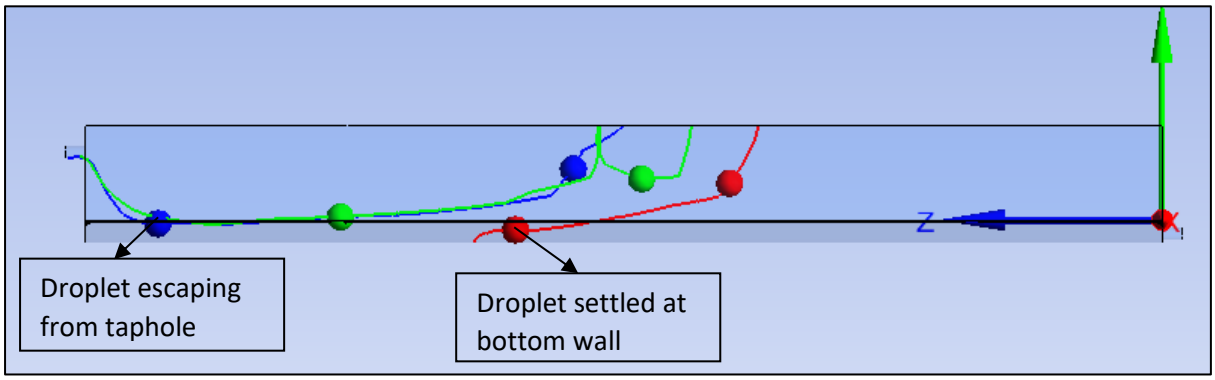

Figure 41: Droplet escaping from taphole and bottom wall

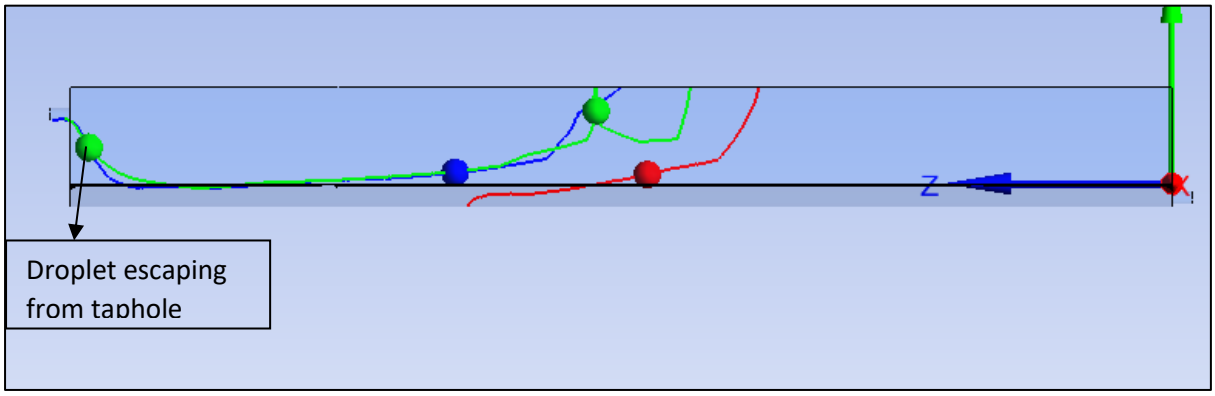

Figure 42: No interaction between droplets

Case 2

In case 2, 50 matte droplets are injected as parcels by cone injector at point 1. Remaining settings are similar to case 1. The injections are listed as in table 17.

Table 17: Injection definitions made in case 2

Matte diameter	Injection type	coordinate points
300 µm	cone (50 matte droplets as parcels)	point1= (0,0.698,3.0)
300 µm	single	point2= (0,0.698,3.5)
300 µm	single	point 3= (0,0.698,4.0)

During settling process, matte droplets from point 1 interacted with matte droplets from point 2. Droplets from point 1 and point 2 underwent collisions/coalescence and settled through the bottom wall. Droplets from point 3 did not interact with any of the droplets and moved out through tap hole. The post-processing results are as shown in figure 43 and 44.

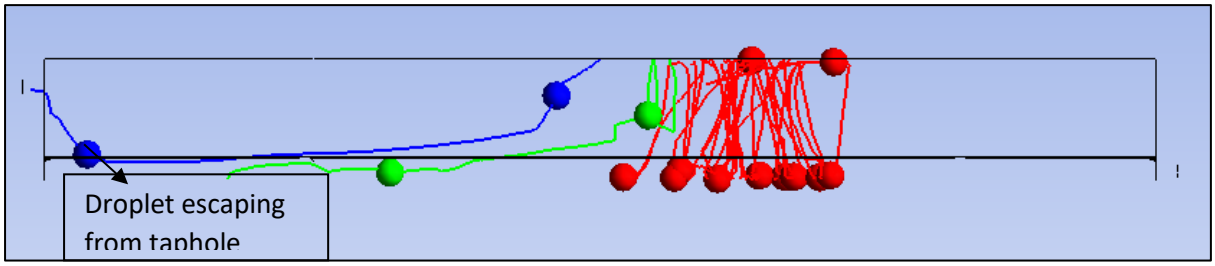

Figure 43:Droplet escaping from taphole

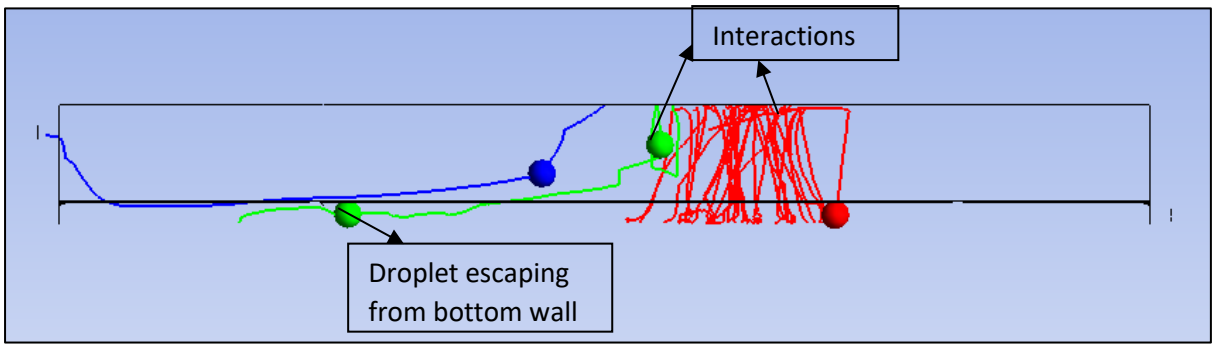

Figure 44: Change in droplet trajectory after collisions/coalescences

Comparing case 1 and case 2, it could be concluded that droplet injected from point 2 changed its trajectory and settled at the bottom wall after collision/coalescence. Thus if droplet have time to undergo collisions/coalescences it changes trajectory and copper loss is minimized.

Computation 2

Similar computation was performed with matte droplets of 100 µm diameter. In case 1 three single injections are made at three points as shown in table 18. The three matte droplets did not interact with each other. All three droplets escaped from the taphole. The post-processing results are as shown in figure 45.

Table 18: Injection definition made in computation 2

Matte diameter	Injection type	coordinate points
100 µm	single	point1= (0,0.698,2.5)
100 µm	single	point2= (0,0.698,3.5)
100 µm	single	point 3= (0,0.698,4.0)

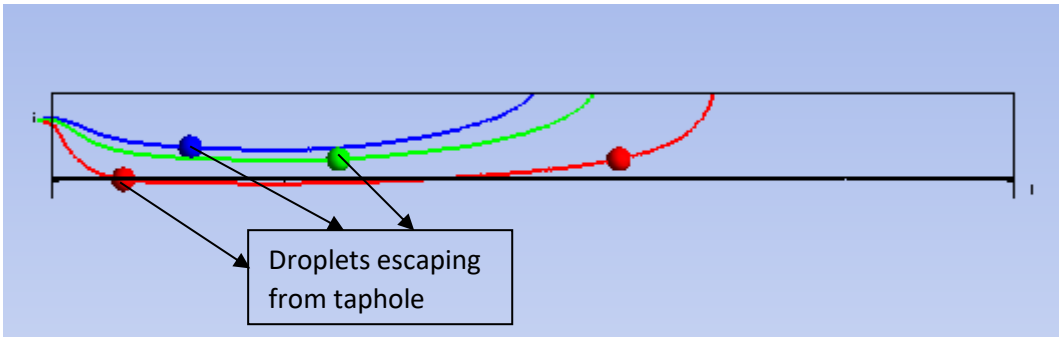

Figure 45:All droplets escaping from taphole

In case 2, 50 matte droplets are injected by a cone injector at point 2. Rest of the setting are kept similar to case 1. The settings are given as in table 19. In this case, matte droplets injected from point 1 and point 3 underwent collisions/coalescence with matte droplets from point 2. Hence, all the droplets settled at the bottom wall as shown in figure 46.

Table 19: Injection definitions made in case 2

Matte diameter	Injection type	coordinate points
100 µm	single	point1= (0,0.698,2.5)
100 µm	Cone (50 matte droplets as parcels)	point2= (0,0.698,3.5)
100 µm	single	point 3= (0,0.698,4.0)

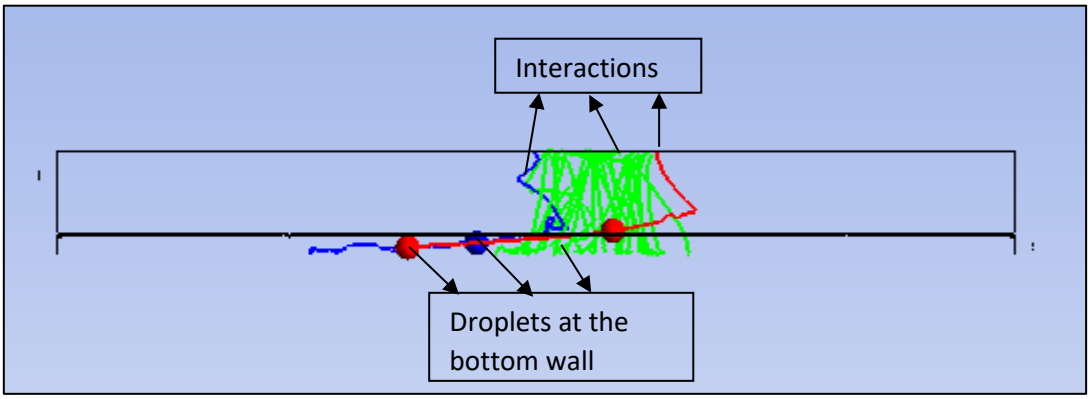

Figure 46: All droplets settled at the bottom wall

By comparing figure 45 and 46 it is quite clear that droplets injected from point 1 and point 2 changed their trajectory after collisions/coalescence and thus it escaped from the bottom wall instead of taphole.

Computation 3

In computation 3, default settings as described in section 3 is used i.e. three cone injectors are placed at three points. Each cone injector injects 50 matte droplets as parcels. The exact settings are as shown in table 20.

Table 20: Injections made in computation 3

Matte diameter	Injection type	coordinate points
300 µm	Cone (50 matte droplets as parcels)	point1= (0,0.698,3.0)
300 µm	Cone (50 matte droplets as parcels)	point2= (0,0.698,3.5)
300 µm	Cone (50 matte droplets as parcels)	point 3= (0,0.698,4.0)

In this case, large number of collisions/coalescences were observed between matte droplets from point 1, point 2 and point 3. High number of collisions/coalescences are due to high turbulence after hitting the slag layer. This large number of collisions/coalescences changed the droplet trajectory and hence, all the droplets settled from the bottom wall of the settler.

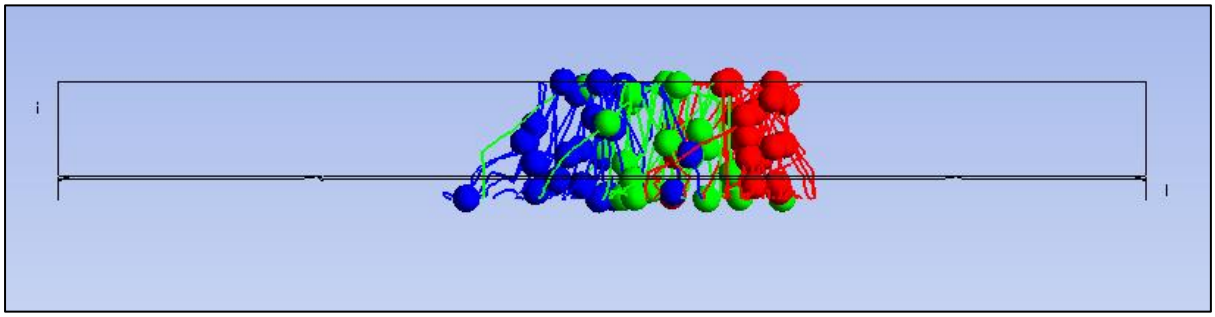

Figure 47: All droplets escaping from bottom wall

By comparing figures in computation 1-3, it is clear that collisions/coalescences change droplet trajectories and make droplets to settle on the bottom wall of the settler. In computation three, the settling is more towards the central region of the settler due to high number of collisions/coalescences. Hence, collisions/coalescences play an important role in settling by changing droplet trajectories and minimizes copper loss. This process is quite complicated and needs to be further studied accurately.

4.5 Settling time

Copper matte droplets may collide each other and coalesce during settling. The droplet diameter increases after coalescence. Previous studies have shown that with increase in matte droplet diameter settling time is lower. To understand this further three computations are run. Settling time of the escaped droplet is measured from the corresponding flow time in particle tracking history.

Computation 1

The injection and setup for computation 1 is similar to computation 1 in previous section. Two cases are run as before.

Case 1

In case 1, two droplets escaped from the tap hole and one droplet escaped from the bottom wall. The particle tracking history shows only droplet escaped, coalesced, flow time, etc. However, it cannot show which particular droplet escaped, coalesced. The sequence of droplets settling is calculated by comparing particle tracking file with the post processing visualizations. The images taken from post processing animation at different instants of time is shown in figure 48 and 49.

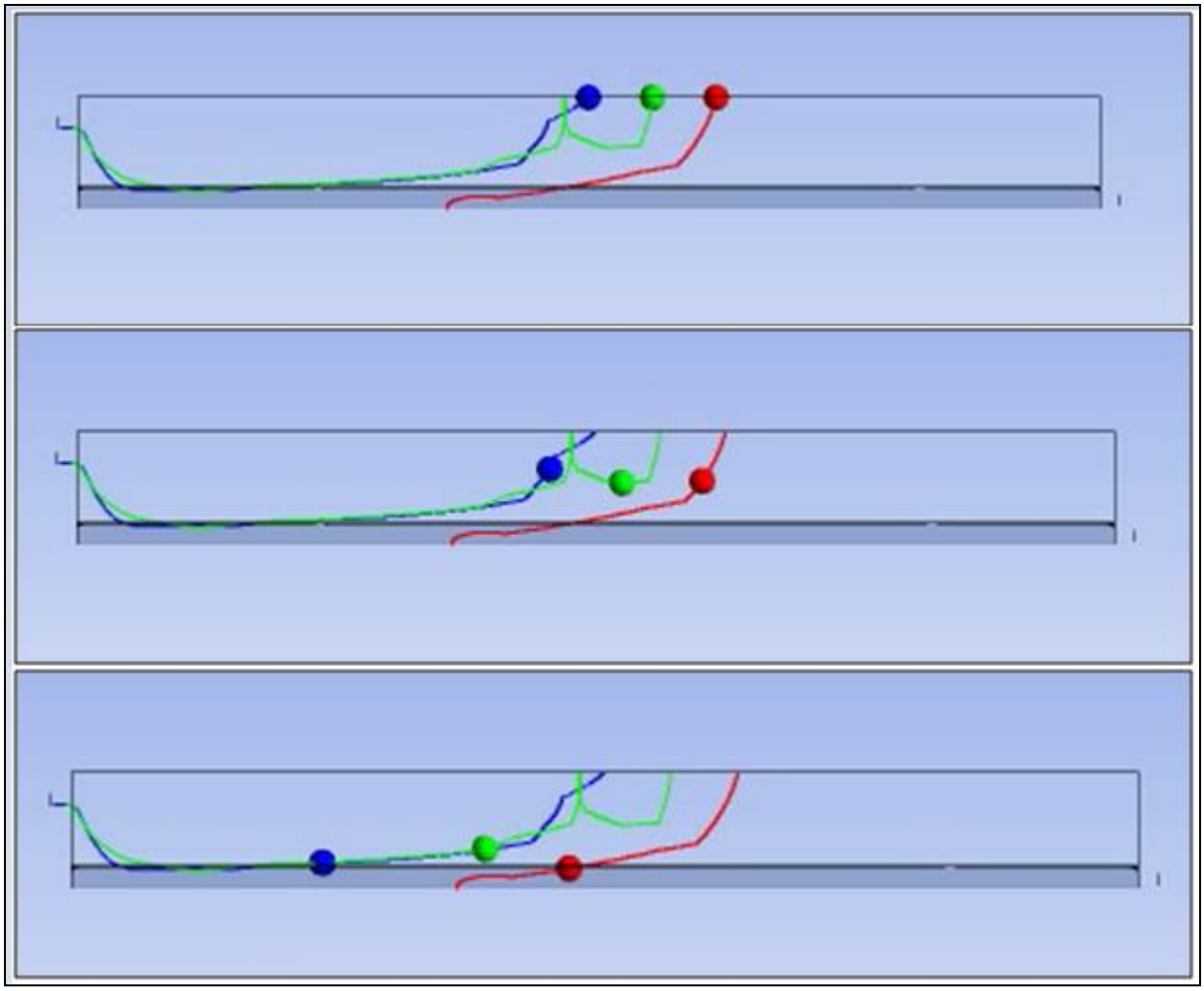

Figure 48: Post processing images at different instants of time

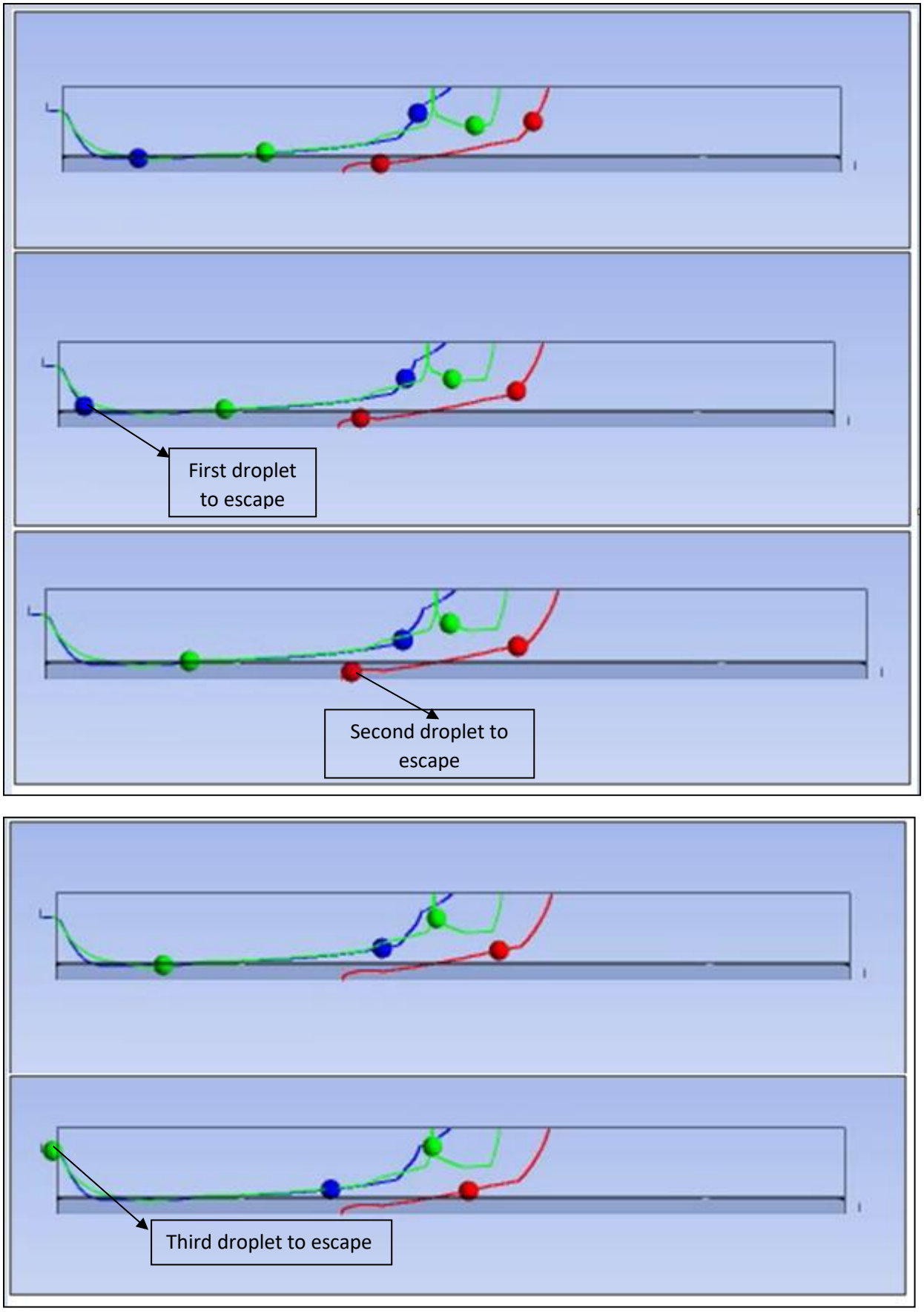

Figure 49: Post processing images at different instants of time

From post processing visualizations and particle tracking history the results could be written as in table 21.

Table 21: Injection definition and settling time in case 1

Matte diameter	Injection type	coordinate points	Sequence of settling	Settling time= corresponding flow time in DPM (s)
300 µm	single	point1= (0,0.698,3.0)	Second droplet to settle	1392.45
300 µm	single	point2= (0,0.698,3.5)	Last droplet to settle	1558.20
300 µm	single	point 3= (0,0.698,4.0)	First droplet to settle	1260.70

Case 2

In case 2, cone injector is placed at point 1. Cone injector injects 50 droplets in the form of parcels and rest of the settings are kept similar to case 1. The post images are as shown in figure 50 and 51. From the post processing images it is quite clear that all 50 droplets (injected from point 1) escaped much before other two droplets (injected from point 2 and point 3). Calculating settling time of 50 droplet is quite confusing and not preferred due to accuracy. 51st droplet settled is the droplet injected from point 2. The droplet did not interact with any of the other droplet. Hence the settling time is similar to case 1. The 52nd droplet to settle is the droplet injected from point 2. Its settling time is 1400.35 s. Thus the settling time is decreased after collisions/coalescence. The results could be summarized as in table 22.

Table 22: Injection definition and settling time in case 2

Matte diameter	Injection type	coordinate points	Sequence of settling	Settling time= corresponding flow time in DPM (S)	Inference
300 µm	Cone (50 droplets)	point1= (0,0.698,3.0)	All 50 droplets settled first	Difficult to calculate because of large number of droplets.	All droplets settled much before other two droplets.
300 µm	single	point2= (0,0.698,3.5)	Last droplet to settle	1400.35	Settling time is decreased compared to case 1. The reason is collision/coalescences
300 µm	single	point 3= (0,0.698,4.0)	51st droplet to settle	1260.70	Did not interact with other droplets. Hence settling time is same as in case 1.

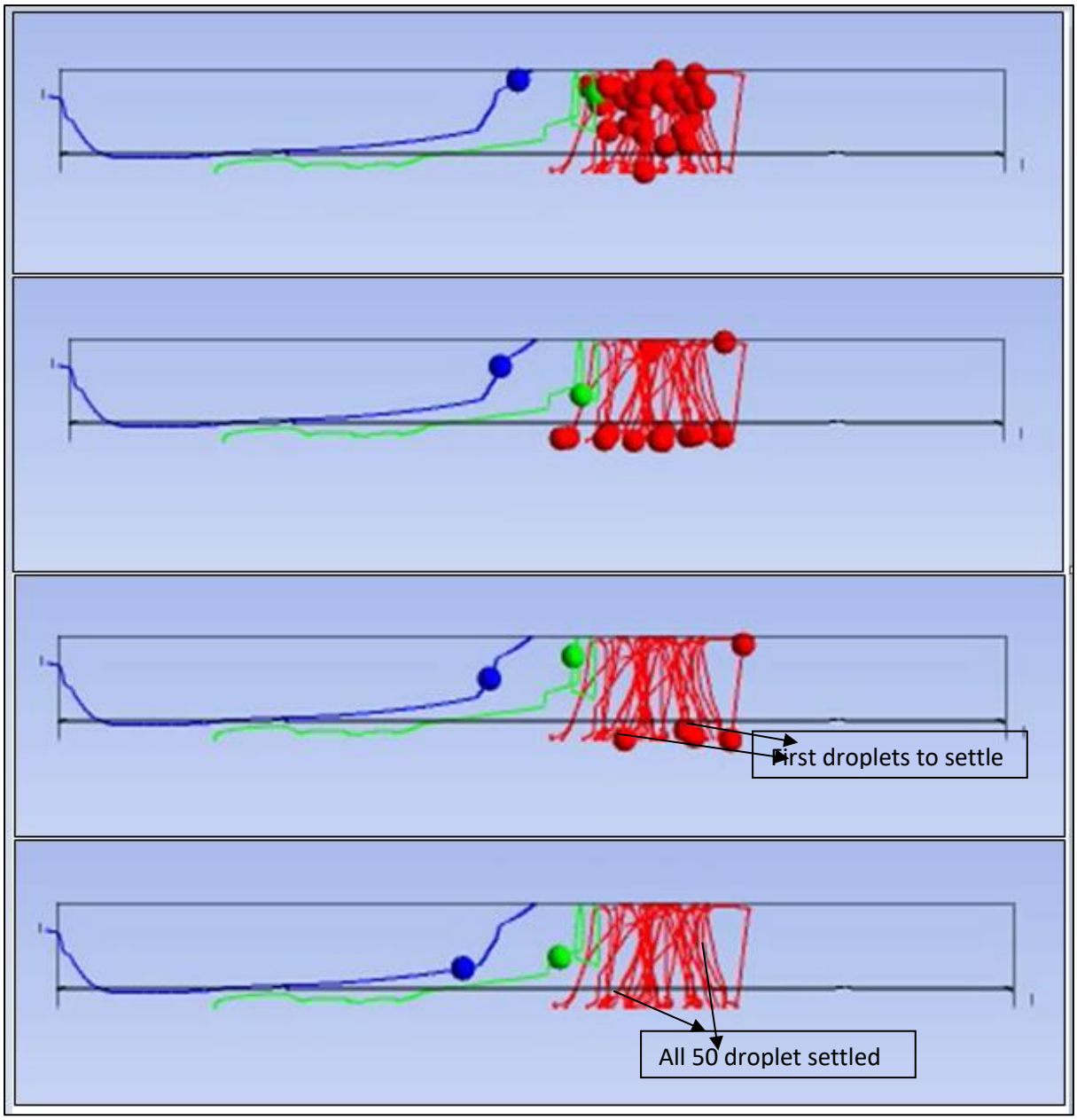

Figure 50: Post processing images at different instants of time

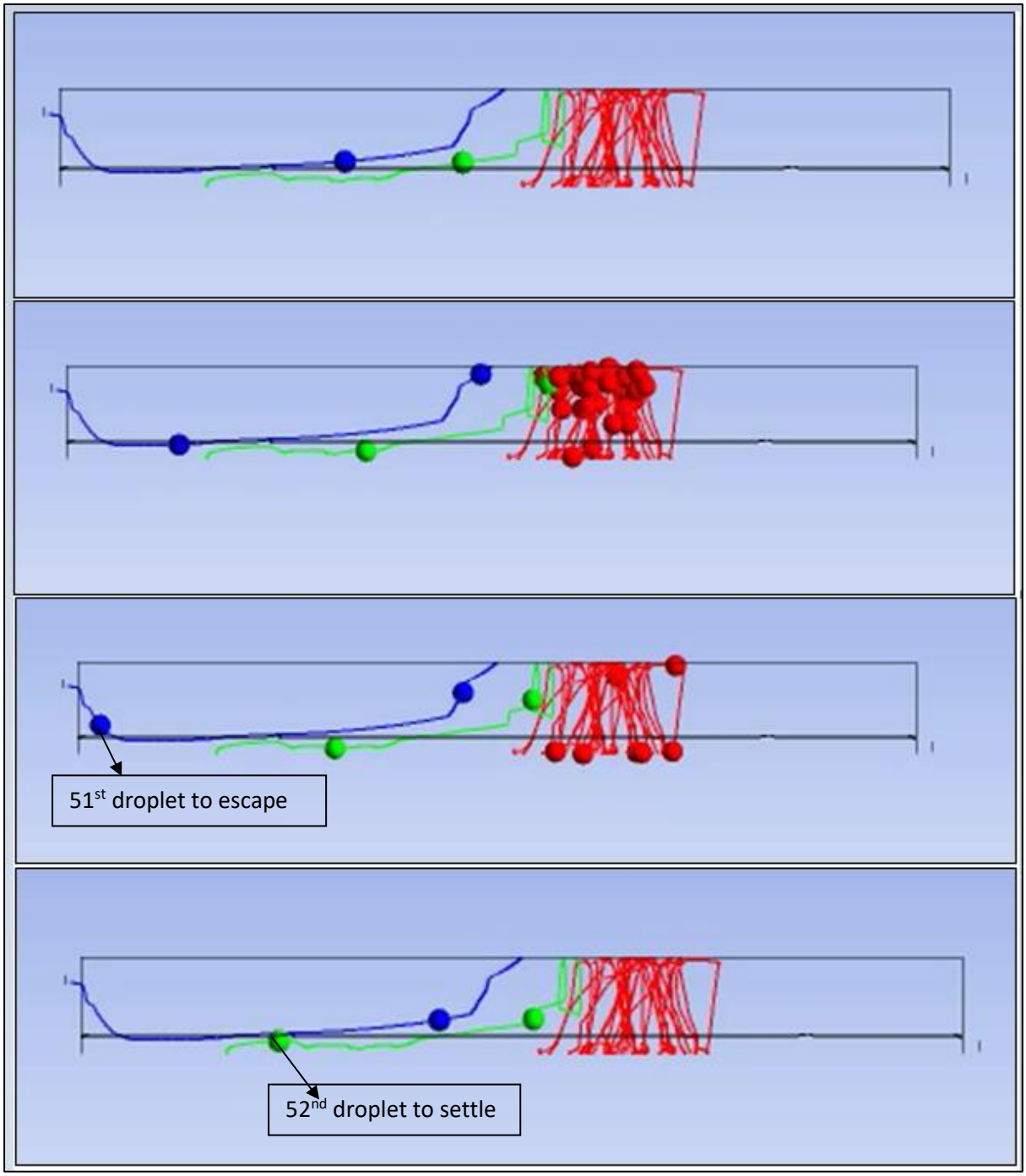

Figure 51: Post processing images at different instants of time

Computation 2

Case 1: Only bouncing outcome (without coalescence)

In case 1, 50 droplets are injected as parcels from point 1, point 2 and point 3. The coalescence outcome is deactivated in the DPM code. Thus, the DPM models only bouncing outcome and no coalescence outcome even though distance between two droplets is lower than the critical offset distance.

The total number of droplets is 150. It is quite difficult to identify individual droplets and calculate its settling time. The manual method of comparing particle-tracking history with animation is quite tedious and not preferred. However, for comparative purpose first seven droplets settled in particle tracking history is documented as shown in table 23.

Table 23: Settling time in case 1

Serial number of settled droplet	Settling time without coalescence case [s]
1	74.50
2	74.90
3	75.85
4	76.25
5	80.85
6	82.50
7	86.10

Case 2: Both coalescence and bouncing outcome

The injection settings of case 2 is similar to case 1. The coalescence outcome is activated in the DPM code. Thus, when the distance between two droplets is lower than the critical offset distance the outcome will be coalescence. Otherwise the outcome will be bouncing.

In this case also, calculating settling time by comparing with post processing video is tedious. The settling time of first seven droplets is documented for comparison as in table 24,

Table 24: Settling time in case 2

Serial number of settled droplet	settling time for Coalescence case [s]
1	38.55
2	42.95
3	47.00
4	55.40
5	59.70
6	62.50
7	62.60

Comparing table 22 with table 23,

- It is quite clear that settling of coalesced droplets started much earlier than uncoalesced droplets. First coalesced droplet settled at 38.55 S, which is much faster than 74.50 S.
- The seven coalesced droplet settled much before the first droplet settled during case 1 simulation. The reason for faster settling is due to increase in droplet size after coalescences.
- It is difficult to compare droplets individually in the DPM code. The particle tracking history displays one of the droplet settled with respect to flow time. However, it fails to identify the name of the settling droplet. When three droplet systems are simulated (like Xia, J. L. et.al (2004) and computation 1) droplets could be identified manually by comparing with the animation. When 150 droplets are injected as parcels manual method is tedious and less accurate.

Computation 3

If two matte droplets collide and coalesce maximum droplet size attained is 378µm. Suppose 8 matte droplets of 300 µm collide and coalesce each other and attain a droplet size of 600µm. Theoretically settling time of coalesced droplet should be equal to settling time of individual 600µm droplet. To investigate this further two cases are simulated.

Case 1

In case 1, 150 matte droplets of 300µm are injected by default settings as shown in table 24. As mentioned earlier (in computation 2) calculating settling time with respect to each droplet is tedious and difficult. Hence settling time of last three droplets are taken for comparison. The settling time of last three droplets are as shown in table 25.

Table 25: Settling time in case 1

Settling time of last three droplets out of 150 droplets	
Serial number of settled droplet	Settling time (S)
148	332.00
149	354.70
150	403.30

Case 2

In Case 2, three droplets of 600 µm are injected at the same three points as in case 1. The injection definition are written in table 26. The post processing video clearly showed all three droplets settled at the bottom wall of the settler. The settling time of three droplets could be written in table 27.

Table 26: Injection definition in case 2

Matte diameter	**Injection type**	**coordinate points**
600 µm	single	point1= (0,0.698,3.0)
600 µm	single	point2= (0,0.698,3.5)
600 µm	single	point 3= (0,0.698,4.0)

Table 27: Settling time in case 2

Settling time of three droplets	
Serial number of settled droplet	Settling time (S)
1	590.60
2	649.20
3	671.15

Comparing case 1 and case 2 the following conclusions could be made:

- In case 1, all 150 droplets settled within 403.30 S.
- In case 2, none of the three droplets settled before 590.60 S, which is a big difference than case 1.
- The last droplet in case 2 took 671.15 S to settle which is 4.46 minutes late than in case 1.
- It should be also noted that some of the droplets might not coalesce in case 1. Thus, it might remain 300 µm diameter in the end. Inspite of few 300 µm matte droplets settling is faster in case 1.
- 600 µm droplet diameter is way bigger than 300 µm droplet. Inspite of the coalesced 300 µm droplets settle very faster than 600 µm . The faster settling in case 1 is not only due to increase in droplet size but also due to change in droplet trajectory after large number of collisions/coalescences. Therefore, it could be concluded that collision/coalescences significantly influences settling time. This is a quite complicated area, which requires in detail research in future.
- The particle tracking history in the present state fails to identify droplets individually. Thus, user-defined functions should be written in future to name droplets individually.

4.6 Number of coalescences

From sections 4.3 and 4.4, it is clear that collisions/coalescences significantly affects the settling time. It is not only increase in droplet size that influences settling time but also the change in droplet trajectory after collisions/coalescences. Hence, number of coalescences is studied further.

The post processing animation and particle tracking for default settings showed large number of coalescences at the inlet of the settler, few in the middle and no coalescences near the bottom wall. All the droplets escaped from the bottom wall of the settler. No droplets escaped from the taphole. The exact details in terms of flow time are as shown in table 28. Number of coalescences in first time step is 37 indicating high turbulence at the inlet. In second time step number of coalesces was 1. No coalescences happened between third and tenth time step. Number of coalescences between eleventh to thousandth time steps is as shown in figure 52.

Table 28: Number of coalescences and settling for every 10 s.

Flow time (S)	number of coalescences	number of droplets settled
0.05-10	52	0
10.05-20	6	0
20.05-30	8	0
30.05-40	5	1
40.05-50	1	2
50.05-60	1	2
60.05-70	0	5
70.05-80	0	3
80.05-90	0	3
90-100	1	4
100.05-110	0	2
110.05-120	0	4
120.05-130	0	7
130.05-140	0	1
140.05-150	0	5

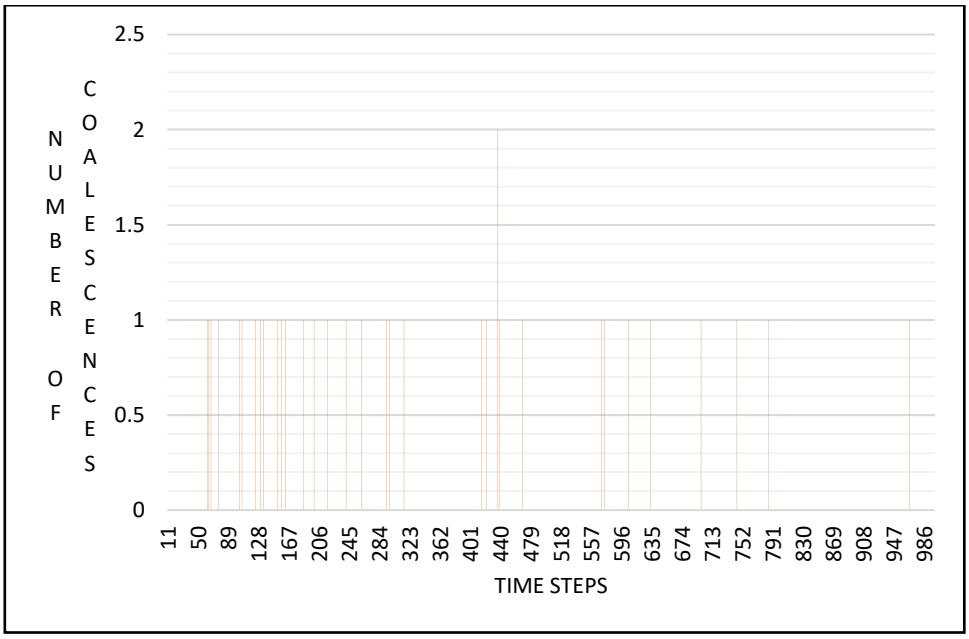

Figure 52: Bar graph showing the number of coalescences from eleventh to one thousand-time step

As mentioned by previous researchers Xia, J. L.et.al (2007) flow underneath the reaction shaft is very complex and turbulent, the large number of coalescences in the beginning of the flow time/time step. The higher turbulence is because of large number of matte droplets striking the slag layer, which results in high number of collisions. As number of collisions are higher, probability of coalescences is higher. Once the droplets pass through the upper layer of the slag, they start taking their own trajectory. The modeled settler has a dimension (8*6) m while matte droplets is (300-600) µm in diameter. The tiny droplets after changing trajectory does not meet at all due to big size of the settler.

Hence very few coalesces are observed in the middle of the settler and no coalescences in the end of the settler. Last coalescence was observed at a flow time of 97.35 S after which the droplets did not coalesced at all.

Parameters affecting number of coalescences are studied. Since high number of coalescences happen in the first time step, it is considered as a reference to study other influencing parameters. The number of coalescences in the first time step for default setup is 37.

Droplet diameter

The default droplet diameter is 300µm. The simulation is carried out for 100,200,400,500µm and number of coalescences in the first time step is noted down. Other settings and parameters are kept similar to default. The graph of droplet diameter is plotted against number of coalescences in the first time step as in figure 53.

It is clear from the simulation values that large number of coalescences happen for lower droplet diameter. It is expected number of coalescence to increase with increase in droplet diameter. However in this simulation number of coalescences decreases with droplet diameter. This is due to the logic of DPM model. DPM gives the coalescence outcome if distance between two droplet is lesser than the critical offset distance. Critical offset distance depends on droplet diameter and Weber number. If b<b_{crit} , the outcome is coalescence or else the outcome is bouncing. Achieving b<b_{crit} is easier for lower droplet diameter as per the equations 37,38,6 and 39. Hence, this is the limitation of using CFD mathematical model results.

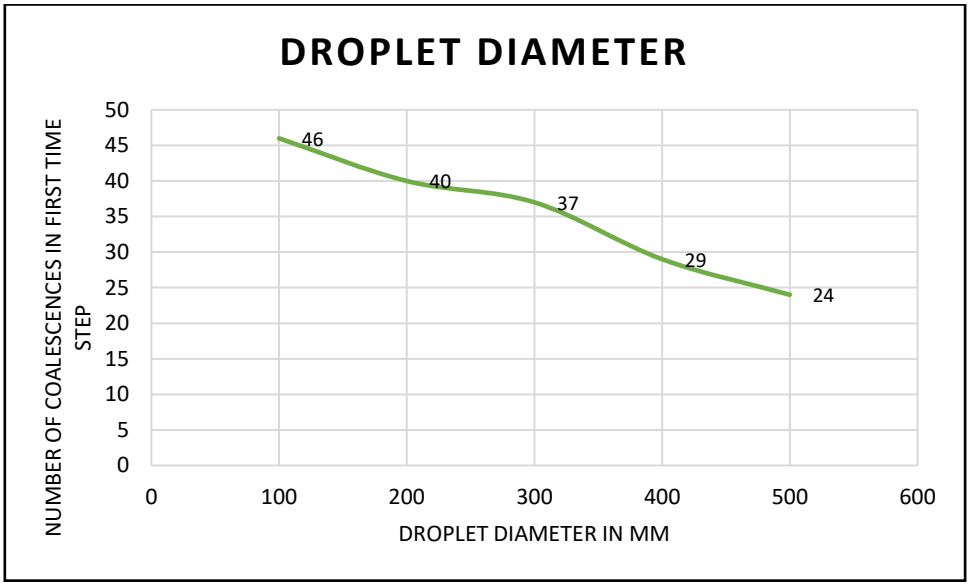

Figure 53: Plot of droplet diameter against number of coalescences in the first time step

Mass flow rate

Mass flow rate is the product of density of matte, projecting area of the injector and velocity of the injection. In this setup density of the matte, angle of injector and velocity of the injection are fixed. Hence, by changing mass flow rate projecting area of the injection changes correspondingly. With increase in projected area of the injection number of droplets injected in the first time step increases.

The default mass flow rate is 4.45 kg/s. The simulation is run for 2,3,4,5,6,7kg/s and number of coalescences at first time step is observed. Rest of the setup was default during the simulations. The graph of inlet velocity against number of coalescences at first time step is as shown in figure 54.

From the values, it is evident that with increase in mass flow rate (area of injection) number of coalescences increases. The reason is with higher mass flow rate large number of droplets comes out from the injector at first time step. The recorded number of coalescence value is the first time step value where high number of droplets collide in the first time step.

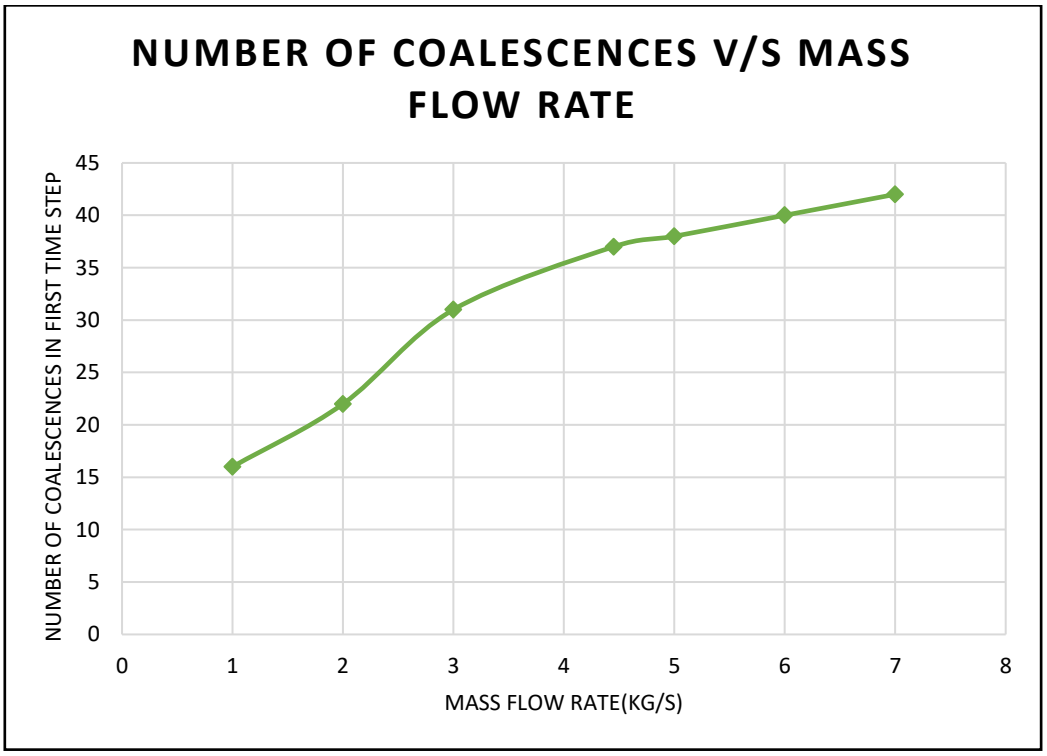

Figure 54: Plot of mass flow rate against number of coalescences in the first time step

Injection velocity

The effect of injection velocity is understood by running the simulation with different injection velocities. The default value of injection velocity in the computational setup is 1 m/s. The simulation is carried out for 0.5,1,1.5,2 m/s and number of coalescences in first time step is noted down. Rest of the parameter settings are made exact to default values i.e density of matte, angle of cone injector and mass flow rate are kept constant. With change in injection velocity projecting area of injector also changes to keep the mass flow rate constant. The graph of injection velocity versus number of coalescences in first time step is plotted as in table 29.

From the graph, it is clear that with change in injection velocity number of coalescences changes abruptly. When injection velocity changes droplets interact in a different way at a different time. Turbulent dispersion effect further increases complications. Thus number of coalesces not only depend on injection velocity but on injection definition as a whole. The way droplets interact with each other play a vital role in determining the number of coalescences.

Table 29: Table showing number of coalesces versus injection velocity

trial no.	Injection velocity	Number of coalescences in first time step
1	0.50	26
2	1.00	37
3	1.50	30
4	2.00	21

Injection positions

The injection positions are understood by placing the injectors in different coordinates. The corresponding number of coalescences at first time step is noted down as in table 30 and table 31. From the readings in table 30 it is quite clear that as the injections are placed closer to each other number of coalescences are higher. This is because of higher number of collisions happening between the closer droplets. In the DPM code distance between two droplets become lesser than the critical offset distance.

From the readings in table, it is evident that even though distance between the injection coordinates are equal different number of coalescences are observed. This is due to turbulent dispersion. The turbulent dispersion is modeled by discrete random walk model in the setup. The need for applying this model is as per the previous researchers Xia, J. L. et.al (2007). The turbulent dispersion changes from point to point in the settler. Turbulent dispersion changes the droplet trajectory, which in turn affects the number of coalescences.

Table 30: Table showing number of coalesces as coordinate distance decreases

trial no.	Injection coordinates	number of coalescences at first time step
1	Default= (0,0.698,4), (0,0.698,3.5), (0,0.698,3)	37
2	(0,0.698,3.8), (0,0.698,3.5), (0,0.698,3.2)	42
3	(0,0.698,3.6), (0,0.698,3.5), (0,0.698,3.4)	51

Table 31: Table showing number of coalesces with equal coordinate distance

trial no.	Injection coordinates	number of coalescences at first time step
1	Default= (0,0.698,4), (0,0.698,3.5), (0,0.698,3)	37
2	(0,0.698,2), (0,0.698,2.5), (0,0.698,3)	36
3	(0,0.698,1), (0,0.698,1.5), (0,0.698,2)	32

4.7 Single injectors

Similar to computational setup done by Xia, J. L. et.al (2004) single point injections are made at three points. Achieving interactions with point injectors at three points seemed tedious and very difficult. The reason is settler is very big and matte droplets are very small. The turbulent dispersion effect further increases the complexity to bring interactions between droplets. Turbulent dispersion changes the droplet trajectory. With a small change in droplet trajectory, the droplet move so far in a big furnace that interaction between other droplets is very difficult to achieve.

4.8 Surface injectors

To check the feasibility of the DPM code to model realistic settling cone injectors are replaced by surface injectors in the DPM module. The particle tracking history did not show any coalescences for surface injectors. In other words, DPM failed to model coalescences for surface injectors. This is due to increase volume fraction. The number of matte droplets injected by surface injector is 5845, which crosses the limit of DPM capacity. Hence, DPM cannot simulate coalescences when surface injectors are used.

4.9 Pattern

Hu, Y. T. et.al (2000) in their study obtained bouncing and coalescence pattern after collision of two polybutadiene drops. They used experimental method to observe collision outcome. The parameter of their interest was Capillary number.

The visualization of bouncing in post processing animation was producing similar images as observed by Hu, Y. T. et.al (2000) i.e. bouncing pattern in figure 55 is similar to bouncing pattern in figure 9.a. Even the matte droplet coalescence pattern observed in post processing visualization is similar to images captured by the researchers i.e. coalescence pattern in figure 56 is similar to coalescence pattern in figure 9.b. The methodology used in this study is CFD. Critical offset distance and Weber number are the parameters.

Thus, CFD simulation produced images whose pattern of coalescence and bouncing is similar to experimental pattern captured by Hu, Y. T. et.al (2000).

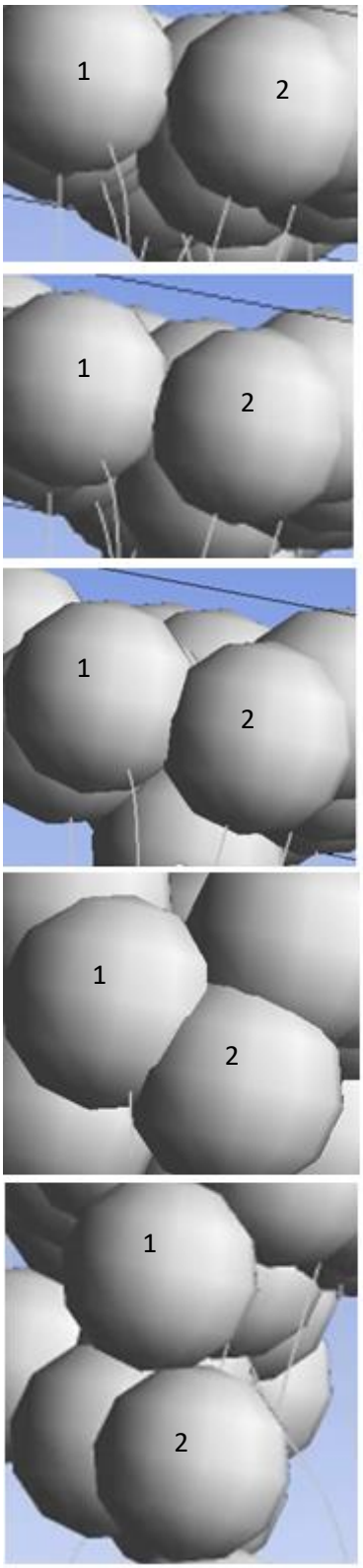

Figure 55: The bouncing outcome at different instant of time comparable with figure 9.a

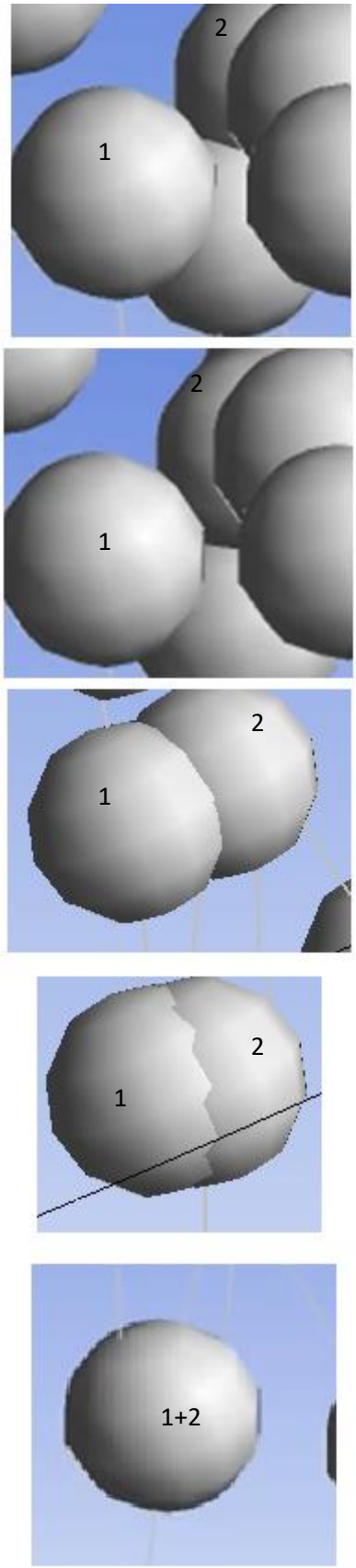

Figure 56: Coalescence outcome at different instant of time comparable with figure 9.b

Mohammadi, M et.al (2011, May)] simulated water droplets coalescence in oil medium and carried out parametric study of collision velocity, offcenter collisions, etc. The pattern of coalescence of water droplets in oil [Mohammadi, M et.al (2011, May)], [Yuan et al (2018)] appeared similar to coalescence pattern images observed in post processing animation. There is no droplet growth in the post processing video. The reason is that DPM technique accounts only particle tracking not the droplet growth in its post processing. However, increase in mass is observed in particle tracking history.

Yuan et al (2018) observed the pattern of water coalescence in oil by solving conservation equations. The pattern of coalescence of oil and water appeared similar to coalescence pattern images in post processing animation. However, after some time interval Discrete phase modeling technique did not account for droplet growth. It accounted only particle tracking in it. Figure 57 shows the results of CFD-post post-processing which could be compared with the pattern obtained by Mohammadi, M et.al (2011, May) and Yuan et al (2018).

Two publications Mohammadi, M et.al (2011, May)] and Yuan et al (2018) used CFD technique to observe coalescence pattern. However, the mathematical model used is Volume of fluid method. In this thesis, CFD is used but DPM is used to simulate coalescence. Hence, it is quite evident that irrespective of the built in model pattern of coalescence would be quite similar if the parametrization is done well.

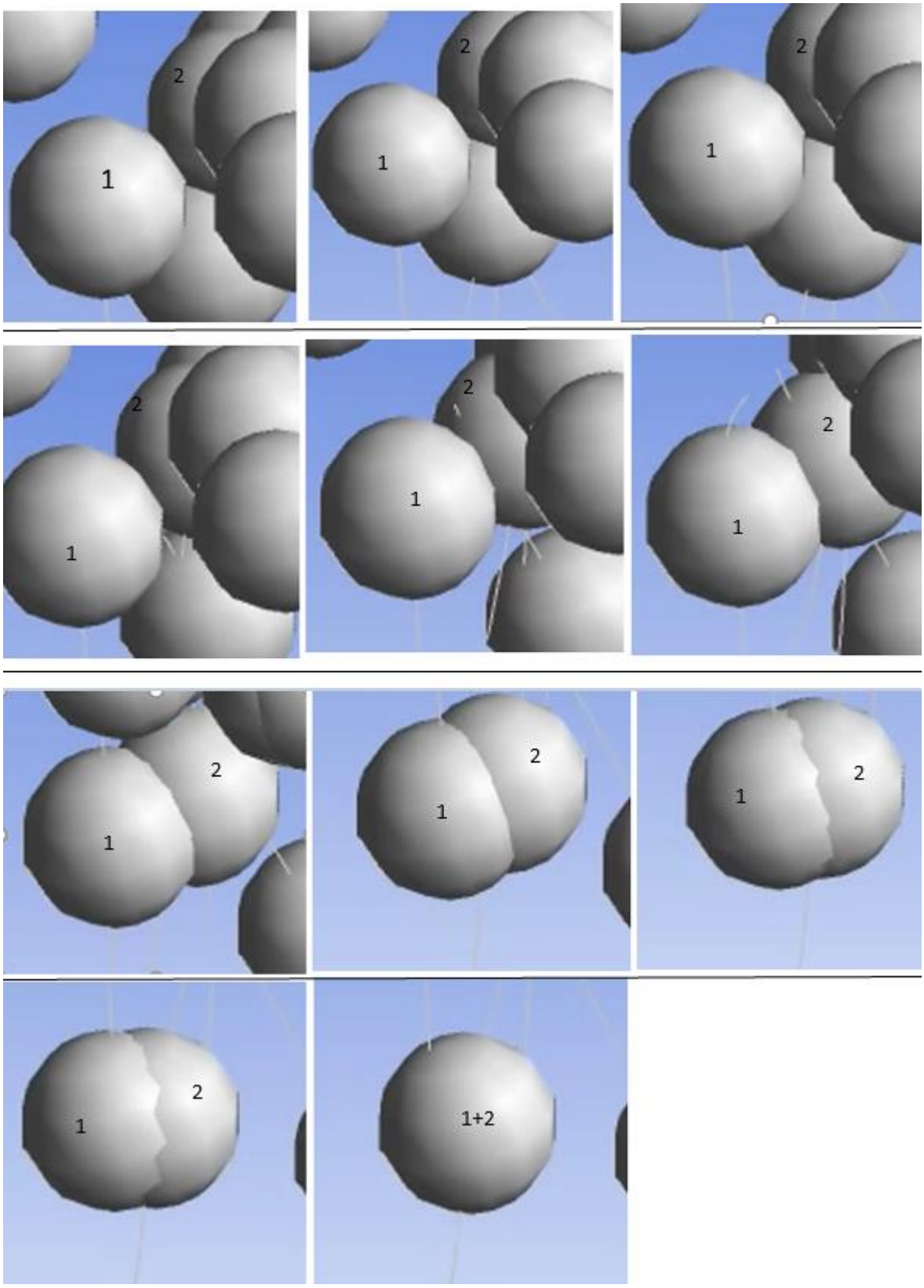

Figure 57: Coalescence outcome at different instants of time comparable with figure 20 and 21

5 Summary and conclusions

Copper droplets entrapped in waste slag greatly influence the cost of copper flash smelting process. Hence, companies give high importance to find ways to minimize copper losses. Previous studies have shown that copper loss in Flash smelting settler could be minimized by increasing matte droplet diameter. Coalescence phenomenon increases droplet diameter and hence should be investigated. It is impossible to take direct measurements in industrial flash smelting settler due to its hostile and aggressive conditions. Hence, flash smelting settler is a target of CFD simulation. CFD solves conservation equations and helps to understand the settling/coalescence phenomena safely from different angles in an economical manner. This thesis work is a first step in CFD modeling of matte droplet coalescence inside flash smelting settler.

Properties of matte and slag and settler dimension are taken from the previous publication. In the computational part settler is reduced in dimension to lower the computational time. Discrete phase model is parametrized to model collision and coalescences. The viability of the parameterized DPM is checked with respect to settling of matte droplets through slag inside the settler.

DPM module uses O'Rourke's method to determine collision outcome and model bouncing, coalescences. It is incapable to simulate shattering and separation. O'Rourke's method determines collision outcome by comparing the offset distance between two droplets with respect to critical value. Critical offset is the function of Weber number and droplet radius of two colliding droplets. If the offset distance is lower than critical value then the outcome is coalescence otherwise the outcome is bouncing. To achieve coalescences in the simulation injections are made in such a way to achieve distance between two droplets lower than the critically measured value. DPM module injects droplets with parcel technique.

DPM model provides three injection types namely point injection, surface injectors and cone injectors. Firstly, point injectors are placed at three points similar to computational setup done by Xia, J. L. et.al (2004). Achieving interactions with single point injections is quite tedious because matte droplets are 100-900µm and settler is (8*6) m in dimensions. Turbulent dispersion changes the droplet trajectory, which in turn increases the complications i.e with a small change in droplet trajectory tiny matte droplets move so far from each other that three droplets does not interact at all inside a big settler. Secondly, surface injectors are tried with the logic that higher turbulences increases the number of collisions. Number of collisions will increase the probability of coalescence outcome. However, the DPM module imposes limitations with respect to volume fraction. Number of droplets injected by surface injector is 5845, which crossed the volume fraction limit of DPM. Thirdly, cone injectors are placed at three points. Cone injectors will reduce the number of droplets injected so that the volume fraction does not cross the maximum limit. 50 droplets are injected from each point making a total of 150 droplets in the computational setup. The angle of cone, number of stream are carefully selected with iterations so that collisions happen.

DPM module allows finding the collision outcome by viewing particle tracking history and post-processing animation. Both particle tracking history and post-processing animation showed coalescences hence the DPM injections and parametrization is successful to model coalescences as the collision outcome. In the post-processing visualization droplet trajectories intersected during collision. One of the droplets and its trajectory disappeared after coalescences while other droplets continued its settling. Parametrized DPM cannot model droplet growth in its visualization.

The post processing visualization clearly showed droplets change their trajectory after collision/coalescences. If the droplet has time to undergo collision/coalescences it will change its trajectory and copper loss is minimized. As number of collisions increases droplets tendency to settle near the central region of the bottom wall increases. Settling is more efficient with high number of collisions/coalescences.

Both particle tracking history and post processing animation showed large number of coalescences in the beginning of the settler, few in the middle of the settler and no coalescences near the bottom wall. The high number of coalescences in the beginning is due to high turbulence created at the inlet of the settler. Droplets experience turbulence at the inlet after hitting the slag layer. Droplets after collision/coalescences change their trajectories near the inlet of the settler. The settler is very big for droplets to interact again after changing the droplet trajectory. Hence, very few coalescences are observed in the middle. Near the bottom wall, tiny matte droplets are so far from each other in a big settler that they do not undergo collisions/coalescences anymore.

The success of the parameterized DPM model was checked by settling literature in the past. Xia, J. L. et al ((2007) proved that time taken for settling is inversely proportional to droplet diameter. In accordance to that study coalesced droplet having bigger diameter settled much faster than the droplets without coalescence. Moreover, the simulation results showed that it is not only the increase in droplet size that influence settling time but also change in droplet trajectory. With higher number of collisions/coalescences droplets settling time decreases significantly due to change in droplet trajectory and increased droplet size. Xia, J. L. et al ((2007) used three droplets for their study. The settling time in three droplets is calculated individually by comparing particle tracking history with the post processing visualization. The total number of droplets injected in the computational setup is 150. It should be noted DPM module injects 150 droplets in parcels technique. Calculating settling time of each single droplets (inside the parcel) by identifying droplets individually out of 150 droplets is very time consuming and not suggested due to accuracy. Further droplets undergoing coalescences are difficult to identify individually. The particle tracking history shows number of droplets coalesced in particular flow time. However, it is unable identify the droplets that are undergoing coalescences i.e. it is difficult to identify out of 150 droplets which droplet coalesced in particular flow time. Manual method is not the preferred way to identify coalescences. Hence, if DPM is used in future then user-defined functions should be written to identify droplets individually for comparison.

This is the first stage of the project wherein built in model is checked for feasibility. The parameterized model could be sophisticated to include reaction kinetics, rate equations by user-defined functions (UDF) in the next stage. However, it should be noted that DPM uses parcels technique, which might create complications for calculating parameters like offset distance, velocity, etc. Introducing reaction kinetics, rate equations, UDF in DPM will increase the computational power. However results are sure to be achieved. Hence, it could be concluded that DPM is feasible for modeling coalescence but robust programming should be done for achieving results. If the robust programming is possible then DPM could be proceeded further. Otherwise, it is suggested to try with other built in models or to develop

a mathematical model exclusively for flash smelting settling. Empirical models defined exclusively with respect to flash smelting would be the best choice.

References

Acevedo-Malavé, A., & Loaiza, N. (2016). Fluid mechanics calculations in physics of droplets–IV: Head-on and off-center numerical collisions of unequal-size drops. *The Journal of Computational Multiphase Flows*, *8*(3), 148-156.

Ahokainen, T., Jokilaakso, A., Vaarno, J., & Järvi, J. (1997, July). Modelling chalcopyrite combustion together with fluid flow simulation. In *Int. Conf. on CFD in Mineral & Metal Processing and Power Generation, CSIRO, Australia* (pp. 213-221).

Ahokainen, T., & Jokilaakso, A. (1998). Numerical simulation of the Outokumpu flash smelting furnace reaction shaft. *Canadian metallurgical quarterly*, *37*(3-4), 275-283.

Ahokainen, T., Jokilaakso, A., Taskinen, P., & Kyto, M. (2006). A new advanced CFD model for flash smelting and converting processes. In *Sohn International Symposium; Advanced Processing of Metals and Materials Volume 8: International Symposium on Sulfide Smelting 2006* (Vol. 8, pp. 529-543).

Ajersch, F., & Toguri, J. M. (1972). Oxidation rates of liquid copper and liquid copper sulfide. *Metallurgical Transactions*, *3*(8), 2187-2193.

ANSYS 18.2 Documentaion

Ashgriz, N., & Poo, J. Y. (1990). Coalescence and separation in binary collisions of liquid drops. *Journal of Fluid Mechanics*, *221*, 183-204.

B. Liu, D. Mather, and R. D. Reitz. (1993). *"Modeling the Effects of Drop Drag and Breakup on Fuel Sprays"*. *SAE Technical Paper 930072*. SAE.

B. Andersson, R. Andersson, L. Håkansson, M. Mortensen, RSTudio, and B.V. Wachem, (2011) Computational Fluid Dynamics for Engineers, Cambridge University Press

Ban, T., Kawaizumi, F., Nii, S., & Takahashi, K. (2000). Study of drop coalescence behavior for liquid–liquid extraction operation. *Chemical engineering science*, *55*(22), 5385-5391.

Carrica, P. M., Drew, D., Bonetto, F., & Lahey Jr, R. T. (1999). A polydisperse model for bubbly two-phase flow around a surface ship. *International journal of multiphase flow*, *25*(2), 257-305.

Charles, G. E., & Mason, S. G. (1960). The coalescence of liquid drops with flat liquid/liquid interfaces. *Journal of Colloid Science*, *15*(3), 236-267.

Chen, P., Sanyal, J., & Duduković, M. P. (2005). Numerical simulation of bubble columns flows: effect of different breakup and coalescence closures. *Chemical Engineering Science*, *60*(4), 1085-1101.

Chevaillier, J. P., Klaseboer, E., Masbernat, O., & Gourdon, C. (2006). Effect of mass transfer on the film drainage between colliding drops. *Journal of colloid and interface science*, *299*(1), 472-485.

Clift, G. (1978). Weber. Bubbles, Drops. and Particles. Technical report, Academic Press.

Coulaloglou, C.A.(1975). Dispersed phase interactions in an agitated flow vessel. Ph.D. Dissertation, Illinois Institute of Technology, Chicago.

Davenport, W. G., & Partelpoeg, E. H. (2015). Flash smelting: analysis, control and optimization. Elsevier.

Davenport, W. G., Jones, D. M., King, M. J., & Partelpoeg, E. H. (2001). Flash Smelting: Analysis. *Control and Optimization, TMS, Warrendale*.

Davenport, W. G., King, M. J., Schlesinger, M. E., & Biswas, A. K. (2002). *Extractive metallurgy of copper*. Elsevier.

Day, P., Manz, A., & Zhang, Y. (Eds.). (2012). *Microdroplet technology: principles and emerging applications in biology and chemistry*. Springer Science & Business Media.

De Wilde, E., Bellemans, I., Campforts, M., Guo, M., Blanpain, B., Moelans, N., & Verbeken, K. (2016). Investigation of high-temperature slag/copper/spinel interactions. *Metallurgical and Materials Transactions B*, *47*(6), 3421-3434.

Dennis, S. C. R., Singh, S. N., & Ingham, D. B. (1980). The steady flow due to a rotating sphere at low and moderate Reynolds numbers. Journal of Fluid Mechanics, 101(2), 257-279.

Dhainaut, M. (2002). Literature Study on Observation and Experiments on Coalescence and Breakup of Bubbles and Drops. SINTEF, Materials Technology. SINTEF

Dreher, T. M., Glass, J., O'Connor, A. J., & Stevens, G. W. (1999). Effect of rheology on coalescence rates and emulsion stability. *AIChE Journal*, *45*(6), 1182-1190.

Eiswirth, R. T. (2014), Binary Droplet Coalescence of Free Rising Droplets, Ph.D. Thesis, University of Kaiserslautern, Germany

Fagerlund, K. O., & Jalkanen, H. (1999). Some aspects on matte settling in copper smelting. In *Fourth International Conference Copper 99-Cobre* (Vol. 99, pp. 539-551).

Fagerlund, K. O., & Jalkanen, H. (2000). Microscale simulation of settler processes in copper matte smelting. *Metallurgical and Materials Transactions B*, *31*(3), 439-451.

Gao, S., & Fritsching, U. (2010). Study of binary in-flight melt droplet collisions. *Materialwissenschaft und Werkstofftechnik*, *41*(7), 547-554.

Guntoro, P. (2017). Experimental investigation of matte-slag interactions in copper flash smelting.

Haider and O. Levenspiel. (1989) "Drag Coefficient and Terminal Velocity of Spherical and Nonspherical Particles". Powder Technology. 58. 63–70.

Hiskey, B. (2000). Metallurgy, Survey. *Kirk-Othmer Encyclopedia of Chemical Technology*.

Hu, Y. T., Pine, D. J., & Leal, L. G. (2000). Drop deformation, breakup, and coalescence with compatibilizer. *Physics of Fluids*, *12*(3), 484-489.

Jakobsen, H. A., Lindborg, H., & Dorao, C. A. (2005). Modeling of bubble column reactors: progress and limitations. *Industrial & engineering chemistry research*, *44*(14), 5107-5151.

Jiang, T., Hwang, J. Y., Alvear, G., Yucel, O., Mao, X., Sohn, H. Y. & Battle, T. (Eds.). (2016). *6th International Symposium on High-Temperature Metallurgical Processing*. Springer.

Jones, R., & Southern, R. (2017, July). Physically-based droplet interaction. In *Proceedings of the ACM SIGGRAPH/Eurographics Symposium on Computer Animation* (p. 5). ACM.

Jorgensen, F. R. A., & Koh, P. T. L. (2001). Combustion in flash smelting furnaces. *JOM*, *53*(5), 16-20.

Kamp, J., & Kraume, M. (2014). Influence of drop size and superimposed mass transfer on coalescence in liquid/liquid dispersions–test cell design for single drop investigations. *Chemical Engineering Research and Design*, *92*(4), 635-643.

Kankaanpää, T. (2007). *CFD procedure for studying dispersion flows and design optimization of the solvent extraction settler*. Helsinki University of Technology.

Kentish, S. E., Stevens, G. W., & Pratt, H. R. C. (1998). Estimation of coalescence and breakage rate constants within a Kühni column. *Industrial & engineering chemistry research*, *37*(3), 1099-1106.

Khan, N. A., & Jokilaakso, A. (2018). Dynamic modelling of molten slag-matte interactions in an industrial flash smelting furnace settler. In *Extraction 2018* (pp. 993-1005). Springer, Cham.

Koh, P. T. L., Nguyen, T. V., & Jorgensen, F. R. A. (1998). Numerical modelling of combustion in a zinc flash smelter. *Applied Mathematical Modelling*, *22*(11), 941-948.

Ko, G. H., & Ryou, H. S. (2005). Modeling of droplet collision-induced breakup process. *International Journal of Multiphase Flow*, *31*(6), 723-738.

Konno, M., Muto, T., & Saito, S. (1988). Coalescence of dispersed drops in an agitated tank. *Journal of chemical engineering of Japan*, *21*(4), 335-338.

Kralchevsky, P. A., Danov, K. D., & Denkov, N. D. (1997). Chemical physics of colloid systems and interfaces. *Handbook of Surface and Colloid Chemistry*, *2*.

Kufås, E. (2008). *Mathematical Modeling of Coalescence of Oil Droplets in Water Flow* (Master's thesis, Institutt for energi-og prosessteknikk).

Leng, D. E., & Calabrese, R. V. (2004). Immiscible liquid–liquid systems. Handbook of Industrial Mixing: Science and Practice, 3952(2006), 639-753.

Li, A., & Ahmadi, G. (1992). Dispersion and deposition of spherical particles from point sources in a turbulent channel flow. Aerosol science and technology, 16(4), 209-226.

Liao, Y., & Lucas, D. (2010). A literature review on mechanisms and models for the coalescence process of fluid particles. *Chemical Engineering Science*, *65*(10), 2851-2864.

Liao, Y., Rzehak, R., Lucas, D., & Krepper, E. (2015). Baseline closure model for dispersed bubbly flow: Bubble coalescence and breakup. *Chemical Engineering Science*, *122*, 336-349.

Liu, H., & Gibbs, B. M. (2002). Modelling of NO and N2O emissions from biomass-fired circulating fluidized bed combustors. Fuel, 81(3), 271-280.

Liu, S., & Li, D. (1999). Drop coalescence in turbulent dispersions. Chemical Engineering Science, 54(23), 5667-5675.

Lo, S. (1996). Application of the MUSIG model to bubbly flows. *AEAT-1096, AEA Technology*.

Lucas, D., Krepper, E., & Prasser, H. M. (2007). Modeling the evolution of bubbly flow along a large vertical pipe. *Nuclear technology*, *158*(2), 291-303.

Lucas, D., Krepper, E., & Prasser, H. ME. (2007). Modeling the evolution of bubbly flow along a large vertical pipe. *Nuclear technology*, *158*(2), 291-303.

Luo, H., & Svendsen, H. F. (1996). Theoretical model for drop and bubble breakup in turbulent dispersions. AIChE Journal, 42(5), 1225-1233.

Ma, X., Cui, Z., & Zhao, B. (2016, January). Simulation of Copper Matte Settlement in Slags Relevant to Bottom Blown Copper Smelting Furnace. In *Copper 2016* (pp. 1148-1158). The Mining and Materials Processing Institute of Japan.

Minto, R., & Davenport, W. G. (1972). Entrapment and flotation of matte in molten slags. *CAN MINING METALL BULL*, *65*(720), 70-76.

Mohammadi, M., Shahhosseini, S., & Bayat, M. (2011, May). CFD Based Simulation of Binary Droplet Coalescence. In *3rd National Conference on CFD Applications in Chemical Industries, Iran University of Science and Technology, Tehran, Iran*.

Morsi, S. A. J., & Alexander, A. J. (1972). An investigation of particle trajectories in two-phase flow systems. Journal of Fluid mechanics, 55(2), 193-208.

Moukalled, F., Mangani, L., & Darwish, M. (2016). The finite volume method in computational fluid dynamics. *An Advanced Introduction with OpenFOAM and Matlab*, 3-8.

Nienow, A. W. (2004). Break-up, coalescence and catastrophic phase inversion in turbulent contactors. *Advances in colloid and interface science*, *108*, 95-103.

Orme, M. (1997). Experiments on droplet collisions, bounce, coalescence and disruption. *Progress in Energy and Combustion Science*, *23*(1), 65-79.

Ounis, H., Ahmadi, G., & McLaughlin, J. B. (1991). Brownian diffusion of submicrometer particles in the viscous sublayer. Journal of Colloid and Interface Science, 143(1), 266-277.

O'Rourke, P. J. (1981). Collective drop effects on vaporizing liquid sprays (No. LA-9069-T). Los Alamos National Lab., NM (USA).

Park, R. W. (1970). Behavior of water drops colliding in humid nitrogen. Thesis (PH.D.)--THE UNIVERSITY OF WISCONSIN - MADISON, 1970.Source: Dissertation Abstracts International, Volume: 31-11, Section: B, page: 6811.

Pedlosky, J. (2013). *Geophysical fluid dynamics*. Springer Science & Business Media.

Prince, M. J., & Blanch, H. W. (1990). Bubble coalescence and break-up in air-sparged bubble columns. *AIChE journal*, *36*(10), 1485-1499.

Qian, J., & Law, C. K. (1997). Regimes of coalescence and separation in droplet collision. *Journal of Fluid Mechanics*, *331*, 59-80.

R.Espejo Guardiola (2008) “Influence of the dispersed phase fraction on drop sizes in liquid/liquid systems“ Diplomarbeit. Technische Universität Berlin

Ramkrishna, D. (2000). *Population balances: Theory and applications to particulate systems in engineering*. Academic press.

ROTH, N., M. RIEBER and A. FROHN: High energy head-on collision of droplets. In 15th Annual Conference on Liquid Atomization and Spray Systems, Toulouse, France, 1999.

Sadeghi, R., Mohebbi, A., & Baniasadi, M. (2011). CFD modeling of the launder of settler of an industrial copper solvent extraction plant: A case study on Sarcheshmeh copper complex, Iran. *International Journal of Mineral Processing*, *98*(1-2), 55-65.

Sadeghi, R., Mohebbi, A., Sarrafi, A., Soltani, A., Salmanzadeh, M., & Daneshpojooh, S. (2011). CFD simulation and optimization of the settler of an industrial copper solvent extraction plant: A case study. *Hydrometallurgy*, *106*(3-4), 148-158.

Schellpfeffer, N. G., & Longmire, E. K. Study of Droplet Coalescence Criteria of a Liquid/Liquid Interface in Micro-and Macro-Gravity Conditions.

Schuchmann, H. P., & Danner, T. (2004). Emulgieren: mehr als nur Zerkleinern. *Chemie Ingenieur Technik*, *76*(4), 364-375.

Sjursen, K. H. (2014). Water Droplets Settling in Crude Oil: Effect of Neighbouring Droplets and Temperature (Master's thesis, Institutt for energi-og prosessteknikk), NTNU.

Suh, I. K., Waseda, Y., & Yazawa, A. (1988). Some interesting aspects of non-ferrous metallurgical slags. *High Temperature Materials and Processes*, *8*(1), 65-88.

ŠUTALO I. D., JORGENSEN F. R. A. and GRAY N. B. (1998a), "Experimental and mathematical investigation of the fluid flow inside and below a 1/4 scale air model of a flash smelting burner", Metallurgical and Materials Transactions B, October 1998, Volume 29, Issue 5, pp 993-1006

ŠUTALO I. D., HARRIS J. A .,. JORGENSEN F. R. A, AND GRAY N. B. (1998b), "Modeling studies of fluid flow below flash-smelting burners including transient behavior", Metallurgical and Materials Transactions B, August 1998, Volume 29, Issue 4, pp 773-784.

Svanberg, M., Ming, L., Marković, N., & Pettersson, J. B. (1998). Collision dynamics of large water clusters. *The Journal of chemical physics*, *108*(14), 5888-5897.

Taskinen, Pekka & Xia, Jilian & Ahokainen, Tapio & Kankaanpää, Timo & Järvi, Juha. (2005). Numerical modelling of copper droplet setting behavior in the settler of a flash smelting furnace. Proceedings - European Metallurgical Conference, EMC 2005. 3.

Wang, T., Wang, J., & Jin, Y. (2005). Population balance model for gas− liquid flows: Influence of bubble coalescence and breakup models. *Industrial & engineering chemistry research*, *44*(19), 7540-7549.

Wang, T., Wang, J., & Jin, Y. (2005). Theoretical prediction of flow regime transition in bubble columns by the population balance model. *Chemical Engineering Science*, *60*(22), 6199-6209.

Wang, W., Li, K., Wang, P., Hao, S., & Gong, J. (2014). Effect of interfacial dilational rheology on the breakage of dispersed droplets in a dilute oil–water emulsion. *Colloids and Surfaces A: Physicochemical and Engineering Aspects*, *441*, 43-50.

Wegener, M., & Paschedag, A. R. (2012). The effect of soluble anionic surfactants on rise velocity and mass transfer at single droplets in systems with Marangoni instabilities. *International Journal of Heat and Mass Transfer*, *55*(5-6), 1561-1573.

Wegener, M., Paul, N. and Kraume, M., 2014, Fluid Dynamics and Mass Transfer at Single Droplets in Liquid/liquid Systems, Int. Journal of Heat and Mass Transfer Vol. 71, pp. 475 - 495.

WHITE, M., HAYWOOD, R., RANASINGHE, D. J., & CHEN, S. (2015). THE DEVELOPMENT AND APPLICATION OF A CFD MODEL OF COPPER FLASH SMELTING. Eleventh International Conference on CFD in the Minerals and Process Industries CSIRO, Melbourne, Australia

Wright, H., & Ramkrishna, D. (1994). Factors affecting coalescence frequency of droplets in a stirred liquid-liquid dispersion. *AIChE journal*, *40*(5), 767-776.

Xia, J. L., Ahokainen, T., Kankaanpää, T., Järvi, J., & Taskinen, P. (2007). Flow and heat transfer performance of slag and matte in the settler of a copper flash smelting furnace. *steel research international*, *78*(2), 155-159.

Xia, J. L., Kankaanpää, T., & Ahokainen, T. (2004). Nickel droplet settling behavior in an electric furnace. *Metallurgical and Materials Transactions B*, *35*(5), 839-845.

Yuan, Shuxia & Dabirian, Ramin & Mohan, Ram & Shoham, Ovadia. (2018). Simulation of Coalescence and Breakup of Dispersed Water Droplets in Continuous Oil Phase. 5th joint US-European Fluids Engineering Summer Conference FEDSM2018.

Zhou, P., Yu, J. P., Chen, H. R., & Mei, C. (2006). Settling mechanism and influencing factors on matte droplets in settler slag of copper flash smelting furnace. *Chinese journal of nonferrous metals*, *16*(12), 2132.